

Aus der Klinik für Hals-, Nasen- und Ohrenheilkunde,  
Universitätsklinikum des Saarlandes, Homburg/Saar

# **Biocompatibility studies for novel therapeutic strategies at the tympanic membrane level**

**Dissertation zur Erlangung des Grades  
eines Doktors der Naturwissenschaften  
der Medizinischen Fakultät  
der UNIVERSITÄT DES SAARLANDES**

2022

vorgelegt von:

Katharina Sorg

geb. am: 25.04.1989 in Saarbrücken

Tag des Kolloquiums 06.07.2022

Dekan: Herr Univ.-Prof. Dr. Michael Menger

Berichterstatter : Frau Univ.-Prof. Dr. Jutta Engel

Frau Prof. Dr. Dr. Gentiana I. Wenzel

## **Eidesstattliche Versicherung**

Ich erkläre hiermit an Eides statt, dass ich die vorliegende Arbeit ohne unzulässige Hilfe Dritter und ohne Benutzung anderer als der angegebenen Hilfsmittel angefertigt habe. Die aus anderen Quellen direkt oder indirekt übernommenen Daten und Konzepte sind unter Angabe der Quelle gekennzeichnet. Die Arbeit wurde bisher weder im Inland noch im Ausland in gleicher oder in ähnlicher Form in einem anderen Verfahren zur Erlangung des Doktorgrades einer anderen Prüfungsbehörde vorgelegt.

Ich versichere an Eides statt, dass ich nach bestem Wissen die Wahrheit gesagt und nichts verschwiegen habe.

Die Bedeutung der eidesstattlichen Erklärung und die strafrechtlichen Folgen einer unrichtigen oder unvollständigen eidesstattlichen Erklärung sind mir bekannt.

Homburg, 10.02.2022

Katharina Sorg

## Vorwort

Die nachfolgende Arbeit entstand unter der Anleitung von Frau Prof. Dr. Gentiana Wenzel und Fr. Univ. Prof. Dr. Jutta Engel in der Abteilung für experimentelle Hörforschung in der Arbeitsgruppe „Laser Hearing Aids“ der Fachrichtung Hals-, Nasen-, Ohrenheilkunde der Universität des Saarlandes in Homburg (Saar), Direktor Univ.-Prof. Dr. Bernhard Schick, im Zeitraum von Januar 2016 bis Juli 2021. Diese Arbeit war finanziert durch den Europäischen Forschungsrat (engl.: *European Research Council*) im Rahmen des spezifischen Programmes „Ideen“ zur Durchführung des Siebten Rahmenprogramms der Europäischen Gemeinschaft für Forschung, technologische Entwicklung und Demonstration (Starting Grant Nr. 311469) sowie im Rahmen des Wissenschaftsexzellenz-Programmes Horizon 2020 (Proof-of concept Grants Nr. 789948 und Nr. 842613).

# Content

Vorwort .....	I
Abbreviations .....	IV
Zusammenfassung .....	VI
Summary .....	VIII
Papers included in this thesis.....	X
1 Introduction .....	1
1.1 Background and aims of this thesis .....	1
1.2 The hearing system.....	2
1.2.1 The peripheral hearing system.....	2
1.2.2 The inner ear (labyrinth).....	6
1.2.3 The auditory system .....	7
1.3 Pathologies of the ear .....	8
1.3.1 Pathologies of the outer ear .....	8
1.3.2 Pathologies of the middle ear .....	8
1.3.3 Pathologies of the inner ear .....	14
2 Results .....	19
2.1 Biocompatibility margins for optical stimulation at the eardrum via 532 nm laser pulses (Appendix 1).....	19
2.2 Cytotoxicity studies of an optoacoustic stimulation strategy for the development of laser-based hearing aids (Appendix 2).....	20
2.3 Optoacoustic stimulation efficiency can be improved using an absorbing film (Appendix 3) . .....	21
2.4 Self-adhesive silicone microstructures for the treatment of tympanic membrane perforations reduce a conductive hearing loss induced by perforation (Appendix 4).....	23
3 Discussion.....	25
3.1 Biocompatibility margins of optoacoustic stimulation.....	26
3.2 Enhanced efficiency of optoacoustic stimulation due to the use of absorbing patches .....	30

3.3 Reduced conductive hearing loss by covering eardrum perforations with self-adhesive patches.....	32
Appendix .....	37
1) First biocompatibility margins for optical stimulation at the eardrum level via 532-nm laser pulses in a mouse model .....	37
2) Cytotoxicity studies of an optoacoustic stimulation strategy for the development of laser-based hearing aids .....	49
3) Optoacoustically induced auditory brainstem responses in the mouse model enhanced through an absorbing film .....	65
4) Self-adhesive silicone microstructures for the treatment of tympanic membrane perforations .....	80
References .....	96
Further publications of the author .....	XI
Danksagung .....	XII
Lebenslauf .....	XIII

## Abbreviations

aABR	acoustically induced auditory brainstem responses
ABR	auditory brainstem responses
Ag	<i>Argentum</i> = silver
CAP	compound action potential
CDKN1A	cyclin-dependent kinase inhibitor 1A
CW	continuous wave
dB SPL	dB sound pressure level
DPOAE	distortion product otoacoustic emissions
ECM	extracellular matrix
fABR	frequency-specific ABR
FTH1	Ferritin heavy chain 1
GADD45A	Growth arrest and DNA-damage inducible gene 45 alpha
GADD45G	Growth arrest and DNA-damage inducible gene 45 gamma
HCH	human chondrocytes
HOB	human osteoblasts
HSP	heat shock protein
ICC	inferior colliculus
IFNG	Interferon gamma
INS	infrared neural stimulation
IO	Input-Output
LDH	lactate dehydrogenase
LLLT	low level laser therapy
LMR	laser modulation rate

LPR	laser pulse rate
MSCs	mesenchymal stem cells
NBN	Nibrin
NHDF	normal human dermal fibroblasts
oABR	optically induced ABR
PBM	photobiomodulation
PDMS	poly (dimethyl) siloxane
PTS	permanent threshold shift
qPCR	quantitative polymerase chain reaction
SNR	signal to noise ratio
SQSTM1	Sequestosome 1
SSA	soft skin adhesive
TLR4	Toll-like receptor 4
TM	tympanic membrane
TMP	tympanic membrane perforation
TTMPs	traumatic tympanic membrane perforations
TTS	temporary threshold shift
TXNRD1	Thioredoxin reductase 1
WST-1	water-soluble tetrazolium salt-1
XPC	Xeroderma pigmentosum, complementation group C

## Zusammenfassung

Die vorliegende Arbeit beschäftigte sich mit der Anwendbarkeit und dem Nutzen neuartiger Strategien zur Behandlung zweier Ohrpathologien: zum einen der optoakustischen Stimulation des Hörsystems, die zur Behandlung von Hörverlusten eingesetzt werden soll. Zum anderen wurde die Applikation von selbstklebenden Silikonpflastern zum unkomplizierten und direkten Verschluss von Trommelfellperforationen untersucht. Zentraler Applikationsort beider Methoden war dabei das Trommelfell. Das Trommelfell ist ein essenzieller Bestandteil des Hörsystems und spielt eine wichtige Rolle für das Hörvermögen, da es die Schallwellen, die gesammelt durch den äußeren Gehörgang auf die dünne, elastische Membran treffen, aufnimmt und durch diese zum Schwingen gebracht wird, dem ersten Schritt im Hörvorgang. Andererseits fungiert es als Grenzfläche zwischen äußerem Ohr und Mittelohr auch als physiologische Barriere und schützt das Mittelohr vor dem Eindringen von Keimen. Ist das Hörvermögen eines Menschen eingeschränkt, z.B. durch altersbedingte Schwerhörigkeit, kommen Hörsysteme zum Einsatz. Diese dienen der symptomatischen Behandlung des Hörverlustes und sollen somit den Patienten wieder die Teilnahme am Leben ermöglichen. Nachteile der konventionellen Therapie sind allerdings eine geringe frequenzspezifische Auflösung des Eingangssignals mit folgender Differenzierungsstörung trotz ausreichender Verstärkung, geminderter Tragekomfort durch einen Verschluss- und damit verbundenen wiederkehrenden Entzündungen des äußeren Gehörganges usw.

Die optoakustische Stimulation bietet eine alternative Stimulationsmethode des Hörsystems mit einer zu erwarteten erhöhten Frequenzauflösung und gleichzeitiger Verbesserung des Tragekomforts, da der Verschluss des Gehörganges bei Nutzen dieser Methode entfallen würde. Dabei werden kurze Laserpulse eingesetzt, um Vibrationen im bestrahlten Gewebe, z.B. dem Trommelfell oder weiteren vibrationsfähigen Komponenten des peripheren Hörsystems, zu erzeugen. Als grundsätzlicher Baustein dieser neuen Stimulationsmethode war ein Ziel dieser Arbeit die Analyse ihrer Biokompatibilität, welche im Tiermodell und in Zellkulturen untersucht wurde. Hierbei konnte am Trommelfell der Maus gezeigt werden, dass für einen gepulsten Laser, mit 532 nm Wellenlänge, ab einer Schwelle von 89 mW mittlerer Laserleistung, Zonen mit apoptotischen und nekrotischen Zellen entstanden, die mit steigender Laserleistung in ihrer Größe zunahmten. Es konnte kein negativer Einfluss auf das Hörvermögen der Tiere durch die Stimulation nachgewiesen werden. In Zellkulturversuchen mit drei humanen Zelllinien konnte gezeigt werden, dass die erhaltenen Schädigungsschwellen je nach Zelllinie deutlich höher waren. Außerdem konnte hier eine reduzierte Zellviabilität nachgewiesen werden, die wiederum abhängig von der Strahlungsintensität war und sich in der Ausprägung zwischen den Zelllinien unterschied. Überdies wurden durch die Bestrahlung regulatorische Prozesse in den Zellen induziert, die sich über Genexpressionsanalysen nachweisen ließen.

Das Hörvermögen kann, neben der Altersschwerhörigkeit, auch durch Trommelfellperforationen maßgeblich beeinträchtigt sein. Durch die Perforationen wird die Schallweiterleitung erheblich geschwächt und es entsteht eine Schalleitungsschwerhörigkeit. Des Weiteren können durch die Perforation Keime in das Mittelohr eindringen und dort akute Entzündungen auslösen, die weitreichende Folgen, etwa die Entstehung von chronischen Prozessen und die Bildung von Cholesteatomen, mit sich bringen können. Um eine direkt wirksame Behandlung von Trommelfellperforationen zu ermöglichen, hat die AG um Prof. Dr. Arzt vom Leibniz Institut für Neue Materialien (INM) in Kollaboration mit uns selbsthaftende Silikon-Pflaster zur Abdeckung der Perforationen entwickelt. Diese wurden in zwei verschiedenen Ausführungen, unstrukturiert und mikrostrukturiert, produziert und dienen, neben dem Verschluss, später auch der verbesserten Heilung der verletzten Trommelfelle. Beide Pflaster zeigten sich *ex vivo* als gut haftend auf dem Trommelfell der Maus. *In vivo*, im lebenden, narkotisierten Tier, fanden wir signifikant erhöhte Hörschwellen und signifikant reduzierte Distorsionsprodukte otoakustischer Emissionen (DPOAE) nach Induzieren einer Perforation. Das Abdecken der Perforation mit den neuartigen Pflastern erhöhte die DPOAE-Signale signifikant, die Hörschwellen in der Click-ABR (engl. *auditory brainstem responses*)-Messung wurden hingegen nicht signifikant verbessert. In weiteren Versuchen konnten wir zeigen, dass die Applikation von dickeren Pflastern keine signifikante Verbesserung der DPOAE-Signale mit sich brachte. Das Aufbringen der Pflaster auf das gesunde Trommelfell führte bei der dicken und der dünnen Ausführung zu einer signifikanten Reduzierung der DPOAE-Signale.

Zusammenfassend erbrachten beide therapeutische Ansätze vielversprechende Ergebnisse, die zusammen mit weiteren translationalen Untersuchungen, auf einen zukünftigen Einsatz im klinischen Alltag hoffen lassen.

## Summary

The presented thesis investigated the applicability and benefit of two innovative therapeutic strategies for the treatment of ear pathologies: on one side, the optoacoustic stimulation as an alternative stimulation method for the hearing system affected by hearing loss. On the other hand, the application of self-adhesive silicone patches for the simple and direct coverage of tympanic membrane perforations. The central site of application of both methods thereby was the tympanic membrane. The tympanic membrane, or eardrum, plays an essential role for the hearing function, as it collects incoming sound waves, traveling from the outer ear canal and is thereby set into vibrations, the first step of the hearing process. Furthermore, the eardrum forms the interface between the outer ear and the middle ear and functions as a physiological barrier to protect the middle ear from the entering of pathogenic germs. If the hearing function of people is impaired e.g., by presbycusis, age-related hearing loss, hearing aids are needed. Conventionally, patients get supplied with hearing aids that are meant to compensate the hearing loss symptomatically aiming to enable the patients to participate in everyday life. The main drawbacks of conventional hearing aids are the insufficient frequency resolution of the input signal leading to insufficient auditive discrimination of sounds despite sufficient amplification, discomfort wearing them in the occluded ear canal and because of occlusion, recurrent infections.

The optoacoustic stimulation offers an alternative stimulation method with an estimated high frequency resolution and a non-occlusive way of application. Thereby, short laser pulses are used to induce vibrations in irradiated tissues e.g., the tympanic membrane or further vibratory components of the peripheral hearing system. As one basic element of this innovative stimulation method, one major goal of the presented work was the investigation of its biocompatibility that was performed in an animal model and in cell culture experiments. The optoacoustic stimulation at the murine tympanic membrane, with our currently used laser parameters, was demonstrated to be safe up to 89 mW. Areas with apoptotic and necrotic cells could be detected starting at 89 mW and increased in their dimensions with rising laser power. We could not identify any negative effect of the stimulation on the hearing function of these animals. In cell culture assays of three human cell lines, our group noticed significantly higher damage thresholds, depending on the irradiated and analyzed cell line. Furthermore, the cell viability was reduced through irradiation with an intensity that was depending on the irradiation power and the respective cell line. Also, regulatory processes were induced by irradiation in the cells, which were investigated by gene expression analysis.

Besides age-related hearing loss, eardrum defects play a crucial role in the loss of hearing function as well. Tympanic membrane perforations significantly affect sound transmission, and a conductive hearing loss occurs. Furthermore, pathogenic germs may enter the middle ear through the perforated membrane, predictably leading to acute inflammations that may cause multiple complications up to

chronic inflammatory processes and cholesteatoma formation. To allow a very direct and quick therapeutic method for tympanic membrane perforations, in collaboration with the group led by Prof. Dr. Eduard Arzt from the Leibniz Institute for New Materials (INM), self-adhesive silicone patches have been designed. Two different conformations of these patches have been analyzed and presented in this work. The unstructured and the microstructured patches aimed to cover the perforation and to support the healing process in the future. The patches demonstrated *ex vivo* good adhesive characteristics on the murine tympanic membrane. *In vivo*, acute eardrum perforations in anesthetized mice induced significantly increased hearing thresholds and significantly reduced distortion product otoacoustic emissions (DPOAE) signals. Covering the perforation with our patches, significantly increased the DPOAE signals, however, the click-ABR thresholds were not significantly affected. In further experiments, we demonstrated that applying patches with higher thicknesses could not improve the DPOAE signals anymore. Additionally, the application of thin and thick patches on the intact tympanic membrane reduced the DPOAE signals significantly.

To sum up, both innovative therapeutic strategies at the eardrum level demonstrated significant positive results warranting further translational work that could introduce them into the daily medical practice.

## Papers included in this thesis

The present thesis is composed as a cumulative work comprising of four different publications.

- 1. First biocompatibility margins for optical stimulation at the eardrum via 532-nm laser pulses in a mouse model (Appendix 1)**

Katharina Sorg, Patricia Stahn, Lukas Pillong, Marius P. Hinsberger, Larissa Heimann, Hans-Jochen Foth, Bernhard Schick, Gentiana I. Wenzel

Journal of Biomedical Optics 24(8), 085003 (2019), DOI: 10.1117/1.JBO.24.8.085003.

- 2. Cytotoxicity studies of an optoacoustic stimulation strategy for the development of laser-based hearing aids (Appendix 2)**

Lukas Pillong, Patricia Stahn, Marius Hinsberger, Katharina Sorg, Bernhard Schick, and Gentiana I. Wenzel

Journal of Biomedical Optics 25(6), 068002 (23 June 2020), DOI: 10.1117/1.JBO.25.6.068002

- 3. Optoacoustically induced auditory brainstem responses in the mouse model enhanced through an absorbing film (Appendix 3, \*shared first authorship)**

Katharina Sorg\*, Larissa Heimann\*, Gabriela Moreira Lana, Achim Langenbucher, Bernhard Schick, Eduard Arzt, Gentiana I. Wenzel

Journal of Biomedical Optics 26(9) 098001 (3 September 2021), DOI: 10.1117/1.JBO.26.9.098001

- 4. Self-adhesive silicone microstructures for the treatment of tympanic membrane perforations (Appendix 4, \*shared first authorship)**

Gabriela Moreira Lana\*, Katharina Sorg\*, Gentiana I. Wenzel, Dietmar Hecker, René Hensel, Bernhard Schick, Klaus Kruttwig, Eduard Arzt

Advanced NanoBiomed Research., 1: 2100057 (22 June 2021), DOI: 10.1002/anbr.202100057

# 1 Introduction

## 1.1 Background and aims of this thesis

The hearing sense, as one of many senses humans have, is the most differentiated. It is essential for people to take part in their daily life including the connection with the environment and other people as basic human needs. Therefore, pathologies affecting the hearing function have far-reaching consequences like affected language development, reduced psychosocial well-being, social isolation, diminished quality of life, educational deficits, etc.[86,89,109]. Hearing-impairing ear pathologies can occur at the outer-, middle- or inner ear level and can be congenital or acquired during a lifetime. According to World Health Organization (WHO), “globally more than 1.5 billion people experience some decline in their hearing capacity during their life course, of whom at least 430 million will require care”. Additionally, the number of people with disabling hearing loss rises each year [36]. Hearing loss is thought to be the fourth leading cause of disability globally [20,134]. In parallel, unaddressed hearing loss is a big issue worldwide causing annual costs of over \$ 980 billion [36]. Out of these, a high percentage of affected people is not sufficiently supplied with hearing aids or further treatments. The high number of patients with unaddressed hearing loss demonstrates the need for effective and available interventions to prevent or compensate the hearing loss including pathologies leading to it.

The goal of this thesis was to contribute to the huge work that needs to be implemented for the potential treatment of hearing impairment within two innovative approaches: first, the optoacoustic stimulation as a novel approach to activate the hearing system and second, the treatment of eardrum perforations, a common cause for hearing impairment, using novel silicone patches.

The optoacoustic stimulation is based on the optoacoustic effect, a physical phenomenon that transforms short laser light pulses into mechanical vibrations and has the potential to activate the hearing system. To be used to stimulate the hearing system, the optoacoustic stimulation’s biocompatibility margins must be defined, and the safe applicability of the method must be ensured. One goal of this thesis was therefore, to define the biocompatibility thresholds of the optoacoustic stimulation for given laser parameters and to search for methods of using it to stimulate the hearing system in a safe and efficient manner.

The further method investigated in this thesis was the treatment of tympanic membrane perforations with innovative self-adhesive polymer patches that allow a quick and direct closure of the perforation without packing the outer ear canal, the current state of the art procedure for this pathology. The adhesion properties, as well as the possible effects of this novel therapeutic strategy on the hearing function, have been assessed as an essential step before considering their application in humans.

Both branches of this thesis contribute to the final preparations for the translation to clinical application. To make both techniques available for patients in the future and, create a chance for them to be applied as individualized therapeutic strategies meeting the patients' specific needs has been the driving force behind the herein presented work.

## 1.2 The hearing system

The hearing system in mammals is a complex system with astonishing potential. The hearing capabilities in humans are so well-developed that we can recognize a familiar voice when hearing one single word. The human hearing system senses a bright range of different intensities, from a pin dropping to an explosion. Thereby, the hearing system performs a large degree of transformation, by converting the mechanical energy of the sound waves into electrical energy represented by neural signals. This mechano-electrical transduction which is the basis of the hearing process occurs on the way of sound from the outer ear to the inner ear. It can be broadly divided into the sound transport, the sound transduction in the cochlea, the stimulus transmission via the nerve up to the stimulus processing in the central auditory system.

### 1.2.1 The peripheral hearing system

The hearing system (Fig. 1) consists of three major parts: the outer ear, middle ear, and inner ear. The outer ear contains the ear canal (*meatus acusticus externus*) and the pinna. It is responsible for the collection and transfer of sound waves from the surrounding environment to the tympanic membrane (TM). The ear canal in humans is around 3 cm long having an s-shape. It consists of the outer cartilaginous and the inner bony part. Sound waves travel through the outer ear canal to the tympanic membrane, the first part of the middle ear. The middle ear is an air-filled cavity, consisting of the tympanic membrane, the Eustachian tube, tympanic cavity, the ossicular chain, and pneumatized cavities.

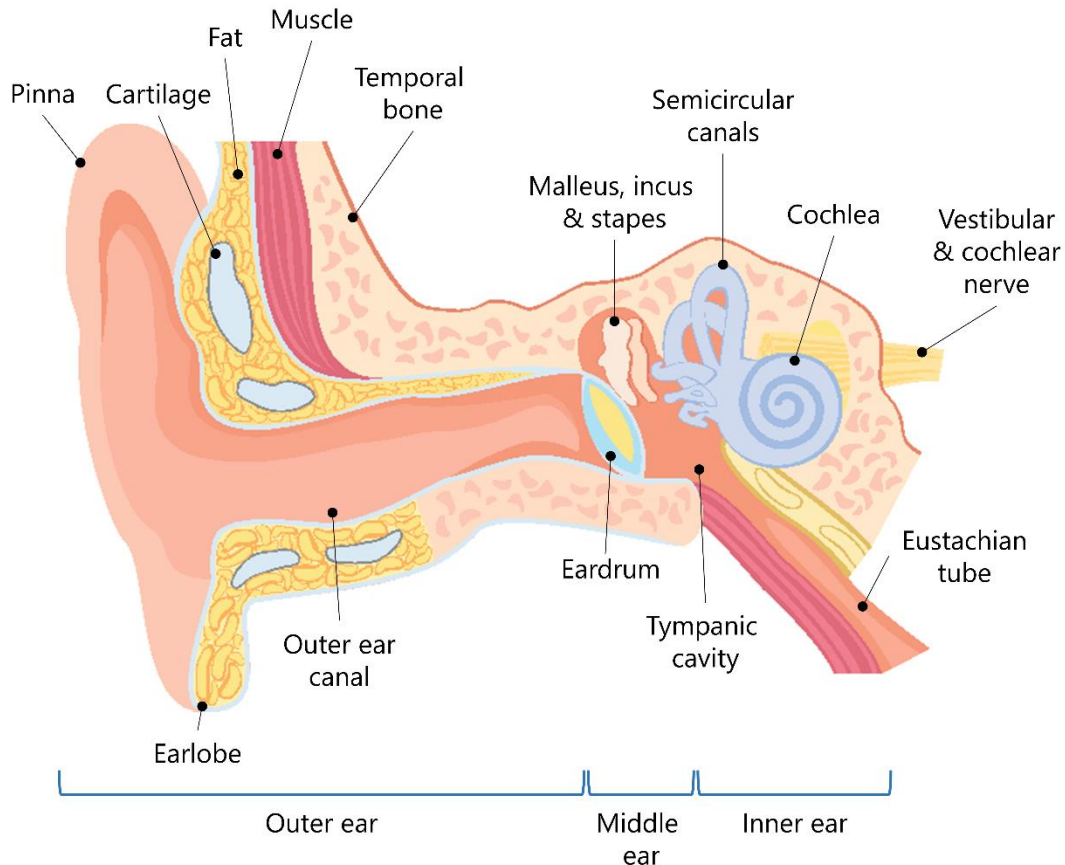


Fig. 1: The hearing system consists of the outer ear, middle ear, and inner ear. The outer ear is containing the pinna and the outer ear canal. The middle ear consists of the eardrum (tympanic membrane), the tympanic cavity and the ossicles malleus, incus, and stapes. The stapes is connected to the cochlea, the inner ear, which transfers the sound energy into nerve impulses that are transferred over the auditory nerve to the brain. ©istock.com/iLexx

The tympanic membrane(TM) (Fig. 2), also called the eardrum, is a thin elastic membrane that separates the outer ear canal from the tympanic cavity. It is embedded with its fibrocartilaginous ring (*annulus fibrosus*) inside the bony *sulcus tympanicus* into the tympanic cavity. The tympanic membrane is an oval membrane with around one cm diameter in humans and around 100  $\mu\text{m}$  thickness. It has the form of an inner-shaped funnel, with the deepest point represented by the umbo, the lower end of the first ossicle, the malleus. The membrane is divided in two major parts, the bigger lower and tense part is called *pars tensa*, and the upper smaller part without tension is the *pars flaccida*. The handle of the malleus is directly bounded and grown together with the tympanic membrane in the *pars tensa*. The membrane can be divided by two lines, one following the malleus and one perpendicular to it, into four different parts: The upper anterior (*anterior superior*), lower anterior (*anterior inferior*), upper posterior (*posterior superior*), and lower posterior (*posterior inferior*) part, also called quadrants.

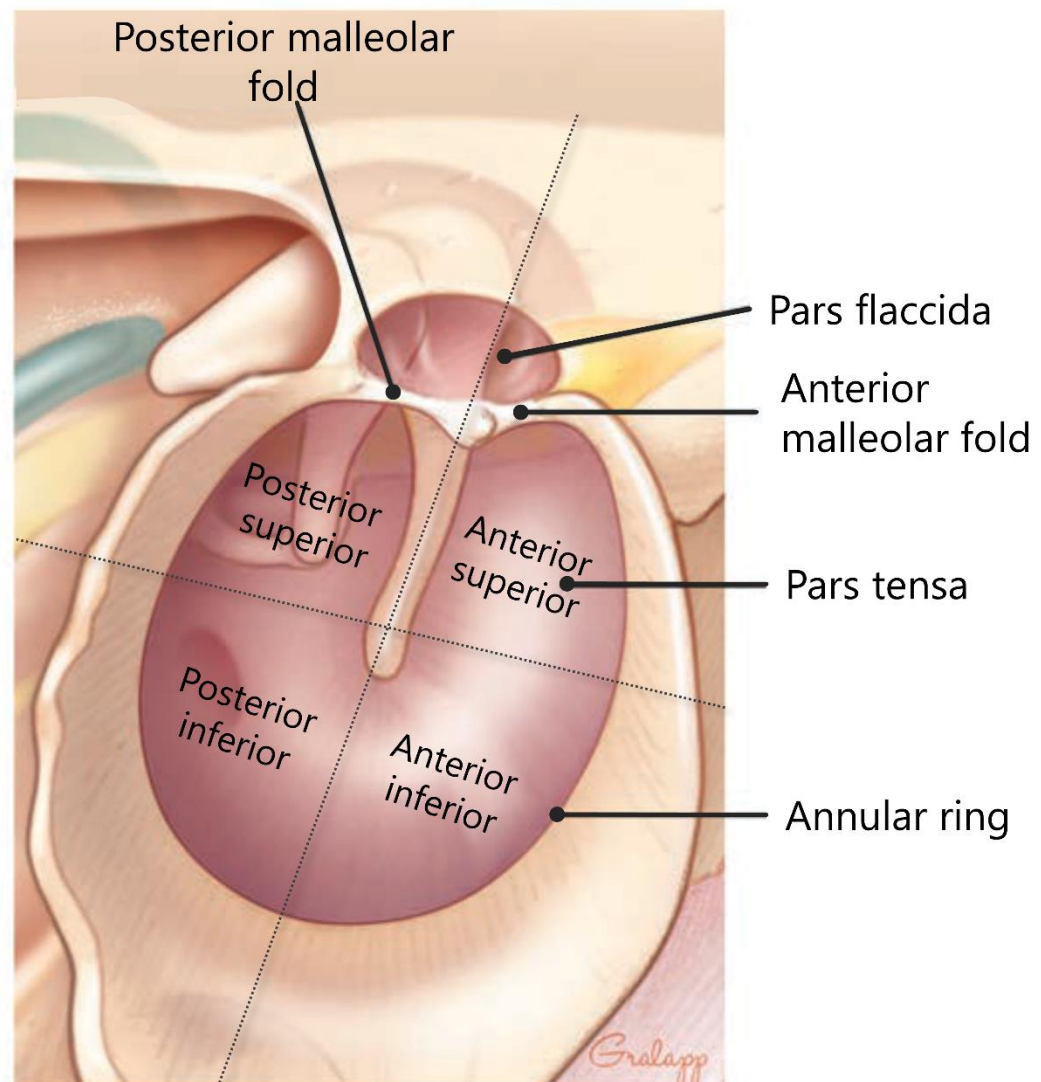


Fig. 2: The human tympanic membrane is a thin membrane consisting of the *pars flaccida* and the *pars tensa* embedded in the annular ring (*annulus fibrosus*). The membrane can be divided into four different parts by two lines: the upper anterior and superior parts and the lower posterior and anterior parts. The image was modified from: Robert K. Jackler.; *Ear Surgery Illustrated: A Comprehensive Atlas of Otologic Microsurgical Techniques*, 2019 [54].

The eardrum is an epithelial structure (Fig 3). The *pars tensa* consists of three different layers: the *stratum cutaneum* on the outside, the *stratum mucosum* on the middle ear side, and a *stratum fibrosum* (*lamina propria*) in between. The outside is an epithelial layer, consisting of a multilayer squamous epithelium as a continuation of the epithelium of the outer ear canal. The *stratum mucosum* is a single-layered epithelium with microvilli. The *lamina propria* consists of two different types of collagen fiber bundles: radial fibers directed towards the outer ear canal and a circular fiber layer that is directed towards the middle-ear side. The *lamina propria* furthermore contains blood vessels (Fig. 3).

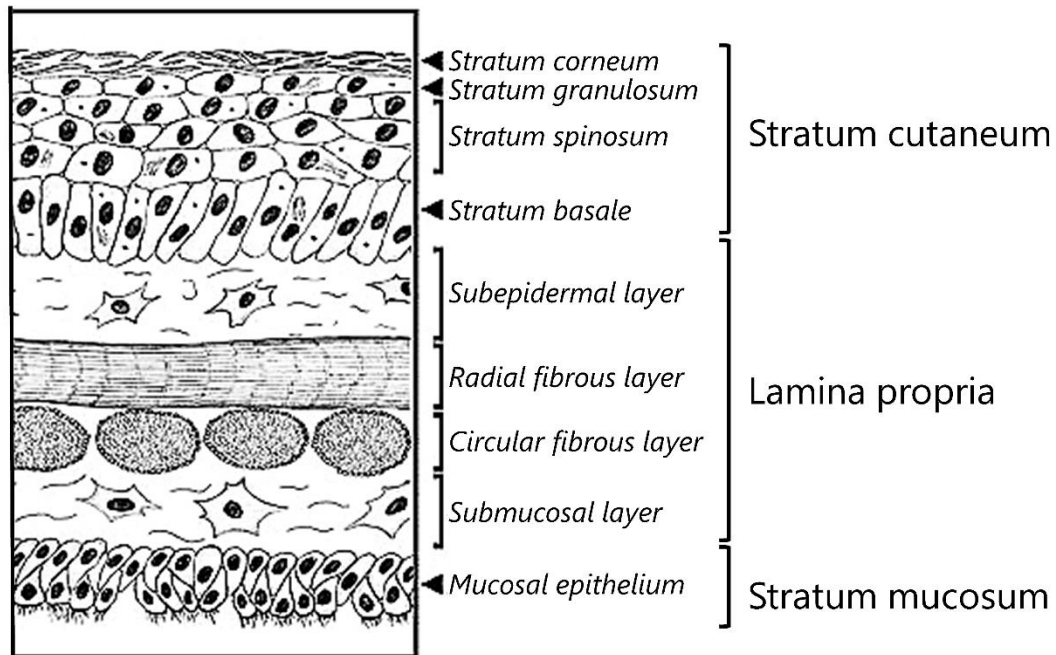


Fig. 3: Histological structure of the tympanic membrane in the *pars tensa*. The *stratum cutaneum*, oriented towards the outer ear canal, consists of a multilayer squamous epithelium, the *lamina propria* contains circular and radial oriented collagen fibers and blood vessels, and the *stratum mucosum*, directed towards the middle ear, consists of a mucosal epithelium. The image was modified from Teh et al. 2013 [116].

The *pars flaccida* only consists of two different layers: the epithelial layer and the mucosal layer without connective tissue. The *pars tensa* is mainly responsible for the vibrational characteristics of the tympanic membrane, whereas the *pars flaccida* does not play a significant role for the sound transfer. The tympanic membrane is set in vibrations by the incoming sound waves and the sound energy is transmitted further through the ossicular chain into the inner ear. The ossicular chain is located inside the tympanic cavity and consists of three different ossicles: malleus, incus, and stapes. The malleus is the first ossicle that is moved directly by the incoming vibrations because of its adhesion of its handle to the membrane. The malleus is connected to the incus by a saddle joint. The incus is attached with its long handle to the stapes, which consists of head, posterior and anterior handle, and the stapes footplate. The footplate is attached on the oval window of the cochlea, one part of the inner ear.

### 1.2.2 The inner ear (labyrinth)

The inner ear is the part of the hearing system where the sound waves are transduced into electrical signals that are then transmitted to the brain. The labyrinth is embedded inside the petrosal bone. It is divided into the bony and the membranous labyrinth. The bony labyrinth surrounds the membranous labyrinth as a capsule being divided into the hearing organ, the cochlea, and the vestibular organ responsible for balance.

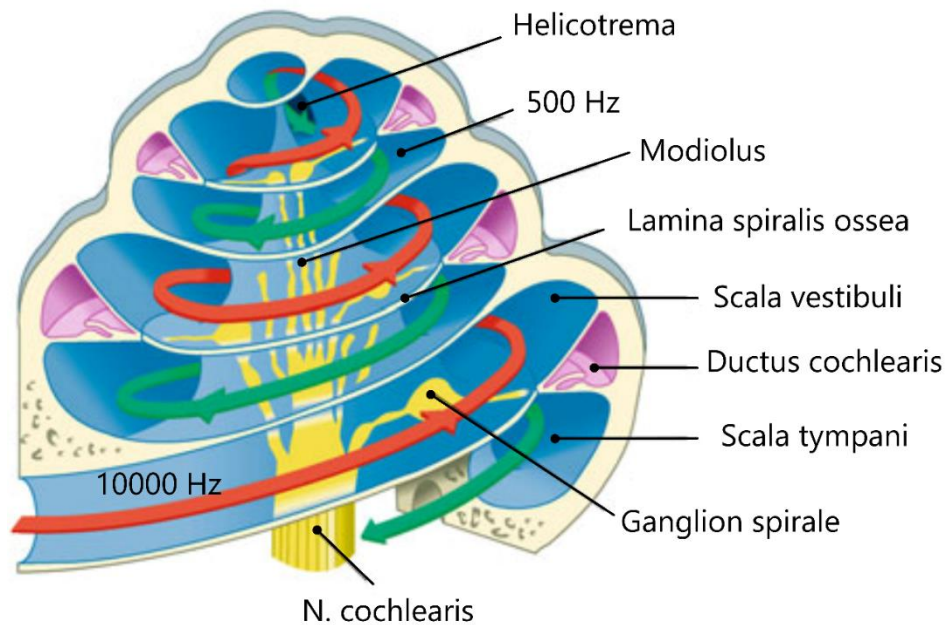


Fig. 4: Cross section of the cochlea along the modiolus axis. The perilymph movements are displayed as red and green arrows along the coils. The frequency spectrum is displayed as 10000 Hz at the basal turn and 500 Hz at the helicotrema of the cochlea. The picture was modified from the book “Hals-, Nasen-, Ohrenheilkunde” of T. Lenarz and H. Boenninghaus, 2012 [72].

The bony cochlea is constructed like a snail and coils helical 2.5 times around its bony longitudinal axis, the modiolus, containing nerve fibers and blood vessels (Fig. 4). The coils are separated by the *lamina spiralis ossea* and the *ductus cochlearis* into three parts that are filled with perilymph: the *scala vestibuli* that is connected with the vestibule and *scala tympani* that is in connection with the round window and in-between both the *scala media*. *Scala tympani* and *scala vestibuli* are connected in the top of cochlea, the helicotrema. The base of the *scala media* is built by the basilar membrane. The membranous cochlea is built by the *ductus cochlearis* that is filled with endolymph. The upper wall of the *ductus cochlearis* is the Reissner's membrane that separates the ductus against the *scala vestibuli*. The lower wall of the *ductus cochlearis* is formed by the basilar membrane, which separates it from the *scala tympani*. On top of the basilar membrane, the organ of Corti is located. The organ of Corti contains the sensory epithelium for acoustic signals. It is formed by highly prismatic epithelial cells consisting of sensory and supporting cells, covered by the tectorial membrane, a gelatinous-like structure. The sensory cells are embedded in between the supporting cells and consist of one row of inner hair cells and three rows of outer hair cells.

The tectorial membrane is in contact with the sensory villi of the outer hair cells. The inner hair cells have 50-60 stereovilli whereas the outer hair cells have 60-120 stereocilia that are connected with the tectorial membrane. *Scala vestibuli* and *scala tympani* are forming the perilymphatic space that is filled with a sodium-rich fluid, the perilymph. *Scala media* is filled with a potassium-rich fluid, the endolymph.

### 1.2.3 The auditory system

The sound waves, meaning oscillations of sound pressure, are travelling through the outer ear canal and finally reach the tympanic membrane that is set in vibrations. The movements of the tympanic membrane are transmitted to the ossicles that function as vibrating masses and finally are transmitted into the perilymph by the stapes footplate. During the hearing process, the whole auditory system amplifies the incoming sound pressure on the way from the outer to the inner ear. The tympano-ossicular system plays a key role by intensifying the sound pressure first through the surface ratio between the tympanic membrane and stapes footplate within the oval window, the first being 16 times bigger than the second one. The second factor influencing the sound amplification is represented by the special anatomic structure of the ossicles generating a lever action. The construction of the handle of the malleus leads to 1.3 times higher leverage effect compared to the process of the ambos. Thereby, the force generated by the incoming sound waves, called sound pressure, is enhanced by the factor 22 from the tympanic membrane to the cochlea. Through this, the impedance mismatch of the ear is diminished, meaning that the sound waves are further transmitted into the perilymph rather than being reflected by hitting the liquid surface inside the cochlea that has a high impedance compared to the air. This effect is called impedance conversion transformation [72,104].

The incoming movements of the stapes lead to pressure waves inside the perilymph. The elastic round window membrane allows pressure compensation inside the cochlea. Because the walls of the *scala media* are not stiff, the *scala media* gets moved by these mechanical processes together with the Reissner's membrane and the basilar membrane. These vibrations within the basilar membrane spread in the form of a travelling wave in direction of the helicotrema. The increasing diameter of the basilar membrane, its elasticity properties, and the decreasing diameter of the cochlear duct leads to the special characteristics of the travelling wave: its amplitude is increasing to a maximum and then decreases very suddenly. Notably, the full characteristics of a travelling wave require active processes i.e., electromotility of the outer hair cells (see below). The place of the maximal amplitude of vibration is the region where the sensory cells are stimulated the most. Thereby, the oscillations are spatially spread inside the cochlea depending on their frequencies. The maximum of a travelling wave of a high frequency is placed near the stapes, the maximum of a travelling wave with a low frequency is placed near the helicotrema. The sound pressure wave induces a shear movement of the basilar membrane relative to the tectorial membrane and the sensory cilia get moved. This movement induces the conversion of mechanical energy into electrical signals, the so called mechano-electrical transduction. One of the key players in this mechanism is the difference in ion potentials between the endolymph that

is outside of the hair cells and the perilymph where the hair cells are embedded in. By the movement of the cilia, ion channels on the apical side of the hair cell membrane are opened leading to an influx of potassium ions. By this membrane depolarization, an influx of calcium ions is initiated, and in turn neurotransmitters are released into the synaptic cleft. This generates a series of action potentials that are further transmitted through nerve fibers. Tightly packed piezo-electric membrane proteins of the outer hair cells called prestin [139], enable them to respond mechanically as they contract and elongate in response to acoustic stimulation. These active processes lead to a reinforcement of the amplitude of the travelling waves and simultaneously damping of neighbored basilar membrane sections. This cochlear amplifier mechanism allows the inner hair cells to react to very low acoustic stimuli. Furthermore, these active processes build the fundamental basis for the generation of otoacoustic emissions. By the induced movements of the perilymph, the sound conduction can be reversed and travels back through the ossicular chain and the tympanic membrane. This sound can be detected as acoustic signals, the otoacoustic emissions, inside the outer ear canal.

### 1.3 Pathologies of the ear

Pathologies of the ear may originate from different causes. Depending on their concrete forms, pathologies of the ear can influence the hearing function in a critical manner. In the following, pathologies of the outer, middle, and inner ear are described and how their characteristics could influence the hearing function.

#### 1.3.1 Pathologies of the outer ear

Pathologies of the outer ear involve anomalies and malformations, non-infectious processes like injuries or hematomas, inflammations, and tumors. Besides the cosmetic consequences, these processes may also influence the hearing of the patient, in special in the case of pathologies of the ear canal or when the middle or inner ear are affected as well. Aural-atresia for example, is the absence of a patent ear canal that may be acquired or congenital. To treat this pathology, an operative treatment to rebuild the outer ear canal is performed. In parallel, the conductive hearing loss should be treated through a middle ear implant or a bone-anchored hearing aid to enhance the life quality of the patient.

#### 1.3.2 Pathologies of the middle ear

Pathologies of the middle ear can be divided into injuries, dysfunctions of the auditory tube, inflammatory processes, facial nerve paresis, tumors of the petrosal bone and otosclerosis. The most important part of middle ear pathologies that will be discussed in this thesis are injuries of the middle ear, especially injuries of the tympanic membrane (TM).

TM injuries are distinguished into directly and indirectly caused injuries. Directly caused TM injuries include impalement lesions, caused by e.g., matchsticks or Q-tips, inclusions of hot metal drops during welding, the breakdown of scars during rinsing of the ear or scuba diving, and combustions or acid

burns. Indirectly caused TM injuries are caused by rapid changes in the air pressure e.g., during explosions, a hit on the ear, or hitting a water surface with the head. Worldwide, TM perforations (TMPs) have different leading causes. In China and Nigeria, they are mostly caused by a hit on the ear [4,21,75]. In the US, they are also mostly caused by ear slaps, followed by accidents during water sports and injuries caused by cotton swabs [41]. In Germany, hits on the ear seem to be the most prominent cause of TM perforations as well, followed by injuries caused by cotton swabs and again, accidents during water sports [65]. Regarding the position and size of perforations, it must be distinguished into central, mesotympanic and epitympanic TM defects. Central TM perforations are located in the *pars tensa* are round- or kidney-shaped and have different dimensions. They don't affect the *annulus fibrosus* (Fig. 5a). The *pars flaccida* is only rarely affected by TM perforations.

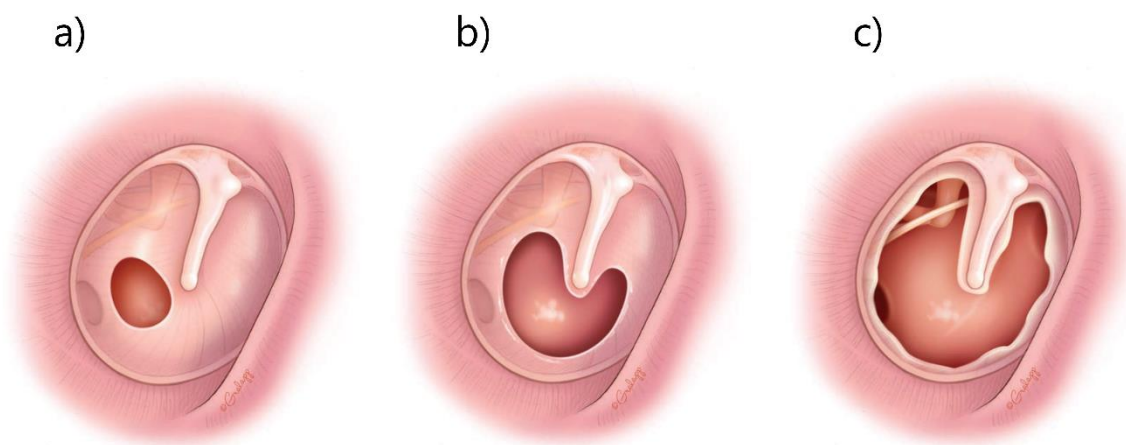


Fig. 5: Perforations of the tympanic membrane in different extents. a) Posterior central tympanic membrane perforation without affecting the annulus fibrosus. b) Typical “kidney bean shaped” central tympanic membrane perforation often occurring during chronic otitis media. c) Near-total tympanic membrane perforation with a small remaining rim at the annulus. The image was modified from: Robert K. Jackler.; Ear Surgery Illustrated: A Comprehensive Atlas of Otologic Microsurgical Techniques, 2019 [54].

TM injuries are a severe health problem because of the complications that may come along with them. Thereby, infections of the middle ear, injuries, or dislocations of the ossicular chain, hearing loss, and tinnitus may occur [81]. If the oval window or the medial wall of the tympanic cavity is affected by the injury, the cochlea is opened and affected. If pathogenic germs enter the middle ear during a TM perforation (TMP), an infection, the acute otitis media, may occur. This infection leads to a protrusion of the TM and to an outflow of secretion from the middle ear into the outer ear canal. If infections are recurrent, they may lead to chronic otitis media. One typical clinical characteristic of the chronic otitis media is the persistent perforation of the TM that is centrally located in the *pars tensa* and has a round, oval, or kidney-shaped form, which does not affect the *annulus fibrosus*, also (Fig. 5 b). A more severe form of chronic otitis media is chronic suppurative osteitis, whereas the inflammation affects the neighbored bone leading to severe complications if it is not treated adequately. Another severe complication of TM perforation is the formation of cholesteatoma, a tumorous formation that consists

of desquamated, devital epithelial cell masses that are layered in an onion-shell form, surrounded by a layer of squamous epithelium and an inflammatory perimatrix. The ongoing inflammatory stimulus in cholesteatoma leads to the degradation of the surrounded bone. The cholesteatoma rises from a TM perforation in the *pars tensa* when squamous epithelia cells protrude from the outer ear canal into the epitympanum. There are also other forms of cholesteatoma that have different causes, but all together form a severe possibly life-endangering health issue that must be treated surgically.

Besides the infectious risks of TMPs, an injury of the eardrum also causes direct impairment of the auditory function. Due to the perforation of the TM, the amplification factor of the sound pressure reaching the stapes is reduced causing a conductive hearing loss. The amount of hearing loss is thereby strictly dependent on the size of the perforation and not reported to be greater than 50 dB [79,94,97,123–125]. Some studies reported trends of differences in the amount of hearing loss depending on the site of the perforation that was mostly not statistically significant. Thereby, some authors stated that the conductive hearing loss would be increased, if the perforation was located in the posterior half of the TM when compared to the anterior half of the TM [34,79,94,97]. In the late 80's, Griffin made a proposal dividing TM perforations into four different grades in regard to their size: grade I affecting 25 % or less of the *pars tensa*, grade II with 25 to 50 % perforated proportions or multiple perforations in two quadrants, grade III from 50 to 75 % or three quadrants affected by multiple perforations and grade IV with 75 to 100 % perforation [41]. Already at that time, the observation was made, that bigger perforations were less likely to heal spontaneously, a fact that is still actual today. Nevertheless, the therapy of TM perforations is not standardized yet. For small perforations, most authors propose to follow observant therapeutic management, as small perforations show a good spontaneous healing rate of around 80 % [3,47,90,103,131]. On the other hand, treatment of larger perforations is performed quite differently and is also dependent on the patient's level of suffering. If for example, a conductive hearing loss is induced by the perforation, covering of the perforation may lead directly to an improvement in hearing function [6,91]. In acutely induced perforations, sterile covering with a silicone foil is used in the clinical daily routine. The silicone foil thereby functions as a seeming material to cover the perforation and to protect the middle ear. The silicone foil is positioned over the TM perforation under local anesthesia and kept in position by packing the outer ear canal with cotton. If TM perforations do not heal properly spontaneously or are recurrent, they are called chronic. Such chronic TM perforations have a prevalence of 0 to 2.3 %, dependent on the geographic distribution [15,57,101,115] and must be further treated surgically. This is mostly recommended if perforations don't heal within 3-6 months and if the perforation is associated with a significant conductive hearing loss, recurrent drainage, desire to participate in water activities, and wearing hearing aids [22,91].

The surgical treatment, called tympanoplasty, must be considered also if the ossicular chain is affected by the perforation. This operation at the sound conduction apparatus has the goal to restore the hearing of the patient. The easiest way to perform a tympanoplasty is a type I operation, also named myringoplasty. Type I tympanoplasties aim to restore the function of the tympanic membrane and are

indicated if the membrane has a defect not affecting the ossicular chain. During this surgery, the injury in the TM is relined with autologous material e.g., fascia, perichondrium, or cartilage. Type II tympanoplasty is the reconstruction of a new tympanic membrane and of an interruption in the ossicular chain in cases of a perforation of tympanic membrane with an erosion of the malleus or part of the incus. Another possibility is to perform a type III tympanoplasty that is indicated when the ossicular chain is defect up to the stapes (IIIA) and including the stapes (IIIB). Thereby, the sound pressure is directly transferred from the TM to the inner ear by including an autogenous part of the incus or a prosthesis (titanium or other materials) between the TM and the maintained stapes. In type IV and V tympanoplasties, no sound pressure transfer over the ossicular chain is possible anymore. To sum up, type I-III aim to restore the sound-transfer component of the hearing impairment while tympanoplasties type IV and V do not allow sound pressure transformation anymore. In these last cases the patient has a hearing impairment after surgery of at least 25 dB. Other middle ear pathologies will not be addressed in this thesis.

#### *1.3.2.1 Graft materials for the treatment of eardrum perforations*

Materials used for eardrum perforation treatment involve a wide range of grafts that could be broadly divided into autologous and non-autologous materials. Dependent on the type and size of the perforation, different materials are used. After acute perforations, the covering of the perforation using paper or silicone patches is an approved direct treatment. If larger perforations or persistent perforations are presented, surgery treatments are needed using autologous materials, like fat, fascia, cartilage, or perichondrium. The use of temporal fascia or perichondrium remains the gold standard in clinical usage. However, autologous materials have some disadvantages such as requiring an incisional harvest from the patient, structural properties that are not optimal for the membrane reconstruction, and eventually structural defects that can subsequently lead to weakness, retraction, and re-perforation [37]. Patching with paper is thought to be the most established method historically as it is inexpensive, easy to obtain and simply applied [17,39,110]. Paper patch, like other implant materials, functions as a scaffold material for the wound closure of the TM but also brings some drawbacks as easy detachment, non-resistance to infections, stiffness, or non-transparency [37,52]. Also, surgical techniques and known graft materials have some drawbacks, like i) the high cost of the operation, ii) the need for general anesthesia with all its general risks, and iii) the eventual need for a further incision for harvesting of the autologous graft material [69]. Therefore, the scientific community is aiming to find new materials and technologies for the treatment of TM perforations.

One evolving technology is tissue engineering that uses patient-specific scaffold materials for the treatment of TMPs. As scaffold material mostly serve decellularized tissues and polymers. Decellularized tissues are obtained after the cell removal of allografts and xenografts and preserve most of the biological and mechanical properties of the original extracellular matrix (ECM) [122]. As decellularized templates for TMP repair, for example, urinary bladder matrix was used [95]. Other studies involve dermis or dura mater as ECM scaffolds [23] or even commercial forms of decellularized

dermal tissue in the form of AlloDerm® that was successfully used in the chinchilla model of acute TMPs [43,78].

Polymers, on the other hand, have the advantage of being easy to be changed in their size, shape, porosity and thereby are easier to be produced so that they fit their future application. They are biocompatible and biodegradable, easy to synthesize and handle, and can be produced on a large-scale basis. Their degradation and mechanical properties can be easily controlled [122]. Polymers that are used in the closure of TMP's are e.g., Gelfoam®, silk fibroin, or chitosan as polymers of biological origin and synthetic materials like Polyglycerol sebacate (PGS). Mota et al. 2015 presented biomimetic scaffold substrates consisting of two copolymers: poly (lactic-co-glycolic) acid (PLGA) plus a random block copolymer of poly (ethylene oxide terephthalate) and poly (butylene terephthalate) (PEOT/ PBT) produced by electrospinning in different conformations. They found that their scaffold constructs had no negative effect on cell viability, cellularity, and protein content in cell culture experiments with human mesenchymal stem cells (MSCs) [84]. In another study, further polymers were successfully used for the treatment of TMPs such as e.g., Gelfoam®, Epifilm® or crosslinked thiolated chondroitin sulfate in the guinea pig model [96].

Silicone has also been reported in literature to be an affordable patching material [14,48]. Branica et al. described it as being an interesting patching material by improving the healing, reducing the possibility of ear infections in blast injury cases, and slightly improving hearing abilities in small and medium TMPs. Hempel et al. concluded that, although the success rate of myringoplasty was 88.9 %, the best therapy for traumatic TMPs (TTMPs) is still controversial, especially because of a lack of systematic and standardized documentation of perforation size. Furthermore, all the above-mentioned grafting materials for TM repair need to be kept in position during the healing time, mostly achieved by packing of the ear canal, a very threatening procedure for the patient. To avoid this procedure, patching with adhesive materials, such as Steri-strips was also considered. The advantage of using adhesive material is to avoid repeated placements of the patching material, such as needed when e.g., paper patches were used. Aslan et al. 2011 reported that all their patients treated with Steri-strip patching immediately noticed a hearing improvement directly after treatment. The healing rate in this study was around 90 % two months after the treatment [6]. Another group compared Steri-strips patching with paper patching and observational therapy. They reported a decrease in the need for repeated procedures and shorter healing times in the Steri-Strip group compared with the observation group that was not patched. Nevertheless, the group around Park et al. demonstrated an increased rate of otorrhea in the Steri-Strips group and there was no difference in hearing improvement between the three treatment groups after three months [98].

Another promising material to be used in TMP treatment is poly-(dimethyl) siloxane (PDMS). PDMS is a silicone elastomer with spacious usages as skin adhesives [7,18,26,55,67]. It offers great potential for the application as wound dressings as it is biocompatible, physiological inert, and has good mechanical properties [1,74,87]. PDMS material is also investigated to be suitable for use in cochlear

implants [2,135] and is analyzed as a novel material to be used for the treatment of TMPs [28,63]. Farhadi et al. proved PDMS patches, in combination with immobilized collagen, as useful to treat small TMPs in a clinical study and reported a healing rate of 70 % [28]. Nevertheless, the PDMS patches had to be fixed on the TM by using Gelfoam®, leading to a conductive hearing loss in treated patients. To combine the advantages of adhesive patching materials with a biocompatible silicone material, avoiding the need for chemical fixing agents and mechanical fixation by packing of the outer ear canal, self-adhesive PDMS-composite films consisting of PDMS and one subclass of it, soft skin adhesives (SSAs) were proposed as a novel patching material for the application on the TM (Fig. 6). SSAs adhere to rough surfaces including wet skin, reveal a high water vapor permeability, and good compatibility with pharmaceutical compounds [7,31,55].



Fig. 6: Schematic drawing of the application of a self-adhesive transparent PDMS patch on a central perforation of the human tympanic membrane. © INM Leibniz Institute for New Materials

The SSAs allow gentle attachment and detachment, combining a secure adhesion to the thin membrane and an atraumatic removal. Composite films of SSAs and Sylgard 184, two elastomeric silicone materials, demonstrated to be well applicable on the murine tympanic membrane and showed strong adhesion in peel-tests [13].

One drawback of using silicone materials as wound dressings is the high hydrophobicity of the material, hindering cellular spreading and adhesion, one major factor regarding the healing of the tympanic membrane. The functionalization of the elastomer surface is however one possibility to enhance their cellular compatibility. Boyadzhieva and coworkers evaluated the physical adsorption of proteins to this adhesive and showed promising results combining the adhesion of synthetic material and scaffolding abilities through functionalization for a novel material for the treatment of TMPs [12,13,31].

### 1.3.3 Pathologies of the inner ear

Pathologies affecting the inner ear can be as well, inflammations, injuries, or tumors. Additionally cochlear and vestibular pathologies are the most important pathologies to be mentioned here, as well as acoustic trauma, presbycusis and other hearing disorders. One cochlear pathology is acoustic trauma, a damage and possible degeneration of hair cells and other structures in the organ of Corti, caused by blasts, explosions, noise, or blunt traumas of the skull. The acoustic trauma leads to a temporary or permanent threshold shift (TTS/ PTS) due to the damage of high sound pressure levels that can be fully repaired (TTS) or not (PTS). This acoustic trauma leads to metabolic disorders and direct mechanical destruction of the hair cells. Once degenerated, hair cells are not able to recover. The combination of duration and level of the acoustic trauma determines the type of trauma. A short, acute damage is called blast trauma. Usually, the hearing impairment of a blast trauma does not proceed. A longer acoustic over exposure induces a burst trauma that often comes along with TM perforations and or luxation of the ossicular chain. These patients suffer from a combined conductive hearing impairment with sensorineural hearing loss.

Another cochlear pathology is the presbycusis or age-related hearing loss caused by age-related physiological and pathological degenerative processes mostly in the organ of Corti. These processes are often caused by extended exposures to several exogenous and endogenous factors like noise, cardiovascular problems, ototoxic substances, nutrition, and diabetes. Furthermore, the degenerative processes in the brain that come with age comprise another factor that play a role in presbycusis. Patients who suffer from presbycusis demonstrate a sensorineural hearing loss on both sides, especially in the higher frequency range. Those patients have problems communicating in a noisy environment and if various people are involved in the communication, like at conferences or parties. Some patients also suffer from tinnitus in quiet surroundings. In these cases, hearing aids, or in severe forms cochlear implants, are used to compensate the age-related hearing loss.

Another pathology of the inner ear are toxic injuries, also known as ototoxicity. Several infectious diseases like influenza, mumps, or meningitis, metabolic disorders, ototoxic drugs e.g., aminoglycoside antibiotics, the use of ototoxic substances in ear drops during a TM perforation, and the exposure to industrial products like cadmium, hydrogen cyanide and its salts, and chemical solvents, e.g., toluene and xylene cause ototoxicity. Ototoxic substances and infections cause non-reparable damage to the hair cells in the inner ear, leading to an ongoing hearing disorder, reaching finally the state of deafness,

dizziness, and tinnitus. The patients are diagnosed with a sensorial hearing loss of different extents, mostly on both ears.

Additional to the inner ear pathologies that are gained during adulthood or with age, there are several forms of hearing disorders that are congenital or acquired in early childhood. These forms are very critical for the development of young patients because good hearing is necessary for speech development. Thus, it is very important to check for hearing impairment already in newborns. In these early forms, it must be distinguished between hereditary and acquired forms of hearing impairment. The cause of hereditary forms are mutations in the genetic code, causing errors during encoding of proteins responsible for specific cellular functions, like connexin 26 or myosin VII. Acquired forms of hearing impairment can occur prenatally, perinatally, or postnatally. Infectious diseases e.g., virus infections, trauma during birth, or metabolic diseases of the mother play the major role in these cases.

#### *1.3.3.1 Hearing aids*

Hearing aids aim to treat the hearing impairment symptomatically. They need to compensate the hearing loss in a range to enhance the patient's speech understanding sufficiently so that daily communication needs are satisfied. Hearing aids collect the sound from the environment using a microphone and enhance the signal that is then transferred to the hearing system of the patient. Normally, the signal is transferred into the outer ear canal, on the skull bone, directly onto the ossicles, or into the inner ear. There exist several types of hearing aids; the most important are air conduction systems, bone conduction hearing aids, and implantable as well as partially implantable hearing devices.

Air conduction systems use an electro-acoustic converter as a small speaker that transmits the sound into the outer ear canal and to the TM. For patients with more severe hearing loss, the outer ear canal must be sealed by an ear mold. There exist two different types of air conduction hearing aids, behind the ear and in-ear hearing aids. They are used for mild to severe sensorineural hearing loss, as well as for conductive- or combined hearing loss if the outer ear canal is functional.

Bone conduction hearing aids transfer the target signal directly onto bone and can be divided into transcutaneous, and percutaneous systems. The signal is transferred onto the bone of the skull mostly onto the mastoid. These systems are used for treating conductive hearing loss that cannot be treated sufficiently through surgery e.g., malformation or acquired occlusion of the outer ear canal, chronic secretion from the ear due to chronic otitis externa or media.

Furthermore, implantable hearing aids may help patients with sensorineural hearing loss that cannot be treated with air conduction systems. Implantable hearing devices transform the sound signal into electrical voltage variations that move an electromagnetic or piezoelectric transducer attached to the ossicular chain or at the inner ear. Thereby, the ossicular chain or the inner ear is set into vibrations directly by mechanical stimulation. Besides the advantages that hearing devices help hearing-impaired people to better hear, communicate and improve their quality of life they also have some disadvantages that can lead to a poor compliance. These include e.g., feedback noise that occurs when the ear canal is not sealed perfectly by the ear mold, the occlusion effect of the outer ear canal by the shielding of deeper

frequencies as well as recurring ear canal inflammations leading to the impossibility to wear the hearing device. Furthermore, hearing aids may have an inadequate sound quality due to distortions of the microphone and resonances inside of the ear canal. Finally, hearing aids directly show the patient's problem of hearing impairment to the public.

When patients suffer from a hearing loss that originates from damage in the inner ear, affecting hair cell functions, a cochlear implant may be used. Cochlear implants are electronic hearing prostheses that replace the function of the inner ear. They short-cut the function of non-functional hair cells by sound-driven electrical excitation of peripheral dendrites of auditory nerve cells. Cochlear implants are high-technology products consisting of an externally worn speech processor coupled to a microphone for sound collection and an auditory processor that is responsible for transducing the transferred auditory information into a digital signal, which in turn is processed and encoded into a radio frequency signal. The resultant radio frequency signal is sent to the implanted receiver where it is decoded and converted into electrical signals that are transmitted to the electrode carrier responsible for the stimulation of the cochlea. The electrodes, which are positioned at certain distances in the *scala tympani* stimulate nearby peripheral dendrites of spiral ganglion cells the axons of which form the auditory nerve. Cochlear implants are indicated for patients with bilateral or unilateral sensorineural hearing loss up to deafness with no sufficient benefit from amplification using conventional hearing devices, bone conduction hearing aids or active middle ear implants.

All these therapies are however not suitable to sufficiently treat every patient with hearing loss. Studies on the prevalence of hearing aid use reported that only 14-24 % of people with hearing loss use a hearing aid in the US [19], and around 30 % in Europe [102]. These low numbers of hearing aid acceptance have different reasons. In a survey from 2004, the according hearing aid refusers, stated as reasons for not wearing a hearing experiences with issues in performance, disappointing results and poor reliability of hearing aid use [62]. In Europe, people stated as the main reason for the non-adoption of hearing aids, that they think, they hear well enough. Another reason is the belief of people, that hearing aids were uncomfortable [102]. In general, the overall satisfaction for hearing aid users with their devices ranges from 72 to 86 %. Notably those users who acquired their hearing aid in the past four years, were more satisfied with their hearing aid than others. Thereby, the level of satisfaction strongly depends on the performance of the hearing devices in different listening conditions. The performance of hearing devices in easy-listening situations, like a conversation with one person or within small groups, watching TV and leisure activities is sufficient to good, whereas challenges remain in more complex situations such as conversations in large groups, the use in a noisy environment and on the telephone [102]. Taken together, factors like the sound quality, speech clarity, easy and comfortable wearing, the amount of background noise and the user expectations about the use of hearing aids are important points in the decision of using hearing aids or not [11]. Given, that hearing aids treat hearing loss only symptomatically by improving the audibility of sound by amplification rather than restoring the hearing function to normal, these factors require further research in and optimization of hearing devices.

### 1.3.3.2 *Optical stimulation as an alternative method for hard of hearing people*

Recently, to improve the quality of auditory devices, alternative stimulation methods to classical acoustic or electric stimulation have been proposed. One of them, optoacoustic stimulation, uses light energy instead of mechanical or electrical energy to activate the hearing system. The optoacoustic stimulation works based on the optoacoustic effect. Here, short light pulses irradiating the surface of a medium, e.g., the tympanic membrane, ossicles, or the round window membrane are absorbed and induce a periodic thermal expansion and relaxation of the medium thus creating a sound source [56].

The idea to use light as a sound source was created by Alexander Graham Bell in the 1880's. His idea was to build a "Photophone"- an apparatus to allow communication by the conversion of sunlight into hearable sounds. His successful demonstration of a tube placed on the ear, catching a sunlight beam that was interrupted periodically, leading to "a clear musical tone" that was heard, was the first demonstration of the optoacoustic effect detected by human ears [9]. Since optoacoustic stimulation could be applied on every vibratory stimulation target of the peripheral hearing system, it has the potential to be used for a new generation of auditory prostheses [111,112,129,138].

The first report on optoacoustic stimulation of the inner ear was published by Fridberger and Ren in 2006. They used a 1.3 W diode laser to stimulate the organ of Corti of gerbils and guinea pigs with pulsed laser light and recorded light-induced basilar membrane vibrations as well as the activation of the hearing system by electrophysiological recordings of cochlear microphonics. They even recorded nerve activities in response to application of the laser on the middle ear (the ossicles and bulla) but classified the recorded signals as artefacts [33]. In a study from 2009, Wenzel and colleagues demonstrated, that optoacoustic stimulation with laser light of 532 nm wavelength activated the hearing system in guinea pigs when applied on the round window membrane of guinea pigs and thereby induced optically evoked auditory brainstem responses (oABR), which resembled in shape and amplitude the acoustical reference waves and moreover were tunable in their amplitude by adjusting the applied laser pulse energy [129]. In the same year, the optoacoustic stimulation could also be proven to induce vibrations of the basilar membrane by using two different wavelengths of 355 and 532 nm, whereas the laser light was applied on the osseous spiral lamina [136]. Later, Schultz et al. demonstrated the stimulation of the inner ear in guinea pigs with nanosecond pulses at different wavelengths. By applying the laser fiber outside the cochlea in front of the round window membrane or intracochlear within the *scala tympani* they recorded cochlear responses to optical stimulation as compound action potentials (CAPs). Similar to the amplitudes of the oABR recordings, CAP amplitudes increased with rising laser intensities, and with slopes that depended on the wavelengths used [106]. Another study demonstrated the optoacoustic effect to be responsible for laser-induced cochlear responses by assessing CAP amplitudes as a function of i) constant pulse energy, ii) constant peak power, iii) wavelength and iv) the absorption coefficient by using two different laser systems, one with a tunable wavelength and one with a fixed wavelength of 1860 nm [58].

Recently, our group has demonstrated, that our stimulation with pulsed green laser light placed in the peripheral hearing system of guinea pigs induced vibrations of the eardrum and in parallel activated the hearing system in a frequency-specific manner. The activation of the hearing system has been proven by stimulation of different loci in the peripheral hearing system: the umbo at the TM, the round window membrane, and the otic capsule. The frequency-specific activation of the hearing system was determined by recordings of neural activities in the inferior colliculus (ICC). In parallel, the results were validated by vibration measurements at the umbo by using different target frequencies, named laser modulation rates (LMRs) and different laser pulse rates (LPRs). All results were also in good agreement with modeled data [114]. Furthermore, we recently demonstrated, that the magnitude of optoacoustically induced vibrations of the guinea pig's tympanic membrane strongly depend on the laser wavelength used. We assume that TM tissues have specific absorption characteristics for different wavelengths [45].

## 2 Results

### 2.1 Biocompatibility margins for optical stimulation at the eardrum via 532 nm laser pulses (Appendix 1)

The aim of this work was to define safety margins for our stimulation strategy at the eardrum while using 10 ns laser pulses of a laser with a wavelength of 532 nm and a laser repetition rate of 50 kHz. The eardrum of anesthetized mice was irradiated for two minutes with different average laser powers and the eardrums were examined three hours after irradiation as *ex vivo* whole mount specimens. For this purpose, I transferred a fluorescence-based viability staining known from cell culture (see Appendix 2, work from Lukas Pillong) to the mouse model. To gain information about the viability of the murine tympanic membrane after irradiation, I established a surgery method to dissect the membrane, spanned over the *annulus fibrosus* with the surrounding bone of the tympanic bulla as whole-mount specimens and used fluorescence-microscopy to detect healthy, apoptotic, and necrotic cells in irradiated TM specimens and the related controls. The results of the fluorescence staining demonstrated that from 89 mW average laser power onwards, areas of necrotic cells resulted from the irradiation at the umbo and the *pars tensa* that grew in their size with increasing laser power (Appendix 1, Fig. 2). Interestingly, the proportions of areas with necrotic cells grew from 0 to 19.5 % of the total area of the TM after irradiation at the umbo and from 0 to 6.4 % after the irradiation at the *pars tensa* (Appendix 1, Fig. 3). On the electrophysiological level, the effect of the laser irradiation was evaluated by using recordings of auditory brainstem responses (ABR) before and after the irradiation in anesthetized mice. First, we determined the hearing thresholds in all mice, after irradiation at the umbo and at the *pars tensa*, as well as in negative control mice. The hearing thresholds were determined as the lowest intensity where the Jewett complex was clearly identifiable (Appendix 1, Fig. 4). The electrophysiological monitoring demonstrated no significant changes in the hearing thresholds after irradiation in all groups. The negative control mice did not demonstrate any change in thresholds, also (Appendix 1, Fig. 5).

A more detailed analysis of amplitude and latency values of wave I at threshold, as well as 10, 20, and 30 dB above, brought the following results: after irradiation at the umbo, no significant changes in amplitude values occurred (Appendix 1, Fig. 6a). Notable, there was a tendency for higher amplitude values after irradiation with 125 mW average laser power. After irradiation at the *pars tensa*, all amplitude values were slightly higher after irradiation in comparison to before (Appendix 1, Fig. 6b). This fact was again the most obvious after irradiation with 125 mW. The analysis of latency demonstrated some significant changes, e.g., a decrease of ca. 0.01 ms at +10 dB over threshold after irradiation with 50 mW (Appendix 1, Fig. 7a, column 2) or an increase of ca. 0.09 ms at +0 to +20 dB over threshold after irradiation with 99 mW at the umbo (Appendix 1, Fig. 7a, column 4). Despite the value at +30 dB over threshold in latency analysis, the negative control demonstrated no significant

changes in amplitude or latency values (Appendix 1, Fig. 7, column 1). After the irradiation at the *pars tensa*, no significant changes in latency values could be observed at all laser power levels (Appendix 1, Fig. 7b). Further analysis of frequency-specific ABR thresholds (fABR) demonstrated no significant changes of the irradiation (Appendix 1, Fig. 8). To evaluate whether an incubation time of three hours in anesthesia before the fluorescence staining influences the hearing function, we performed a further control experiment in mice irradiated with 125 mW at the umbo and analyzed their hearing function before (pre), directly after (post1) and three hours after the laser irradiation (post2). The analysis of this control experiment demonstrated no significant changes in their hearing thresholds, amplitudes, latencies of frequency-specific thresholds, although hearing threshold, amplitude and latency values showed a trend for higher values after three hours of incubation (Appendix 1, Fig. 9).

## 2.2 Cytotoxicity studies of an optoacoustic stimulation strategy for the development of laser-based hearing aids (Appendix 2)

To examine the effects of optoacoustic stimulation on the cellular level, we designed a protocol that would allow us to assess cytotoxicity and cellular viability on three different primary cell lines: human dermal fibroblasts (NHDF), human chondrocytes (HCH), and human osteoblasts (HOB). These cell types were used as representatives for cell types existing in the hearing system to represent natural conditions as closely as possible. The cells were seeded on glass-bottom cell culture plates and irradiated with our stimulation protocol (Appendix 2, Fig. 1) that was also used in the mouse model. After the irradiation, the following assays were performed: i) fluorescence staining of healthy, apoptotic, and necrotic cells, ii) lactate dehydrogenase (LDH) assay, iii) water-soluble tetrazolium salt-1 (WST-1) assay and iv) quantitative polymerase chain reaction (qPCR) analysis (RT<sup>2</sup> Profiler™ PCR Array). The fluorescence assay demonstrated different irradiation thresholds for the three different cell lines. For fibroblasts, no significant effects on cellular viability, marked by circular areas of necrotic cells, could be observed for laser powers up to 223 mW (Appendix 2, Fig. 4a, second column). For chondrocytes, this threshold appeared between 223 mW and 250 mW (Appendix 2, Fig. 4b, second column) and for osteoblasts, first effects could be observed at 285 mW (Appendix 2, Fig. 4c, second column). For laser powers exceeding 250 mW, the LDH assay demonstrated significant increases in the cytotoxic response of fibroblasts in the irradiated group in comparison to the non-irradiated control group. Thereby, the cytotoxicity of ca. 1.8 % at 250 mW increased to around 10.4 % at 500 mW (Appendix 2, Fig. 5a). For chondrocytes, the cytotoxic effects could be observed first after irradiation with 281 mW with a significant cytotoxicity of ca. 2 % that increased with rising laser power (Appendix 2, Fig. 5b). The LDH release in osteoblasts was significantly higher after irradiation of 315 mW laser power in comparison to the control group, increasing as well with higher laser power (Appendix 2, Fig. 5c). The irradiation with 199 mW had no significant effect on the viability of fibroblasts as measured by the WST-1 cell viability assay. After irradiation with 223 mW and 500 mW, however, viability was

significantly decreased by 4.2 % and 18.5 % respectively (Appendix 2, Fig. 6a). In chondrocytes, irradiation with 354 mW decreased the viability significantly by 10.9 %, similar as irradiation with 397 mW (to 11.1 %, Appendix 2, Fig. 6b). In osteoblasts, a significant decrease in viability was observed after irradiation with 281 mW of ca. 4.6 % (Appendix 2, Fig. 6c).

To investigate the effects of the irradiation on the cellular regulatory level, we performed qPCR analysis of genes involved in cytotoxicity and cell stress response. Therefore, cells were irradiated with parameters below and above each cytotoxicity level and ran qPCR arrays analyzing 84 key player genes in parallel. For fibroblasts, we found 21 genes upregulated after irradiation with 500 mW that derived from different pathways, like DNA-damage response (GADD45A, XPC, NBN, and CDKN1A), oxidative stress (FTH1, SQSTM1, and TXNRD1), heat shock response, inflammatory response, hypoxia, and autophagy (Appendix 2, Fig. 7a). We could not find any significantly downregulated genes in this panel. After irradiation with 199 mW, only one gene was found to be upregulated: GADD45A (Appendix 2, Fig. 7b). In chondrocytes, we found genes from the heat shock response, unfolded protein response, DNA-damage and hypoxia signaling pathway significantly upregulated after irradiation with 500 mW (Appendix 2, Fig. 7c). The irradiation with lower levels did not lead to any significant up- or downregulation (Appendix 2, Fig. 7d). In osteoblasts, the irradiation with 500 mW induced an upregulation of genes related to osmotic stress, heat shock protein (HSP) response/ unfolded protein response, autophagy, cell cycle arrest and DNA-repair pathway (Appendix 2, Fig. 7e). Here, the irradiation with 199 mW induced an upregulation of TLR4 and a downregulation of IFNG, two genes that are linked to inflammatory response pathways (Appendix 2, Fig. 7f).

### 2.3 Optoacoustic stimulation efficiency can be improved using an absorbing film (Appendix 3)

To assess whether the optoacoustic stimulation could be used in the mouse model as well, we established the recording of optoacoustically induced ABR (oABR) waves in mice. The resulting wave I amplitudes were analyzed and the effectiveness of optical stimulation versus acoustic stimulation by click-ABR (aABR) was compared. To gain a higher efficiency of the optical stimulation, we tested whether an absorbing layer positioned on the TM, enhanced the resulting ABR waves. We assessed the effects of poly (dimethyl) siloxane (PDMS) patches for this purpose (Appendix 3, Fig. 1). These patches were self-adhesive and similarly designed to treat TM perforations (Appendix 4). The absorbing patches were further optimized using a reflective Ag layer and an absorbing layer on top (Appendix 3, Fig. 2b) and were positioned centrally over the umbo, the soft skin adhesive layer in tight contact to the TM and the absorbing layer facing the outer ear canal (Appendix 3, Fig. 1b). The analysis of the transmission and absorbance of the patches demonstrated a plateau of approximately 94 % transmission above 300 nm, being 93.72 % at 532 nm, whereas the absorbing structure demonstrated a constantly low transmission, with 0.24 % at 532 nm (Appendix 3, Fig. 3a).

The absorbance of the patches was calculated as  $Abs = \log(1/T)$  whereas  $T$ =transmission, and was at 532 nm 2.574 for the absorbing patch and 0.028 for the control film (Appendix 3, Fig. 3b).

We compared the resulting ABR waves between i) irradiation at the native TM without any patch, ii) using a non-absorbing patch and iii) using an absorbing patch between the laser modulation rates (LMRs) of 1, 8 and 10 kHz from 2 to 79 mW average laser power with 50 kHz laser pulse rate (LPR). Thereby we were able to reproducibly record signals that resembled in their shape acoustically induced waves (Appendix 3, Fig. 4). It was striking that oABR waves had significantly lower amplitudes compared to aABR when the irradiation was performed on the native TM (Appendix 3, Fig. 4a) or using a non-absorbing patch (Appendix 3, Fig. 4b). However, using an absorbing patch on the TM, the oABR wave amplitudes were considerably higher and resembled the ones recorded for 80 dB SPL acoustical stimulation (Appendix 3, Fig. 4c).

To analyze the efficiency of the optical stimulation in more detail, we analyzed wave I amplitude of oABR waves between 2-79 mW average laser power and compared the results to aABR from 0-80 dB SPL (Appendix 3, Fig. 5). The irradiation at the native TM led to a nearly linear growth of wave I within the applied laser power levels (Appendix 3, Fig. 5a top row, left three panels). In contrast, using a non-absorbing film reduced the resulting amplitude values to ~ 33 % (Appendix 3, Fig. 5b middle row). Finally, applying an absorbing patch, the amplitude values at 79 mW were demonstrated to be 6.8, 4, and 3.5 times higher for LMR of 1, 8, and 10 kHz respectively, compared to the stimulation at the native TM (Appendix 3, Fig. 5c bottom row). To analyze the effect of the patch application itself on the hearing function of mice, we analyzed click-ABR data of wave I amplitude before and after patch application between 0 and 80 dB SPL stimulation and found significantly lower amplitude values at all sound pressure levels. Especially between 30 and 60 dB SPL, the amplitude values were highly significantly lower after patch application (Appendix 3, Fig. 6). To take this effect into account, we further normalized wave I amplitude to the results obtained after acoustical stimulation with 80 dB SPL with as well as without patch (Appendix 3, Fig. 7). Thereby, we found that the amplitude values normalized to aABR with patch demonstrated slightly higher amplitudes and smaller error bars at 80 dB SPL in comparison to the aABR amplitudes recorded without a patch. Nevertheless, the difference between both normalization methods was less than 5 %. The normalization of the data resulted in amplitude values of around 60 % of the aABR amplitude level at 80 dB SPL for 1 kHz LMR (Appendix 3, Fig. 7 left column), and 50 % with 8 and 10 kHz LMR (Appendix 3, Fig. 7, middle and right column). To simulate the theoretical laser power that would be necessary to induce higher levels of equivalent acoustic stimulation, the averaged oABR and aABR amplitudes of both groups, with absorbing film and irradiation at the native TM, were fitted and set equal. The result of the fitting process were input-output (IO) functions with the resulting dB SPL level as a function of laser power (mW). Thereby, we demonstrated the dynamic range of the IO function of the absorbing film to be close to 70 dB SPL (Appendix 3, Fig. 8b), whereas the dynamic range of the IO function of the native TM group was 20 dB SPL lower (Appendix 3, Fig. 8a).

## 2.4 Self-adhesive silicone microstructures for the treatment of tympanic membrane perforations reduce a conductive hearing loss induced by perforation (Appendix 4)

To investigate how tympanic membrane perforations could be treated to compensate the functional defect quicker and better compared to standard methods, we evaluated the use of self-adhesive silicone elastomers for tympanic membrane perforations in a mouse model. The self-adhesive elastomers were designed as film-terminated structures with microstructures and a backing layer consisting of Sylgard 184 and an adhesive layer on top, consisting of MG7-1010, a soft skin adhesive (SSA) polymer. The elastomers were conceptualized as a microstructure form and a respective unstructured control film, with the same calculated weight as the microstructures but smaller thickness (Appendix 4, Fig. 1). Since the roughness of the tympanic membrane is one important characteristic strongly influencing the adhesion of silicone elastomers, we first characterized it using confocal microscopy on silicone replicas of explanted TM specimens (Appendix 4, Fig. 2). The assessed roughness of the TM was compared to an epoxy substrate that was used in further examinations of the elastomer's adhesion properties in laboratory conditions. The arithmetic mean height of the replicas of explanted TMs was  $0.14 \pm 0.04 \mu\text{m}$ , whereas the arithmetic mean height of the epoxy substrate was  $0.41 \pm 0.01 \mu\text{m}$ . As the next step, we evaluated the adhesion properties of the elastomers against the epoxy substrate and thereby found significantly higher pull-off stress of the microstructure compared to the unstructured control after applying pre-stresses of 11 and 23 kPa (Appendix 4, Fig. 3). The elastomers were further examined regarding their adhesion on the murine TM *ex vivo* and applied on acutely induced TM perforations *in vivo*. Thereby, we used two different conditions of the TM: i) intact and ii) perforated membranes (Appendix 4, Fig. 4a). To investigate the adhesion of the patches on the murine TM, we used a custom-made adhesion evaluation device (Appendix 4, Fig. 4b&c), allowing us to apply and detach patches with a defined speed and pressure. The patches were applied with a pre-stress of about 25 kPa that was held for 10 seconds followed by the retraction (Appendix 4, Fig. 4d). The tensile stress was used to analyze the strength of adhesion of the different samples: i) microstructured, named as "FT" ii) unstructured named as "Control" and iii) as a further control, non-adhesive backsides of control patches, named "Control non-adh." (Appendix 4, Fig. 5). The film-terminated, as well as the unstructured patches demonstrated significantly higher adhesions on the intact TM, in comparison to the non-adhesive control while the difference between microstructured and control patches was not significant (Appendix 4, Fig. 5a). On the perforated membrane, the tensile stress used for detachment was overall lower compared to the intact condition. Interestingly, the adhesion of microstructured patches appeared to be higher than the adhesion of the control patches, however again the analysis demonstrated this difference to be non-significant. Both patch samples, microstructured and unstructured, adhered statistically significantly better than the non-adhesive control group (Appendix 4, Fig. 5b).

To further assess the functional effects of treating TM perforations regarding hearing, we used electrophysiological recording of auditory brainstem responses and DPOAEs in anesthetized mice with intact, perforated, and patched TMs. The analysis of click-ABR hearing thresholds demonstrated a significant increase from 12 to 34 dB SPL after inducing a perforation in both groups. After application of patches, no significant improvement of the hearing threshold could be recorded in neither group (Appendix 4, Fig. 6). To analyze the effects on the hearing function in a frequency-specific and finer way, we used the recording of DPOAE signals between 10 and 18 kHz for the same conditions (Appendix 4, Fig. 7). After perforation, the averaged DPOAE signals clearly decreased in intensity, measured as signal-to-noise ratio (SNR) over all frequencies and increased when a patch was applied on the perforation (Appendix 4, Fig. 7a&b). After the application of a microstructured patch, the improvement was more prominent in the frequency range up to 15 kHz (Appendix 4, Fig. 7a). In comparison to this, the increase of the SNR after applying an unstructured patch was smaller, however observable over the whole frequency range (Appendix 4, Fig. 7b). In a more detailed analysis, we separately analyzed DPOAE signals in the frequency ranges from 10-15 kHz and 15.5-18 kHz. In the lower frequency range, the SNR significantly dropped from 26.4 to 17.5 dB after perforation and increased to 21.8 dB after applying a microstructured patch (Appendix 4, Fig. 7c). In mice treated with the unstructured patch, the control group, the DPOAE values of the perforated TM were both improved (Appendix 4, Fig. 7d). In the higher frequency range, this situation was reversed. The significant decrease from 30 dB to 23 dB after perforation was not improved after applying a microstructured patch (Appendix 4, Fig. 7d) whereas the DPOAE signals increased after covering the perforation with unstructured patches (Appendix 4, Fig. 7f). The DPOAE-signals were not improved to the level of the intact condition after closing the perforation, in any of the groups.

To examine whether this effect was caused by the weight of the patches, we performed experiments using patches that were applied on the intact tympanic membrane. In these experiments, we also applied thicker patches and compared the results with those of patches in the thinner form used in the former experiments. Thereby, we showed that DPOAE signals were significantly reduced after applying patches on the intact tympanic membrane in all cases (Appendix 4, Supplementary Fig. S1). As expected, the decrease in DPOAE levels was higher after applying thick microstructured or thick control patches (Appendix 4, Fig. S1 c&d) compared to the patches of the thinner conformation (Appendix 4, Fig. S1 a&b). The DPOAE levels were not improved by application of thick patches on perforated TMs neither with nor without microstructure, (Appendix 4, Fig. S2).

### 3 Discussion

Pathologies of the ear range from malformations, inflammatory processes, injuries, and tumors up to functional impairment of the two senses hearing and balance. Independent of their type, these pathologies strongly influence the patient's life especially due to the affected sense of hearing. Hearing is important to get into connection with the environment, to orientate in daily life, and communicate with other people. If the hearing function is diminished for any reason, and the hearing loss is kept unaddressed, it impacts many aspects of people's life: daily communication, development of language and speech in children, cognition, education, employment, mental health, interpersonal relationships etc. [36]. Globally, around 1.57 billion people are affected by hearing loss, of whom 460 million people suffer from a disabling hearing loss among which 34 million are children [35,105]. In Germany, the prevalence of hearing loss is estimated to be 0.1 - 128 per 1000 children and adolescents [105]. Experts estimate that worldwide by 2050, around 2.45 billion people suffer from hearing loss, with 698 million people having a moderate to complete hearing loss [35]. In the global burden of disease (GBD) study in 2019, hearing loss was demonstrated to be the third-largest cause of global years lived with disability (YLDs) [35]. Besides the personal impact of untreated hearing loss, the world health organization (WHO) estimates, that unaddressed hearing loss leads to annual global costs of 660 billion Euros. On the other side, the WHO approximates, that 60 % of hearing loss in children could be prevented by avoiding ear infections such as otitis media and virus-induced pathologies such as meningitis [133]. All these facts demonstrate the importance to develop strategies to treat and to prevent hearing loss.

One pathology of the ear affecting hearing are tympanic membrane perforations. They have different causes such as traumatic events e.g., impalement lesions by cotton swabs or inclusion of foreign bodies, explosions, hitting a water surface or slaps on the ear. Regardless of their origin, tympanic membrane perforations cause a conductive hearing loss due to the reduced sound capture and transmission to the middle ear. On the other hand, pathogenic germs may enter the middle ear through the injured membrane, leading to infections. Traumatic perforations occur approximately with a frequency of 1.4 to 8.6 / 100.000 people [3,41,128]. The therapy of small and acute perforations is controversy discussed in the scientific and medical community. Some clinicians prefer to keep these perforations untreated and observe the patients until they heal spontaneously. Others treat perforations by covering them with silicone foil or paper patches to seal them in the acute stage. Closing the perforation immediately clearly has the advantage to restore the sound conduction mechanism of the membrane and rebuild the physiological barrier between the outer ear and the middle ear. This protects the middle ear from pathogenic germs that could possibly lead to otitis media and could have further far-reaching consequences e.g., hearing loss, chronic infections etc.

The objective of this work was to investigate two different innovative methods to treat ear pathologies from two different perspectives, having together one major goal: the investigation of their biocompatibility and applicability in preparation to be used in the clinical routine in the future. First, the treatment of hearing loss with an alternative stimulation strategy based on laser light and not on acoustic or electric stimulation has been assessed for its biocompatibility. Second, the treatment of eardrum perforations to reduce the conductive hearing loss and avoid infections was evaluated and presented herein. Therefore, as part of the translation of both methods to the daily clinical routine, the investigation of their biocompatibility and usefulness has been the driving goal of this thesis.

### 3.1 Biocompatibility margins of optoacoustic stimulation

The optoacoustic stimulation offers a great potential to be used in the future to activate the hearing system. The advantages of light-energy instead of conventional methods are thereby: light can be applied much focused, contact-free and on every desired site of application. In contrast to electrical stimulation used in cochlea implants, no electric field around the application site would be induced, allowing a high resolution capacity of activation without spreading of the electrical field as happening in cochlear implants [64]. However, scattering effects of light on tissues, such as bone or cartilage, absorption-mediated heating, high energy requirements [112] and possible cytotoxic effects of laser-irradiation [99,111] are possible limits for the practicability. If utilized in air, light can be applied with low scattering and the patients would strongly benefit from the contact-free application that would not require a closure of the outer ear canal, which is needed when classic sound amplifying hearing aids are used.

The optoacoustic stimulation works based on the optoacoustic effect whose underlying mechanism is a photothermal laser-tissue interaction. Thereby, short light pulses, absorbed by irradiated media, induce short, periodic, thermal expansion-relaxation events which in follow lead to the generation of ultrasound waves, thus generating a sound source. The first approach of optoacoustic stimulation of the inner ear was made by Fridberger and Ren in 2006 who used diode lasers to stimulate the cochlea of rats *in vivo*. They analyzed the activation of the hearing system by the recording of cochlear microphonics and vibrations of the basilar membrane [33]. The optoacoustically induced vibrations can be used to activate the hearing system as they are transmitted as acoustically induced vibrations over natural paths [24,45,112,114,136]. Wenzel et al. 2009 described the irradiation of guinea pigs cochleae with 10 ns pulses of Nd:Yag Lasers induced oABR waves *in vivo* [129]. In the same year, this group reported optoacoustically induced basilar membrane vibrations using two different laser wavelengths of 532 and 355 nm [136]. The optoacoustic stimulation was also discovered to succeed if the laser light is applied on the TM and middle ear structures inducing oABR waves and frequency-specific neural spike activities in the inferior colliculus (ICC) in guinea pigs [130]. Later, experiments assessing the amplitude of compound action potential (CAP), as a measure of the efficiency of the optoacoustic stimulation at

the inner ear, for different wavelengths and stimulus intensity, was presented [106]. In 2016, the group around Kallweit et al. demonstrated that the optoacoustic effect is responsible for cochlear responses induced by infrared laser stimulation, formerly thought to be a direct neuronal excitation effect from other groups. They drew this conclusion from *in vivo* experiments in hearing guinea pigs and pressure measurements in water demonstrating a strong relation between the efficiency of optoacoustic stimulation and the absorption coefficient of the irradiated structure [58]. The approach to use the optoacoustic stimulation in the middle and outer ear was studied by our group in parallel, demonstrating the frequency-specific activation of the hearing system. Thereby, the incoming laser signals were modulated in a sinusoid form representing the aimed frequency of activation, the laser modulation rate (LMR). We were able to demonstrate a frequency-specific activation of the hearing system through neural spike activity recordings at the ICC by stimulating at the TM level, the round window membrane and at the otic capsule [114]. The efficiency of optoacoustic stimulation with different wavelengths was further investigated by our group. The vibration amplitude of guinea pigs TMs was analyzed as a function of the wavelength *ex vivo* using laser Doppler vibrometry. The aim of this study was to define the optimal stimulation parameters for the application at the TM [45].

Experimentally, optoacoustic stimulation is currently applied on different structures on the hearing organ, however, to our knowledge, no reports exist regarding its biocompatibility. Most studies focus on electrophysiological effects. To use the optoacoustic effect as a future stimulation method in hearing aids, the safety limits of its application are required. We, therefore, performed biocompatibility analyses in two different ways: on the tympanic membrane of mice and in cell culture. In the mouse model, the irradiation of the TM using green 10 ns laser pulses at 50 kHz laser pulse rate demonstrated a first safety margin at 89 mW average laser power above which laser-mediated generation of areas with necrotic cells around the irradiated zone could be detected (Appendix 1, Fig. 2). The affected area increased in size with increasing laser power and clearly differed in its size between the irradiation at the umbo and the irradiation at the *pars tensa*, indicating absorption-mediated effects (Appendix 1, Fig. 3). One possible reason of increased laser-induced necrotic areas after irradiation at the umbo could be of thermal origin due to: i) the higher absorption of green laser light within the bony structure of the malleus and ii) the coagulation of more central vessels in the umbo than at the *pars tensa* [111]. Based on the principle of stress confinement, no energy dissipation and thereby thermal heating of the irradiated tissues should occur during the generation of the acoustic signal [136]. However, the roles of physics are not easily transferred on the irradiation of the hearing system, since, especially on the tympanic membrane, we irradiated inhomogeneous biological structures, like epithelial cells, collagen fibers and bony structures at once. Therefore, it is impossible to investigate the possible laser-tissue interactions based on theoretical calculations. Furthermore, photothermal interaction depends on diverse characteristics of the irradiated tissue e.g., optical, thermal and mechanical properties, chemical composition, as well as the anatomy and physiology of the irradiated tissue [118]. For the TM, these parameters are not yet sufficiently characterized [111]. We claimed hemoglobin, and collagen / bone as

the major components involved in the absorption events during optical stimulation of the TM. This assumption was also supported by recent studies of our group, assessing the optoacoustically induced vibrations of the guinea pig's TM *ex vivo* using laser Doppler vibrometry in correlation with the absorption spectra of inherent components of the TM [45]. In combination with the absorption occurring during irradiation, another factor leading to necrotic cells in the irradiation zone might be the use of the high laser pulse rate of 50 kHz. Computer modeling of laser irradiation experiments of the human and the guinea pig cochlea suggested that heat conduction reached a quasi-steady state after a few seconds. Here, the temperature rise depended on the laser pulse rate [137]. Besides our findings it is hard to use laser safety parameters from the literature for application at the TM. Reports regarding nondestructive laser application are mostly focusing on the low-level laser therapy (LLLT) [100] or trans-tympanic photobiomodulation (PBM) and therefore are hard to compare to optoacoustic stimulation. For example, PBM is performed with near-infrared laser light and laser parameters similar to the ones used in our experiments, 165-200 mW average laser power followed by macroscopic and microscopic observation e.g., hair cell counts or scanning electron microscopy for investigating the biocompatibility [82]. However, the lasers applied in these studies were CW lasers and subsequently, the biocompatibility findings are not equivalent to the ones after the stimulation with pulsed nanosecond lasers. Another widely used and well-established laser application at the TM is laser Doppler vibrometry. Data from Foth et al. 2000 demonstrated laser Doppler vibrometry to be safe using CW lasers at 633 nm up to experimentally determined thresholds of 7100 W/cm<sup>2</sup>. This value differed considerably from often used 80 W/cm<sup>2</sup> [32]. Other investigations from the literature used infrared neural stimulation (INS). Goyal et al. did not find any significant electrophysiological effect on the cochlea within the signals generated after continuous irradiation below 30  $\mu$ J/pulse. Histologically, they did not observe any structural changes of the tissue while working with a diode laser at 1869 nm and with 100  $\mu$ s pulse length either [40]. On the electrophysiological level, we could not find any significant influence of the irradiation on the hearing function either. This translated into no significant increase in hearing thresholds following the irradiation (Appendix 1, Fig. 5). Although increasing necrotic areas were detectable, amplitude values were not significantly reduced by using higher irradiation values (Appendix 1, Fig. 6). This finding diverged with the result of higher latency values in the data group after irradiation with 99 mW at the umbo. Since this effect was singular and has not been confirmed in groups irradiated with higher intensities, this effect might be caused by random variances inside this group.

Interestingly, in cell culture experiments using the same irradiation parameters and staining method as in the mouse model, higher cell-line specific irradiation thresholds for cellular viability were found. Thus, all three methods confirmed a safe application of our stimulation strategy *in vitro* with laser powers up to 99 mW (2988 J/cm<sup>2</sup>). In accordance with our findings in the mouse model, a trend of an increase in cytotoxicity was found with increasing laser power in all three tested cell types, however with different thresholds for each cell line [99]. For fibroblasts, the threshold was found to be the lowest at 223 mW, for chondrocytes at 250 mW, and for osteoblasts at 285 mW (Appendix 2, Fig. 4). This

might be caused by varying concentrations of photoacceptor molecules of the different cell types or by differences in their growth patterns, respectively [99]. The results of previous experiments (data not shown) in which an exposure-time-dependent increase in affected areas was demonstrated further supported the idea of potential thermal effects as one major damage mechanism in this set of experiments. This hypothesis was supported by qPCR analysis revealing multiple responses from different stress and toxicity pathways after irradiation above threshold like DNA damage response, oxidative stress, heat shock and inflammatory response, hypoxia, and autophagy [99]. The induction of DNA damage response pathways after irradiation with a 532 nm laser has also been described for the human liver cell line HepG2 [88] and hamster fibroblasts [70]. However, there is the well-known problem of poor comparability between the studies because the authors used laser as a picosecond laser and different average radiant exposure and power densities compared with our experiments. The induction of heat shock response after laser irradiation is also known from literature and mostly interpreted as a cytoprotective mechanism and an increased autophagy response. The latter was found in a glioma cell line using a similar experimental setup as ours, but higher cytotoxicity was found after applying 477.5 J/cm<sup>2</sup> only whereas necrosis and destruction of cell structures were found after irradiation with 1910 J/cm<sup>2</sup>. These differences are suspected to be caused by a higher vulnerability or altered response mechanisms to the laser irradiation in the glioma cell line [66]. Sub-threshold qPCR analysis demonstrated upregulation of the stress gene GADD45G in fibroblasts, which could be induced through a potential growth arrest after irradiation with sub-phototoxic laser powers. This finding is in line with a study in 2017 From Kim et al. who perceived a protective mechanism induced by an upregulation of GADD45A after irradiation with visible red light ranging from 620 to 690 nm wavelength [60,99].

Although the upper thresholds for laser safety strongly differed between the mouse model (89 mW) and the cell culture assay (at least 223 mW) the average power density between both models turned out to be a good parameter for comparing both methods. In the mouse model, the upper limit was at 5340 J/cm<sup>2</sup> whereas in cell culture it amounted to 2988 J/cm<sup>2</sup>. Here, one major factor to consider the relatively large distance of the laser fiber to the murine tympanic membrane because of the conical shape and tilted angle of the mouse eardrum. In contrast, the laser fiber was easily adjusted as close as possible to the flat glass bottom of the cell culture plates. Another factor was the difference regarding absorption events between a monolayer cell culture and a much thicker epithelial structure consisting of different cell types and connective tissues organized in layers [99]. A clear advantage of cell culture-based cytotoxicity assays is the possibility of analyzing the effects of laser irradiation for each cell type individually giving additional insight into the different sensitivity characteristics of the irradiated structures [99].

Taken together, we were able to specify for the first-time cytotoxicity / biocompatibility thresholds for optoacoustic stimulation of the hearing organ *in vitro* and *in vivo*. We successfully transferred a method for the detection of cell viability effects from the cell culture model into whole-mount preparations of the murine eardrum. Given these first margins, further steps regarding the underlying phototoxic mechanisms, including laser-irradiation-associated photochemical and thermal effects are needed to define the optimal and biologically safety parameters for optoacoustic stimulation.

### 3.2 Enhanced efficiency of optoacoustic stimulation due to the use of absorbing patches

We were previously able to demonstrate that our stimulation strategy could be used to frequency-specifically stimulate the guinea pig's hearing spectrum *in vivo* [114]. For biocompatibility and energy consumption reasons, the irradiation intensities used for optoacoustic stimulation of the hearing organ need to be as low as possible. One challenge regarding this issue is the efficiency of optoacoustic stimulation, being highly dependent on the light energy [58] as well as its absorption in the irradiated substrate, which is a function of the absorption coefficient [45]. To analyze the *in vivo* stimulation and the *ex vivo* biocompatibility assessment in the same animal the modulation of the stimulation intensity needed to be examined in the mouse model. As a proof of principle, we have demonstrated for the first time that oABR waves could be induced in mice, although they have a nearly transparent tympanic membrane that does not offer an ideal basis for optoacoustic stimulation [46,113]. To enhance the absorption of the murine eardrum, we designed and applied in collaboration with our partners from the Institute for New Materials a novel self-adhesive patch, which is equipped with an absorbing layer on the side directed towards the laser fiber and a reflective layer below.

The results of oABR detection showed that when using the absorbing patch, we were able to record reproducible oABR signals resembling those of aABR. Since analysis of growth functions is a proven method to examine the neural response to the stimulation of the auditory system, we analyzed growth functions of wave I, the most prominent wave in ABR signals in mice [29,132,140,141], and compared the resulting amplitudes to stimulation without a patch and with a non-absorbing patch. The efficiency of optoacoustic stimulation was strongly enhanced using absorbing patches. Interestingly, the higher the LMR was, the lower was this enhancement factor. One reason for this finding might be that the number of pulses in one sine period decreased with increasing LMR leading to less efficient laser stimulation. Furthermore, a higher absorption efficiency does not automatically lead to higher signals. Kallweit et al. 2016 who worked on an optimal absorption coefficient and found a negative correlation between optoacoustic signal amplitude and this absorption coefficient optimum [58]. Another interesting finding was the significantly reduced aABR amplitude recorded after the patch application (Appendix 3, Fig. 6). This finding was most likely caused by the weight of the patch attached to the tympanic membrane,

damping the vibrations, and thereby reducing the sound conduction. Nevertheless, this effect had only a low impact (5 %) on the oABR wave I amplitude normalized to the result after 80 dB SPL stimulation recorded with patch in comparison to the bare TM. Therefore, the effect of patch conformation on the interpretation of oABR signals was at this point negligible. Upon stimulation with 1 kHz LMR and subsequent normalization we were able to reach ~ 60 % of the level that was reached with 80 dB SPL acoustic stimulation (Appendix 3, Fig. 7). This finding was surprising since mice have very low hearing ability at this frequency. It is important to consider that click sounds activate almost the entire cochlea inducing a stronger ABR amplitude due to summing up of neuronal activity in comparison to a very narrow frequency band activated with a frequency-specific stimulation strategy. We used however the method of normalizing our data to click-ABR signals to be in line with research protocols reported by other groups [50,77,121,127]. Upon stimulation with 8 and 10 kHz LMR, we reached levels of 50 % compared to acoustic stimulation with 80 dB SPL. It should be considered that in our currently used stimulation strategy the number of pulses under the sinusoid is smaller the higher the LMR is. Therefore, a direct comparison of the oABR data with an adapted acoustic stimulus is not optimal at this point, which will be changed in future experiments. One option would be the comparison to frequency-specific acoustic stimulation, matching the targeted LMR. In addition, vibration analyses would help to clarify, why the stimulation at 1 kHz LMR was the most efficient, although mice have a poor hearing ability at this frequency. One explanation for this phenomenon could be the induction of harmonics by the absorbing patch or the TM that would create vibrations of other frequencies better perceived in mice contributing to the summation of the induced action potentials.

The results demonstrate that the optoacoustic stimulation can be enhanced using an absorbing film applied on the targeted stimulation site e.g., the tympanic membrane in this set of experiments. Light absorbing patches in the self-adhesive conformation makes them a proper candidate to be further used for this stimulation strategy. Fischer et al. demonstrated that PDMS films securely adhere on rough surfaces and even on human skin [12,30,31]. The biocompatibility of PDMS films, their flexibility, and good adhesion makes them ideal candidates for wearable applications [18]. PDMS patches were also successfully used in a non-adhesive form without SSA but instead with immobilized collagen to treat tympanic membrane perforations [28]. Furthermore, because the patches could be designed in every feasible design and conformation, one could imagine using absorbing films on different stimulation loci of the hearing organ, e.g., middle ear, ossicles, or the otic capsule. Additionally, the characterization of light transmission and absorption of those patches revealed their suitability for other wavelengths as well.

The double-layer design was used to provide a structure embodying two elements at the same time: good adhesion and stability. The SSA surface allows for reliable adhesion to the TM without damaging the tissue [13] whereas the Sylgard fraction ensures the support for the soft SSA film and gives stability for handling and application. The optical properties of the patches were optimally designed for low transmission and high absorption. The low transmission of the film should provide higher safety since

very low amount of the irradiation energy should be transferred to the middle and inner ear. Additionally, the absorbing films demonstrated to be useful for all wavelengths between 200 and 1300 nm. How far adaptation of the absorptive layer would lead to even better results regarding improving the efficiency of the optoacoustic stimulation needs to be further investigated. For example, using a completely pigmented patch would be conceivable as a further beneficial step.

Overall, the results demonstrated that the efficiency of the optoacoustic stimulation can be enhanced using an absorbing film, but still is not efficient enough with our current stimulation protocol. The equivalent oABR levels of ~60 and ~50 % of the levels reached with 80 dB SPL acoustic stimulation seem not to be enough for the future use in a hearing device, especially when considering the high energy input of 89 mW average laser power, possibly leading to biocompatibility issues over time. Therefore, further work is needed to optimize the stimulation parameters with regard to reduced energy consumption, enhanced activation of the hearing system, biocompatibility, and interaction between wavelength and absorbing film. Possible ways to reach this could be the use of a more biocompatible wavelength e.g., in the infrared region with a compatible absorbing film, shorter pulse lengths, or other repetition rates.

### 3.3 Reduced conductive hearing loss by covering eardrum perforations with self-adhesive patches

The eardrum is a thin, elastic, and nearly transparent membrane that separates the outer ear from the middle ear. As the first coupler between the outer ear and middle ear, it is responsible for the transmission and enhancement of sound waves on their way to the inner ear, providing the base of hearing. In parallel, the TM serves as a physiological barrier to protect the middle ear from pathogenic germs. If the membrane is, at least partially ruptured, the collection of sound waves is disturbed and consequently, the sound wave transmission is diminished. Hearing loss and potential infections are the first consequences. Although most of the tympanic membrane perforations heal spontaneously without complications, in some cases, they persist for longer time periods or re-occur several times. Overall, the time of healing and the closure rate strongly depends on the type, size, and duration [27,37]. Recurring and chronic perforations could cause severe health issues due to the risk of infections and the formation of cholesteatoma, a life-endangering complication [76]. Furthermore, TMPs can lead to conductive hearing loss [10,79].

To immediately close the perforation and overcome conductive hearing loss, one well-established method is to seal or cover TMPs with a patch consisting of different materials, including paper, non-adhesive silicone strips, or Steri-strips. One major challenge of paper or silicone patching is to ensure keeping the patch in the right position. The standard solution for this issue is to pack the outer ear canal up to the tympanic membrane with cotton and Gelfoam® to keep the patch in position over the

perforation for at least 1-3 weeks. Using this procedure, the patient is strongly affected in his daily life due to the resulting conductive hearing loss induced by the complete occlusion of the ear canal on the affected side. Unilateral hearing loss impacts the patient in communication, orientation and influences its feeling of safety in public. One possible method to avoid these drawbacks is the use of adhesive materials for TMP treatment. Park et al. 2011 demonstrated that patching large TMPs with Steri-strips lead to a reduced healing time compared to just observing the patient. Additionally, it reduced the number of additional procedures when compared to the treatment using paper patching. However, no significant difference in the hearing gain or in the closure rates between the observed groups could be detected [98].

Our group designed self-adhesive poly-(dimethyl) siloxane (PDMS) composite films as a novel patching material for the application on the TM. PDMS is a silicone elastomer with wide-ranging use as a skin adhesive [7,18,55,68]. The PDMS materials, which were demonstrated to be biocompatible in cell culture experiments, have tunable mechanical properties influencing their adhesion [30]. PDMS patches were also shown to have good adhesion on materials with skin-like roughness [31]. Recently, composite films of two different PDMS materials were established for the application as wound dressings on tympanic membrane perforations. In detail, composite films of soft skin adhesives (SSAs), a subclass of PDMS elastomers, and Sylgard 184 demonstrated to be well applicable on the murine tympanic membrane and presented strong adhesion in peel-tests [13]. The SSA can adhere to rough surfaces and has the advantage of gentle attachment and detachment, combining a secure adhesion to the thin membrane with an atraumatic removal. SSAs, also known as dry adhesives, have the advantage of adhesion without the use of any chemical fixation because of their physical interaction with the adhering surfaces by van der Waals forces [61,92]. This glue-free application together with their ability to adhere to rough surfaces including wet skin, their high water vapor permeability, and good compatibility with pharmaceutical compounds make SSAs to ideal candidates for medical use such as wearable electronics, skin applications, wound scaffold materials, and wound dressings [7,12,31,55,117]. In the past years, the idea to further enhance the adhesion of silicone elastomers by the implementation of microstructures, inspired by nature, emerged. Thereby, the polymers were prepared based on the model of the gecko's foot, having keratinous hairy structures, allowing the climbing on vertical walls by dry adhesion over van der Waals interactions [5]. Such micropatterned structures, created by the use of micropillars in different architectures, are successfully established and applied in robotics and industrial applications where they demonstrated to have advantageous effects on the adhesion [5,8,49]. Besides industrial applications, the use of microstructured silicone materials in medical applications, especially as skin applications and wound dressings created an emerging research field in the past few years. For example, Hwang et al. 2018 proposed encouraging opportunities of different nature-inspired skin adhesive patches for the use of e.g., wound dressings, wearable electronic patches, transdermal approaches, and drug-releasing reservoirs [53]. Further possibilities are the use of microstructured skin adhesives as bioelectronics [7].

Modern manufacturing processes and evolving knowledge on the advantages of using microstructures in silicone elastomers for medical applications led to the idea to implement micropillars in PDMS films to be used for the treatment of TMPs. As in other medical applications, the implementation of microstructures should end in higher adhesion and in parallel, allow better handling and protection of the very sensitive TM by damping effects of the pillars. We, therefore, created patches with a film-terminated design in which the micropillars are covered by a continuous top layer. This design was described from a mechanical point of view from Glassmaker et al. [38] and Noderer et al. [85] pointing out their excellent adhesion due to a crack-trapping mechanism, enhancing the adhesive properties of micropatterned structures compared to flat samples on glass samples. Film-terminated patches are also reported to have good adhesion to rough surfaces due to their superior adaptation to the surface characteristics because of the soft top layer [44,107,108]. A comparable structure was reported to have a better resistance against vibrational resistance with enhanced adhesion and an energy-dissipation matrix, which was inspired by pedal-muscle structures of snails, therefore named snail-inspired adhesive (SIA) [59].

To assess whether a film-terminated micropatterned self-adhesive patch would serve as treatment for TMPs, we evaluated their applicability from different points of view: i) adhesion in tack-tests on epoxy substrates, ii) adhesion on explanted murine TMs *ex vivo*, and iii) effects on the hearing ability of mice *in vivo*. All examinations were performed in comparison to unstructured control patches. Control and microstructured patches adhered reliably on the murine tympanic membrane and could be detached without damaging the sensitive membrane. The adhesion was generally lower when the tympanic membrane was perforated in comparison to the intact condition (Appendix 4, Fig. 5). This outcome was most likely caused by the reduction in the actual contact area by perforation. Another effect could be the reduced tension of the ruptured *pars tensa* after perforation, which would result in a less defined contact and make the mating surfaces more conforming [16,83]. Interestingly, the beneficial adhesion of microstructured patches in contrast to unstructured control patches which was seen in tack tests performed on rigid epoxy substrates (Appendix 4, Fig. 3), was not observed anymore in the *ex vivo* animal model. In general, the adhesion on the murine TM was lower compared to the adhesion measured in the epoxy model. We claimed that at least two factors are responsible for this finding: i) the different geometric complexity (a nominally flat epoxy surface vs. the concave curvature of the eardrum) and ii) different stiffness values between both models.

The tight contact between the patch and tympanic membrane and the reliable adhesion allowed us to use the patches in an *in vivo* animal model to assess the effects of patching of tympanic membrane perforations on the hearing function. Click-ABR thresholds significantly increased after perforation compared to intact conditions. This threshold increase could not be significantly reduced after applying microstructure or control patches on the perforation (Appendix 4, Fig. 6). The ABR thresholds thereby gave us a first insight into the hearing function of mice without detailed information about frequency-specific effects. One method to quantify frequency-specific conductive hearing loss is the measurement

of distortion product otoacoustic emissions (DPOAE). This procedure is well-established in the clinical routine in humans and used in different research approaches regarding hearing function in laboratory animals [25,42,51,73,93,120,126]. DPOAE signals are generated by active processes of outer hair cells inside the cochlea and can be recorded by very sensitive microphones placed in the outer ear canal. We used DPOAE measurements to prove the positive effect on the hearing ability directly after applying a patch on perforated TMs (Appendix 4, Fig. 7)[83]. As hypothesized, the DPOAE signals were significantly reduced after perforation compared to healthy and significantly improved immediately after patch application of microstructured or control patches. Frequency-specific analysis showed that the microstructured patch specifically enhanced hearing at lower frequencies (up to 15 kHz), while the control patch improved hearing at higher frequencies (between 15.5 and 18 kHz) [83]. Altogether the patches could not fully restore the hearing as the patches could not completely return the function of the damaged eardrum. This was mainly caused by the added mass on the tympanic membrane, which influenced the acoustic impedance and dampened the sound conduction. As microstructured and control patches should have the same mass, it is not surprising that we could not demonstrate any differences between both groups regarding this fact. The negative impact of added mass was confirmed by the reduction in DPOAE levels after applying the patches to intact TMs in further control experiments (Appendix 4, Fig. S1).

In general, DPOAE measurement is a very sensitive method to detect sensorineural but also conductive hearing loss. Thereby, the signal level depends on the anterograde and retrograde middle ear transmission and is strongly influenced by mechanical changes in the outer ear and middle ear, such as increased mass or stiffness [119]. Consequently, DPOAE quality is influenced twice by the middle ear constitution, in particular by affecting the incoming tones in the inward direction as well as the returning DPOAE signals in the outward direction [25]. Taken together, DPOAE measurements are a suitable characteristic for assessing the effects of tympanic membrane perforations. In a gerbil model, Dong et al. 2019 analyzed the effects of TM perforations and altered middle ear transmission on the generation of DPOAEs. Those were found to be detectable up to perforation sizes involving about half of the tympanic membrane. In agreement with our results, DPOAE thresholds were not totally restored to normal after 4 weeks of healing, especially in the higher frequency range ( $> 10$  kHz). The authors suggested an incompletely restored middle ear transmission even after the closure of the TMP [25]. In a guinea pig model, it has been demonstrated that increasing TM perforations lead to a decrease in the DPOAE amplitude beginning at 25 % perforation of the TM and ending at 75 % perforation size where DPOAE signals were not detectable anymore [71]. Recently, the group around Lin et al. 2021 supported these findings in their gerbil model, demonstrating DPOAE levels reduced to noise floor after 50 % perforation of the TM, which steadily recovered to the intact level after 4 weeks of spontaneous healing. They concluded from their findings of DPOAE and middle ear transmission measurements, that ME transmission is strongly influenced by increased mass or altered vibratory characteristics of the TM, effects that are a result of wound closure mechanisms of the TM [73]. In conclusion, DPOAEs are a

specific and meaningful tool to investigate the sound conduction apparatus and to gain information about the sound transmission through the middle ear. For treatment of patients with TMPs, patch materials matching the natural characteristics of the TM, e.g., elasticity, vibratory properties, and thickness are needed. This would help to overcome the conductive hearing loss induced by perforation and not only close the perforation.

To sum up, covering acutely induced TMPs with self-adhesive patches in the animal model served as a suitable method to, at least partially, compensate a conductive hearing loss induced by the perforation. The films demonstrated reliable adhesion but were at the same time easily removed from the sensitive TM making them perfect candidates for future application in the daily clinical routine. Although the murine and human TM are histologically identical, future work must be performed to analyze the adhesion properties on the human TM. As roughness is one major point that influences the adhesion, the adhesion behavior is assumed to be different on human TMs which are expected to be rougher than the murine TM. Moreover, the overall material thickness must be adapted to the human TM that is expected to be  $\sim 120 \mu\text{m}$  thick in comparison to the murine TM having  $\sim 5 \mu\text{m}$  thickness in our histological preparations. Another fact that must be discussed in the future is the cellular compatibility and supportive properties for cellular spreading of the novel TM patches. As previous work demonstrated and is well-known from literature, silicone elastomers have hydrophobic surfaces, avoiding cellular adhesion and spreading [12,13,30]. Possible interventions to overcome this issue would be the functionalization by plasma treatment or protein adsorption to enhance cellular compatibility. Nevertheless, the biocompatible, flexible, easy handleable PDMS material, which is tunable in its mechanical characteristics by adaptation of the material composition, makes it an excellent future candidate for the treatment of human TMPs. Patients would benefit from its self-adhesive properties allowing a covering of their perforation without concluding the outer ear canal during the healing phase. Moreover, the use of the film-terminated design with the porous SSA top layer could be used to design a drug-release system between the pillar portions, steadily releasing over time anti-inflammatory and infection-suppressing agents, e.g., cortisone and antibiotics, directly at the desired target location [80,135].

Taken together, the benefits for the patient during and after the healing period, as well as the easy handling, the biocompatibility, and mechanical tunability of the material, offer great potential for micropatterned PDMS patches to be successfully translated into clinical practice soon. Studies regarding the long-term adhesion and effects on hearing, as well as the effects on the healing of injured TMs, along with the vibratory characteristics of the material-TM complex in humans, will give further insight into the applicability of silicone elastomers on human TM perforations.

## Appendix

### 1) First biocompatibility margins for optical stimulation at the eardrum level via 532-nm laser pulses in a mouse model

Katharina Sorg, Patricia Stahn, Lukas Pillong, Marius P. Hinsberger, Larissa Heimann, Hans-Jochen Foth, Bernhard Schick, Gentiana I. Wenzel

Contribution of the authors:

Katharina Sorg developed the study conception and performed the experiments, analyzed the data, and composed the manuscript. Patricia Stahn developed and programmed the software used to perform the experiments. Marius Hinsberger assisted during the experiments. Patricia Stahn, Lukas Pillong, and Larissa Heimann assisted during the experiments and helped with the manuscript preparation. Hans-Jochen Foth assisted in laser-specific questions and with scientific discussions. Bernhard Schick assisted during manuscript preparation and scientific discussions. Gentiana I. Wenzel worked on the study design, data analysis, during manuscript preparation and with scientific discussions.

## **First biocompatibility margins for optical stimulation at the eardrum via 532-nm laser pulses in a mouse model**

Katharina Sorg  
Patricia Stahn  
Lukas Pillong  
Marius P. Hinsberger  
Larissa Heimann  
Hans-Jochen Foth  
Bernhard Schick  
Gentiana I. Wenzel

Katharina Sorg, Patricia Stahn, Lukas Pillong, Marius P. Hinsberger, Larissa Heimann, Hans-Jochen Foth, Bernhard Schick, Gentiana I. Wenzel, "First biocompatibility margins for optical stimulation at the eardrum via 532-nm laser pulses in a mouse model," *J. Biomed. Opt.* **24**(8), 085003 (2019), doi: 10.1117/1.JBO.24.8.085003.

# First biocompatibility margins for optical stimulation at the eardrum via 532-nm laser pulses in a mouse model

Katharina Sorg,<sup>a,\*</sup> Patricia Stahn,<sup>a</sup> Lukas Pillong,<sup>a</sup> Marius P. Hinsberger,<sup>a</sup> Larissa Heimann,<sup>a</sup> Hans-Jochen Foth,<sup>b</sup> Bernhard Schick,<sup>a</sup> and Gentiana I. Wenzel<sup>a,\*</sup>

<sup>a</sup>Saarland University, Department of Otolaryngology, Faculty of Medicine, Homburg, Germany

<sup>b</sup>University of Kaiserslautern, Department of Physics, Kaiserslautern, Germany

**Abstract.** Hearing impairment affects ~460 million people worldwide. Conservative therapies, such as hearing aids, bone conduction systems, and middle ear implants, do not always sufficiently compensate for this deficit. The optical stimulation is currently under investigation as an alternative stimulation strategy for the activation of the hearing system. To assess the biocompatibility margins of this emerging technology, we established a method applicable in whole-mount preparations of murine tympanic membranes (TM). We irradiated the TM of anesthetized mice with 532-nm laser pulses at an average power of 50, 89, 99, and 125 mW at two different locations of the TM and monitored the hearing function with auditory brainstem responses. Laser-power-dependent negative side effects to the TM were observed at power levels exceeding 89 mW. Although we did not find any significant negative effects of optical stimulation on the hearing function in these mice, based on the histology results further studies are necessary for optimization of the used parameters. © The Authors. Published by SPIE under a Creative Commons Attribution 4.0 Unported License. Distribution or reproduction of this work in whole or in part requires full attribution of the original publication, including its DOI. [DOI: 10.1117/1.JBO.24.8.085003]

Keywords: biocompatibility; optical stimulation; tympanic membrane; optoacoustic; laser.

Paper 190084RR received Mar. 25, 2019; accepted for publication Jul. 29, 2019; published online Aug. 21, 2019.

## 1 Introduction

Hearing impairment is a worldwide problem that affects individuals of all ages. There are 460 million people worldwide with hearing impairment and have problems communicating on a daily basis.<sup>1</sup> To compensate for hearing deficit, conventional hearing devices use mechanical energy and, for cases with severe hearing impairment, cochlear implants use electrical energy to stimulate the auditory system. However, for the hard of hearing population who are not yet candidates for cochlear implants and not sufficiently supplied with the currently available auditory prostheses due to multiple reasons, e.g., recurrent outer ear canal inflammations or connectivity issues, further stimulation strategies are needed.<sup>2</sup> Light has been considered as an alternative energy form for the activation of the hearing organ, having the advantage to be a noninvasive and precise noncontact activation method.<sup>3–5</sup> The optical stimulation of the ear has been assessed via three different ways, the infrared neural stimulation (INS),<sup>3,6–9</sup> the optoacoustic stimulation,<sup>10–12</sup> as well as optogenetics, the activation of neural structures that are genetically modified to express light-sensitive ion channels.<sup>4,13,14</sup> The optoacoustic stimulation is induced by the use of very short laser pulses that are absorbed into the irradiated materials and lead to a short thermal expansion that induces mechanical vibrations. It was first proposed and studied for the optical stimulation of the inner ear using a monochrome laser.<sup>15</sup> Recently, we were able to demonstrate that the optoacoustic stimulation has the advantage to induce precise vibrations within all vibrating

structures from the ear drum up to the inner ear without the need of direct contact to the vibratory structure.<sup>2,16,17</sup> Independent of the final irradiated structure, the biocompatibility of this stimulation method has to be defined and characterized. Up to now, just a few specific biocompatibility studies regarding the laser application at the ear drum are to be found in literature. Foth et al. described the power density limits for the laser-induced thermal effects for laser Doppler vibrometry<sup>18</sup> being 7.2 kW/cm<sup>2</sup> for the pig TM. Another set of studies described the effects of laser irradiation for the low-level laser therapy (LLLT) of the inner ear<sup>19</sup> as well as trans-tympanic photobiomodulation (PBM).<sup>20</sup> Both work far below our values using an 830-nm diode laser with power densities of 900 mW/cm<sup>2</sup> in the case of LLLT and 909 to 1363 mW/cm<sup>2</sup> for PBM. However, due to the fact that they used another wavelength (830 nm) and that the laser parameters were not exactly in the range of our used parameters, these reports could not give us enough safety margins for a clinical application of the optoacoustic stimulation either. In addition, the tympanic membrane (TM) is anatomically very complex. It consists of collagen fibers, embedded in epithelium with mucosa on the middle-ear side and epidermis on the outside<sup>21,22</sup> as well as blood vessels. It closes the air-filled tympanic cavity and spans over the bony structure of the malleus. All these together create a very inhomogeneous structure with various absorption characteristics at different locations inducing different laser–tissue interactions. For these reasons, we established a method to assess the biocompatibility margins for light stimulation of the hearing organ and present herein our results regarding the effects of the optoacoustic stimulation with 10-ns 532-nm laser pulses at the TM in a mouse model.

\*Address all correspondence to Katharina Sorg, E-mail: Katharina.Sorg@uks.eu; Gentiana I. Wenzel, E-mail: Gentiana.Wenzel@uks.eu

## 2 Material and Methods

### 2.1 Animal Model

Eight- to 12-week-old female CBA/J mice (Janvier Labs, France) weighing 18 to 23 g were used in our experiments (44 animals in total in this study). The studies were performed according to the guidelines of "The Animal Care and Use Committee of Saarland." All animals were initially anesthetized intraperitoneally with 100 mg/kg ketamine (Ketaset, Zoetis, Berlin; Germany), 10 mg/kg xylazine (Rompun, Bayer, Leverkusen; Germany), and a maintenance dose of  $\frac{1}{4}$  to  $\frac{1}{2}$  of the initial dose intraperitoneally every 30 min. Throughout the experiment, the body temperature of the animal was maintained at 37°C using an electric heating pad, and the animals were supplied with additional oxygen over a tube positioned at nose level. The hearing function of all animals was monitored via auditory brainstem response (ABR) recordings before and within 5 to 10 min after the laser stimulation.

### 2.2 Surgical Procedure

After we trimmed the hair around the outer auditory canal, we made a vertical incision beginning at the *incisura intertragica* and expanding it along the cartilaginous outer ear canal. The TM was exposed by anchoring the edges of the incision with sutures. To assess possible heat-induced changes by laser irradiation on the TM, a positive control based on heat treatment was established. A 70°C to 80°C preheated metal pin of 0.5 mm diameter was carefully pressed on the TM for 20 s without mechanically damaging the membrane. A further control was the contralateral ear that was left untreated, however that received the same manipulation for the exposure of the TM to ensure the detection of preparation-induced necrotic cell conditions.

### 2.3 Laser Irradiation

This stimulation protocol was established in cell culture experiments and has been used for the optoacoustic stimulation in the guinea pig in our group as well.<sup>2</sup> The laser irradiation was always performed on the left ear of the mice. We used a 532-nm pulsed neodymium-doped yttrium orthovanadate (Nd:YVO<sub>4</sub>) laser (Xiton Photonics GmbH, Kaiserslautern, Germany) as the light source. The pulsed laser light was applied through a glass fiber with a diameter of 365  $\mu\text{m}$ , which we directed vertically toward the umbo or the *pars tensa* of the TM, at  $\sim 300$  to 500  $\mu\text{m}$  using a micromanipulator (Narishige, Tokyo, Japan). The final adjustments were performed using a continuous wave (cw) pilot laser with a power of 0.1 mW and duration of maximum of 30 s. The laser irradiation parameters were chosen to replicate our self-designed stimulation strategy creating a sinusoid signal at the targeted frequency, the laser-modulation rate (LMR) (Fig. 1).

We irradiated the selected area for 2 min with an average power of either 50, 89, 99, or 125 mW at a laser repetition rate (LPR) of 50 kHz and LMR of 1 kHz as presented in Table 1.

### 2.4 Electrophysiological Monitoring: Auditory Brainstem Response

The recording of ABRs was performed in the same way as previously reported.<sup>23–26</sup>

The sounds in the form of sine wave stimuli were generated with a digital signal processing system (Agilent 33500 B Series True form Waveform Generator, Keysight Technologies GmbH,

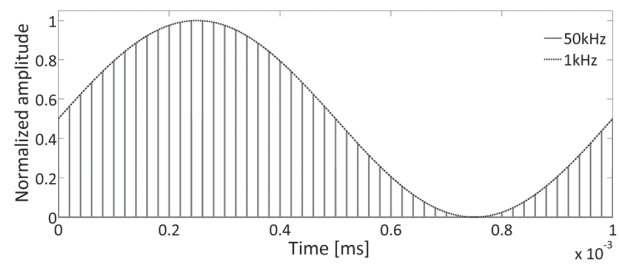


**Fig. 1** Our designed stimulation strategy with the laser modulation rate of 1 kHz (black dotted line) and the LPR of 50 kHz (light gray peaks).

**Table 1** Used laser parameters.

Average power (mW)	Energy per pulse ( $\mu\text{J}$ )	Average radiant exposure ( $\text{J}/\text{cm}^2$ )	Average power density ( $\text{W}/\text{cm}^2$ )	Irradiation at the umbo ( $n$ animals)	Irradiation at the <i>pars tensa</i> ( $n$ animals)
50	1	3000	25	7	6
89	1.8	5340	44.5	8	4
99	1.99	5940	49.5	5	5
125	2.5	7500	62.5	4	5

Germany) and were delivered through a free field speaker (custom made from a DT-911, Beyerdynamic GmbH & Co. KG, Germany<sup>26</sup>) placed in a 5-cm distance in front of the left ear (the irradiated ear). We recorded click- and frequency-specific ABRs using subcutaneous needles: one on the mastoid, one at the vertex (reference), and one at the base of the tail (ground). The recorded signals were then amplified through the biosignal amplifier (g.USBamp, g.tec medical engineering GmbH, Austria), digitized at 19.2 kHz, and filtered to obtain the frequencies from 300 to 2500 Hz. The stimulus intensities ranged from 0 to 80 dB SPL increased in 10 dB steps at 2, 4, 8, 12, 16, 20, 32, and 48 kHz. For click ABRs 500 trials and for fABRs 128 trials were averaged. The speaker output was calibrated periodically. The hearing thresholds were determined visually during the recording as well as offline and were defined by the lowest intensity where the Jewett's wave complex was identifiable (see Sec. 3, Fig. 5). The Jewett complex was first described by Jewett and Williston in 1971.<sup>27</sup> In mice, it typically consists of five vertical positive waves between 1 and 6 ms.<sup>28–30</sup> We focused on the wave I within the ABR-complex, representing mainly the activity of the first neuron of the auditory pathway<sup>31</sup> and through this being the closest measure for the function of each ear independently (no crossing neural pathways yet of the auditory pathway). However, due to the small head shadow (diameter of a mouse head being in average 1.2 cm) of mice, one should keep in mind that free field stimulation will always lead to some deterioration and underestimation of ABR measures (see Sec. 4). The amplitude values of wave I were defined by the total value between the first negative peak ( $I_n$ ) to the first positive peak ( $I_p$ ) whereas the latency was determined at peak  $I_p$  (see Sec. 3, Fig. 4). All animals represented in Table 1 were analyzed ( $n = 44$  in total). In a control experiment, ABR measurements were again repeated after 3 h of incubation

( $n = 4$  animals). We measured the amplitude of the wave I peak and the latency of the positive part of wave I at the hearing threshold as well as 10, 20, and 30 dB above this.

#### 2.4.1 Fluorescence microscopy

We explanted the petrosal bone of each animal and trimmed down the outer ear canal to its bony part. We then removed the main part of the bony ear canal, down to the bony ring expanding the eardrum as well as parts of the petrosal bone, to expose the TM even better. The tympanic cavity was then opened and trimmed down to the *annulus fibrosus* of the TM. By separating the ossicular chain and cutting the tendon of the *tensor tympani* muscle, the TM was extracted tightly bounded to its bony ring. The explanted TM specimen was placed in 37°C preheated Dulbecco's modified eagle medium and incubated in a 5% CO<sub>2</sub> incubator (Forma Scientific) for 3 h to ensure the maturation of possible cytotoxic effects due to the laser irradiation. After incubation, the specimen was stained for the detection of apoptotic, necrotic, and healthy cells (apoptotic/necrotic/healthy cells detection kit-Promokine; Heidelberg, Germany). This staining protocol was transferred from the cell culture experiments results of our group using the same staining dies.<sup>32</sup> The specimen was washed and subsequently incubated in staining solution, substituted with fluorescence marked Hoechst 33342, Annexin V and Ethidium-Homodimer III for 30 min. After removing the staining solution, the TM specimen was examined

and analyzed under a fluorescence stereomicroscope (Leica Microsystems; Wetzlar, Germany). The three used fluorescent dies (Fig. 2) mark different cell conditions: healthy cells nuclei were stained only in blue, nuclei of necrotic cells appeared in red and blue, and cells stained with triple colors were dead cells progressing from the apoptotic cell population. The results of the staining were used to quantify the resulting areas of necrotic cells in relation to the whole TM. This was performed with the help of measuring-tools implemented in the microscope software (LASX software, Leica Microsystems, Wetzlar; Germany) and Microsoft Excel<sup>®</sup>. The calculations were performed manually using the measured diameter of the elliptically formed TM and of the necrosis area.

#### 2.4.2 Statistical analysis

The statistical analysis was performed with OriginPro<sup>®</sup> software. If the data were normally distributed and had homogeneity of variance, we conducted two-sided paired *t*-tests for the analysis of the hearing function. Otherwise, the statistical data analysis was performed by Wilcoxon signed-rank test. In case of amplitude and latency measurements, we considered the result of each acoustic stimulation level as an individual value and compared the results before (pre) and after (post) the irradiation at each stimulation level (Figs. 6 and 7). Likewise, we considered each frequency of the fABR analysis as individual values (Fig. 8) and compared the response at each sound level before

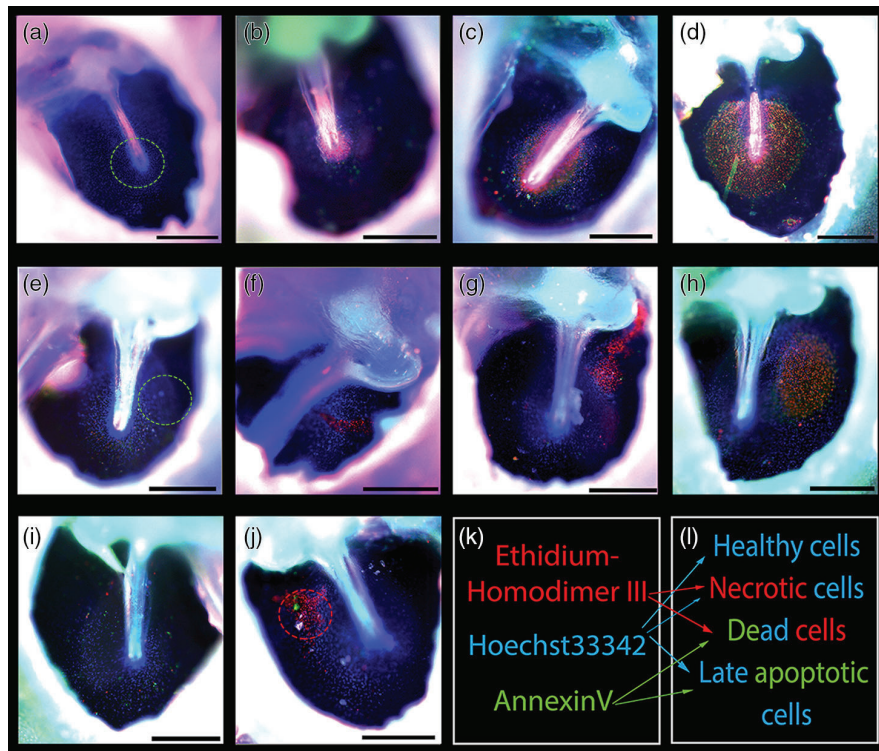


**Fig. 2** Fluorescence staining with apoptotic/necrotic/healthy cells detection assay (Promokine, Germany) after irradiation (a)–(d) at the umbo or (e)–(h) at the pars tensa with average power of (a), (e) 50 mW; (b), (f) 89 mW; (c), (g) 99 mW; and (d), (h) 125 mW, respectively. (i) The negative control was not treated; (j) the heat treatment served as a positive control for necrotic cells (red dotted circle). The irradiated region of all specimens is representatively marked as a green dotted circle in the left column. (k) The assay is based on three different stainings which mark specifically (l) different cell conditions. The images demonstrate representative examples of TM. Scale bar represents 500  $\mu\text{m}$ .

and after irradiation. For the control experiment with three measurements, we performed a univariate ANOVA with repeated measures for normally distributed data and otherwise a Friedman-ANOVA. The reported alpha level was 0.05.

### 3 Results

#### 3.1 Fluorescence Microscopy

We herein present results of the laser application at the umbo and at the *pars tensa* (Figs. 2 and 3). The viability staining performed after laser irradiation gave insight into the distribution of healthy versus apoptotic or necrotic cells within the irradiated TM. The data are presented herein in comparison to the control, nonirradiated ear [Fig. 2(i)] and grouped with respect to the average laser power applied as presented in Table 1. The fluorescence images demonstrate representative examples of the irradiated TM groups.

The results of the fluorescence live/dead staining demonstrated that the laser irradiation with an average power of 50 mW had no effect on the viability of the exposed TM [Fig. 2(a)]. By applying pulses with an average power of 89 mW, first discrete necrotic cell areas around the irradiated location were induced [Figs. 2(b) and 2(f)]. This area of necrotic cells increased in size with increasing laser input (Fig. 3). The irradiations with 99 mW lead to a circular zone of necrotic cells right around the umbo [Fig. 2(c)] and to nearly round areas at the *pars tensa* [Fig. 2(g)]. The necrotic area increased further at 125 mW [Figs. 2(d) and 2(h)]. For the laser application at the *pars tensa*, the thresholds were the same, but the necrotic areas were smaller compared to the irradiation at the umbo. The negative control (nonirradiated TM) [Fig. 2(i)] only demonstrated isolated necrotic or apoptotic cells, which can be attributed to normal physiologic conditions of permanent cell regeneration in the TM. The positive control (heated instrument applied onto the TM) [Fig. 2(j)] leads to an almost round-shaped necrotic cell area similar to the area that was induced through the laser treatment.

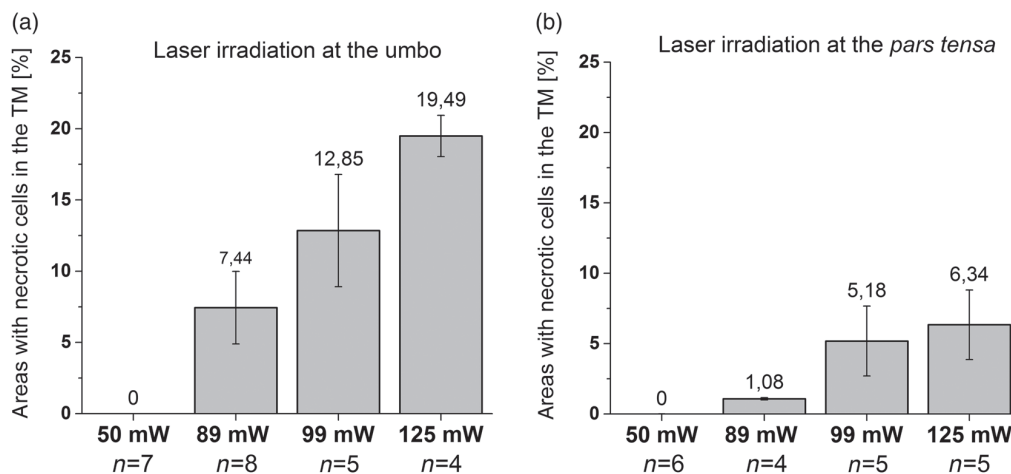
The quantification of the proportions of areas with necrotic cells of all irradiated eardrums (see Table 1) confirmed the visually estimated results within the fluorescence imaging (Fig. 3).

The proportion of areas with necrotic cells after the irradiation at the umbo with 89 mW was around ~7% and raised up to ~20% after the irradiation with 125 mW [Fig. 3(a)]. In comparison, the areas with necrotic cells in the *pars tensa* were clearly smaller and grew less in size after the irradiation [Fig. 3(b)]. The proportions were ~1% after the irradiation with 89 mW going to ~6% after the irradiation with 125 mW. The lower increase in necrotic cell areas after irradiation at the *pars tensa* may be due to the fact of a lower absorption of the laser light on the transparent TM compared to the higher absorption at the umbo region, caused by the bony malleus.

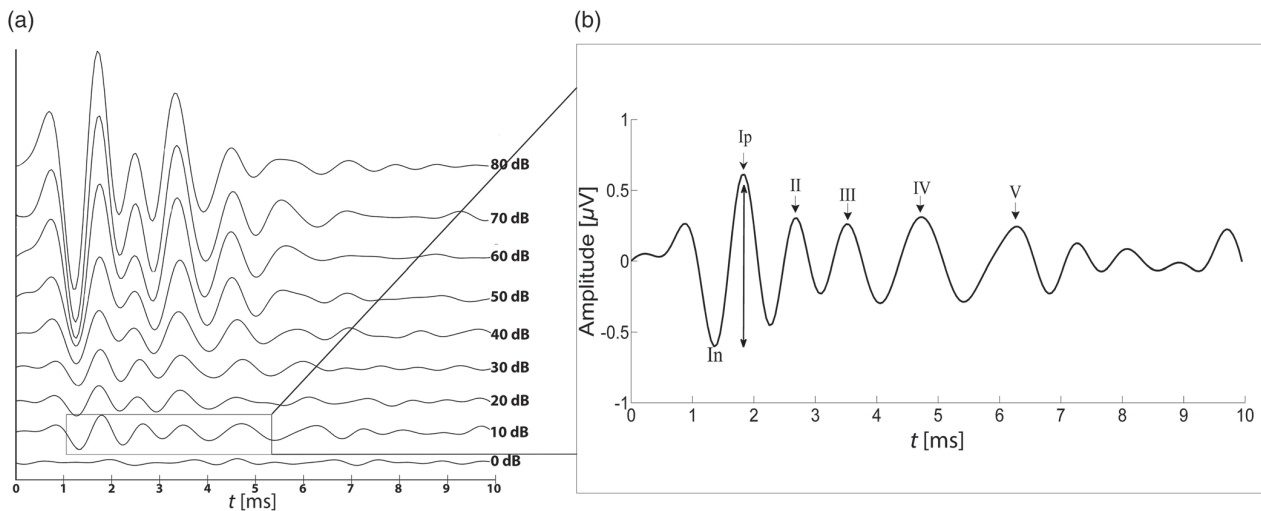
#### 3.2 Electrophysiological Monitoring: Auditory Brainstem Response

Figure 4 shows exemplary the filtered ABR signal of one mouse after the stimulation with click acoustic stimuli from 0 to 80 dB SPL. As described in Sec. 2, the threshold was determined as the lowest intensity where the waveform complex I to V was detectable. Typically, the amplitude value at the threshold was around 1  $\mu$ V. We also analyzed the averaged hearing thresholds to gain an insight into the effect of laser irradiation. This demonstrated that the mice had an overall hearing threshold at the beginning of the experiment between 10 and 30 dB SPL. We compared the results of the mice irradiated at the umbo [Fig. 5(a)] as well as the ones irradiated at the *pars tensa* [Fig. 5(b)] with the results to the negative control mice (not irradiated) [Fig. 5(c)].

After the irradiation with 50 mW at the umbo, the average threshold increased with 5 dB and after the irradiation with 125 mW around 10 dB. Both increases were, however, statistically not significant. In contrast, no threshold shift could be detected at the other power levels (89 and 99 mW) [Fig. 5(a)]. After the irradiation at the *pars tensa*, the average hearing threshold increase was around 10 dB at all power levels; however, being statistically nonsignificant again [Fig. 5(b)]. In addition, we performed a control experiment in which the animals were anesthetized receiving click ABR and fABR at the same time intervals as in the laser experiments, however without laser exposure [Fig. 5(c)]. In these animals, no threshold shift could be observed. To clarify if there are long-term



**Fig. 3** Proportions of areas with necrotic cells of the whole TM after laser irradiation (a) at the umbo or (b) at the *pars tensa* with 50, 89, 99, and 125 mW, respectively. Error bars represent the SEM. The  $n$  indicates the amount of preparations that were analyzed that can also be found in Table 1.



**Fig. 4** Example of (a) an evoked click ABR signal from 0 to 80 dB SPL and (b) a filtered detail plot of ABR waves at the threshold (10 dB SPL in this case). At the threshold, the Jewett wave complex consisting of wave I to V is clearly identifiable for the first time above the noise floor. We analyzed wave I in our study and thereby determined the amplitude from peak  $I_n$  to  $I_p$  and the latency at peak  $I_p$ .

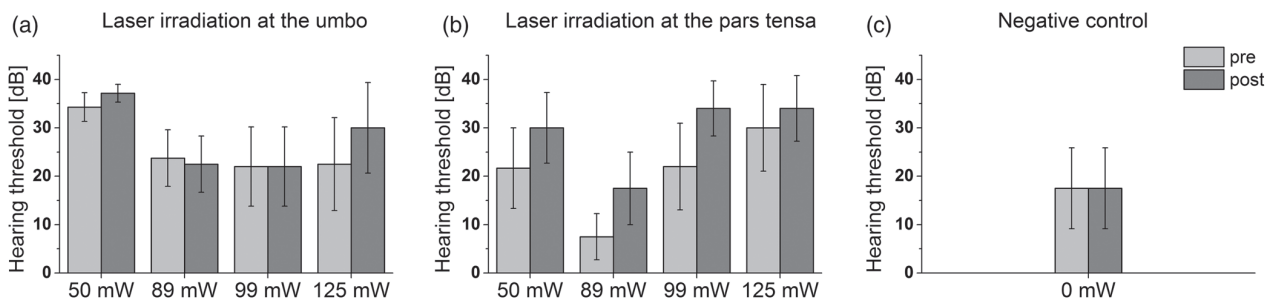


**Fig. 5** Click-evoked hearing thresholds of mice that were irradiated (a) at the umbo or (b) at the pars tensa with 50, 89, 99, or 125 mW, respectively. (c) Negative control mice were not irradiated. The error bars represent the SEM.

consequences of these nonstatistically significant differences after laser exposure, further long-term experiments are planned.

In addition to the hearing thresholds, we also analyzed the wave I amplitude and latency values of wave  $I_p$  before and after the irradiation as a further measure for the functionality of the auditory pathway (analysis exemplary shown in Fig. 4) at threshold and at 10, 20, and 30 dB above threshold.

The amplitude values demonstrated in all cases the typical increase with higher acoustic stimuli (Fig. 6). For the irradiation at the umbo, the amplitude values started to be nonsignificantly higher after the irradiation with 99 mW having after the irradiation with 125 mW an even more visible increase [Fig. 6(a)]. After the irradiation at the *pars tensa*, the amplitude values were not significantly higher starting from 50 mW [Fig. 6(b)]. At 125-mW irradiation power, the increase between the amplitude of wave I before (pre) and after (post) irradiation was the highest, however lower compared to the irradiation with the same levels at the umbo and being still statistically not significant. In the negative control mice group, we could not detect any differences in amplitude values between before and after the incubation time.

The latency values of the positive peak of wave I ( $I_p$ ) before and after the irradiation as a measure for the functionality of the

auditory pathway as well as for comparison to the nonirradiated negative control are presented in Fig. 7.

The average latency of wave I varied between 1.6 and 1.8 ms demonstrating a minimal trend to decrease with increasing intensity of the acoustic stimuli [Figs. 7(a) and 7(b)]. The irradiation with 50 mW at the umbo [Fig. 7(a)] induced a significant increase of the latencies at +10 dB over threshold. The irradiation with 99 mW induced a significant increase of the latencies from +0 to +20 dB but being not significant at +30 dB above threshold. The latency values demonstrated a trend to be lower after the irradiation at *pars tensa* [Fig. 7(b)], especially after the irradiation with 99 and 125 mW, this difference being however statistically nonsignificant. One exception could be observed in the negative control mice that demonstrated a significant increase at +30 dB acoustic stimuli. Considering an increased in latency as a negative neural effect, based on these first experiments, no consistent neural damage after the laser irradiation could be detected. The only exception observed was after the irradiation with 99 mW at the umbo that needs to be further explored in future experiments.

Additionally, we analyzed the fABR thresholds of all irradiated and negative-control mice before and after the irradiation, respectively (Fig. 8).

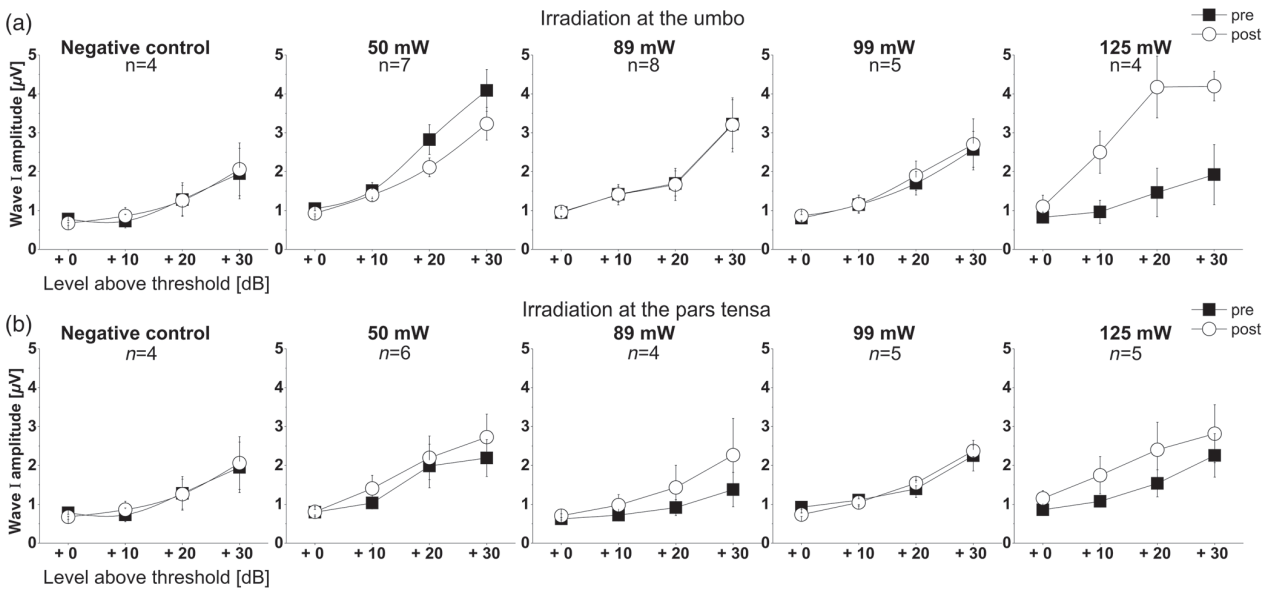


**Fig. 6** Analysis of the wave I amplitude before and after the irradiation with 50, 89, 99, and 125 mW average power (a) at the umbo or (b) at the pars tensa. Black squares indicate the amplitude values before (pre) the irradiation, white circles after (post) the irradiation. In both lines, the negative control (nonirradiated mice) experiment is plotted as the reference. Error bars represent the SEM.

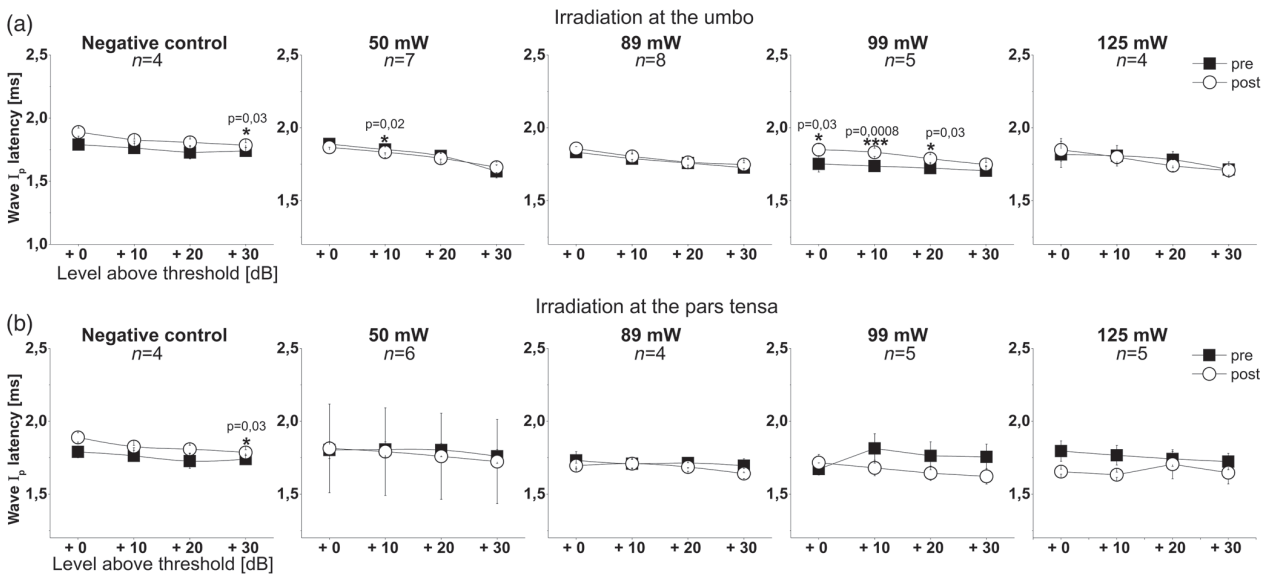


**Fig. 7** Analysis of the positive peaks in wave I latency ( $I_p$ ) before and after the irradiation with 50, 89, 99, and 125 mW average power (a) at the umbo or (b) at the pars tensa. Black squares indicate the latencies before (pre) irradiation, white circles after (post) irradiation. In both lines, the negative control (nonirradiated mice) experiment is plotted as the reference. Error bars represent the SEM and significant different values are marked with a star.

The analysis of the fABR thresholds from 4 to 48 kHz stimulation demonstrated that in all groups the mice had no statistically significant threshold shift with increasing average laser power. The negative control fABRs demonstrated a nonsignificant partial threshold shift as well [Fig. 8(c)]. Interestingly, the threshold shift in these mice after the incubation time was even higher compared to the irradiated mice in the frequencies from 20 up to 48 kHz.

In another control experiment, we analyzed the effects of laser-induced cytotoxicity on the TM on the hearing function within the first 3 h after irradiation on a small collective of animals ( $n = 4$ ). The hearing function was measured before the irradiation with 125 mW at the umbo (pre), directly after the irradiation (post 1) and 3 h later (post 2), analyzing at hearing threshold the wave I amplitude, wave  $I_p$  latency and the frequency-specific thresholds (Fig. 9).

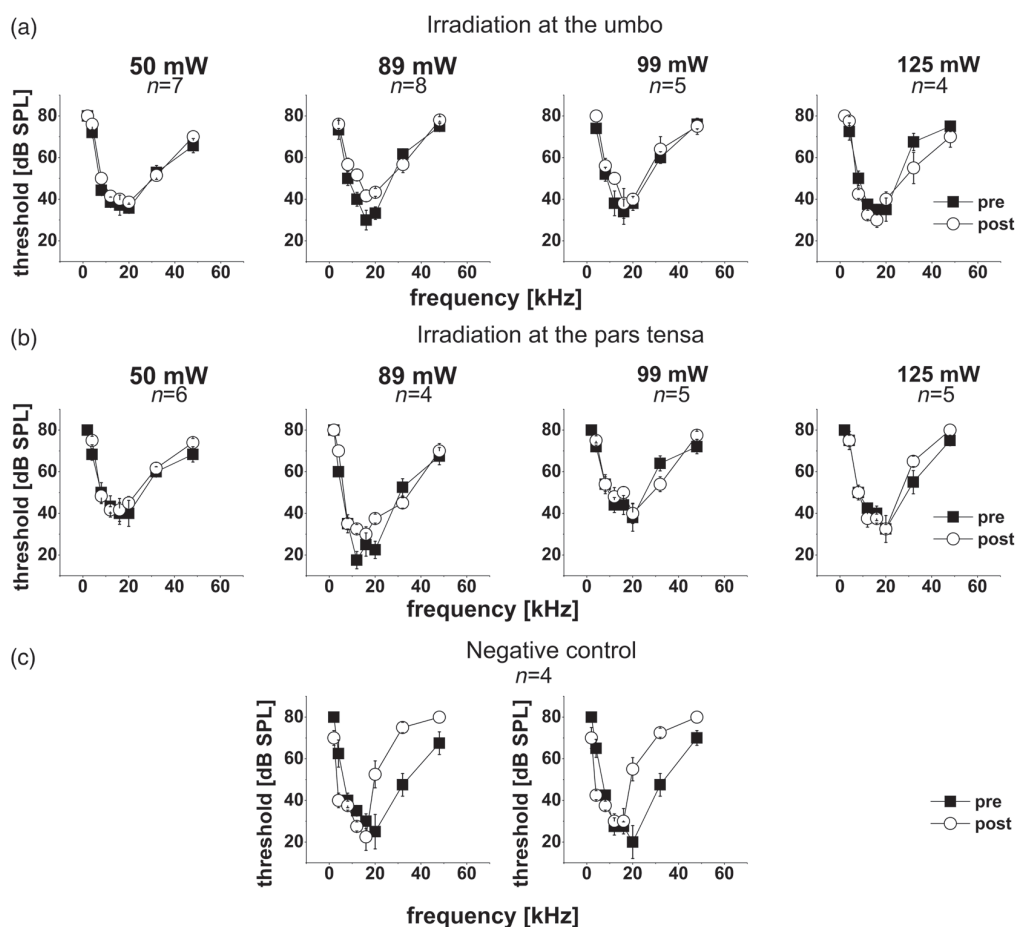


**Fig. 8** Analysis of fABR measurements for the irradiation (a) at the umbo and (b) the pars tensa with 50, 89, 99, and 125 mW average laser power, respectively. (a) fABR measurements of the irradiated ear before (pre) and after (post) the irradiation. (b) fABR measurements of the irradiated ear before (pre) and after (post) the irradiation at the pars tensa. (c) Negative control fABR data of the left and the right ear of mice that were not irradiated. Error bars represent the SEM.

Interestingly, the control experiment demonstrated that the average hearing threshold increased with around 10 dB after 3 h of incubation on the irradiated ear being however statistically insignificant in this small group of animals. The fABR analysis showed no significant threshold shift. However, as already mentioned, the nonirradiated contralateral ear could lead to small

deterioration and underestimation of the monaural ABR measurements in this case as well.

#### 4 Discussion

We were able to establish a method for the detection of cytotoxic effects on the TM in a whole-mount model, herein presented to

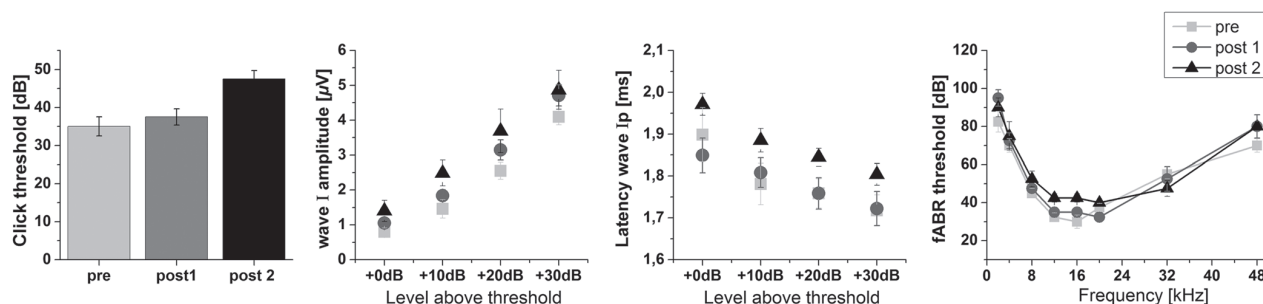


**Fig. 9** Analysis of the hearing function of control mice characterized by click ABR threshold, amplitude values of wave I, latency of  $I_p$ , and fABR threshold which were measured at three different time points: before the irradiation (pre), directly after (post 1), and 3 h after the irradiation (post 2)  $n = 4$ .

our knowledge for the first time in the literature. The simultaneous staining of necrotic, apoptotic, and healthy cells gave us insight into the viability of the laser-exposed membrane *in toto*. Additionally, we established a negative and a positive control demonstrating that the staining specifically and repetitively marked necrotic areas within the whole-mount TM mouse model. Using this whole-mount viability assay, we examined the laser-induced effects on the TM after optoacoustic stimulation applied in a sinusoidal form of the pulse sequences. The irradiation with an LPR of 50 kHz and an LMR of 1 kHz for 2 min duration appeared to be safe up to an average power of 50 mW. In our experiments, the irradiation of the eardrum with average laser power of 89 mW induced discrete areas of necrotic cells around the irradiated zone at the umbo as well as at the *pars tensa*. These results could be due to a thermal effect and/or the absorption of green laser light by the surrounding blood vessels in the TM and/or by bony structures, e.g., the umbo or the surrounding tympanic cavity (*bulla tympanica*). Green laser light has been chosen in the originally designed experiments being considered to have a very good biocompatibility potential as visible light. However, our current data demonstrate that through the high absorption of green light by hemoglobin and its clotting effect within the irrigating blood vessels these laser parameters induced cell damage starting at higher laser intensities. In this regard, diminished nutrition and oxygen supply as well as decreased thermal buffering function of the irrigated area are the mechanisms to be discussed. In addition, the affected areas demonstrated to be bigger in the mice irradiated at the umbo compared to those, which received the irradiation at the *pars tensa*. This effect might be caused by at least two factors: (1) the additional high absorption of green laser light within the bony structure of the malleus inducing supplementary heat formation; (2) the clotting effect onto more central vessels in the umbo then at the *pars tensa*. Both may be induced by the fact that the underlying mechanism of the optoacoustic stimulation is a photothermal-laser interaction. In detail, the optoacoustic stimulation is the result of short photon absorption events within the irradiated tissues.<sup>5,11,16,33,34</sup> The energy introduced by light is converted into kinetic energy, leading to a local increase of the temperature. This rise in temperature will result in a thermoelastic expansion leading at constant volume to an increase in pressure. The permanent alteration between increase and decrease of pressure values during this thermoelastic expansion and relaxation inside of the irradiated material leads to the development of a sound wave that propagates through the irradiated tissue. To gain an optimal stimulation signal, the principle of stress confinement<sup>35</sup> should be fulfilled meaning that the laser pulses have to be shorter than the time the acoustic signal needs to propagate through the tissue. Thereby, no energy dissipation happens during the generation of the acoustic signal.<sup>16</sup> However, since we are irradiating inhomogeneous biological structures, the rules of physics cannot be transferred in an absolute mean, and the thermal side effects at high energies can be observed. The safety limits are therefore mandatory to be defined in order to use the optoacoustic effect for stimulation purposes. In our case, one possible reason for the formation of areas with necrotic cells in the TM might be the induction of heat by the high LPR. The thermal damage in laser-tissue interactions in general is dependent on the tissue temperature, the time the tissue remains at the temperature, and the time intervals between the light exposures.<sup>36</sup> Computer-based modeling of laser irradiation of the human and the guinea pig cochlea

demonstrated a heat conduction that reached a quasi-steady-state after a few seconds. The rise in temperature was thereby dependent on the laser pulse rate.<sup>37</sup> In addition, the photothermal interaction itself is dependent on the diverse properties of the irradiated tissue, e.g., the optical properties (absorption and scattering), the thermal and mechanical properties, the chemical composition as well as the anatomy and the physiology of the irradiated tissue.<sup>36</sup> For the TM, these parameters are not sufficiently characterized, yet. Furthermore, the complex histology of the TM consisting of different materials such as bone, collagen fibers, epithelial cells, and blood vessels makes it difficult to investigate the possible laser-tissue interactions just through theoretical calculations. In our case, the absorption of hemoglobin<sup>38</sup> and collagen/bone<sup>39</sup> appears to play the leading role. Furthermore, the TM as a dry structure, surrounded by air and relatively low-perfused by blood may lead to a low temperature dissipation and therefore to the accumulation of heat during the irradiation period in the TM. Therefore, there is the clear need to define the laser safety parameters and the optical properties of the TM since the laser-tissue interactions are dependent on both: the applied laser parameters and the characteristics of the irradiated structure. As a comparison, in another study in which we chose to use lasers to induce collagen remodeling in the TM, we had to additionally apply a red pigment onto targeted areas of the TM before irradiation to increase its energy absorption and induce the proposed structural changes in our animal model.<sup>23</sup>

As briefly mentioned in Sec. 1, very few investigations regarding laser safety for the application at the TM are available in literature. These reports of nondestructive laser application are focusing on the LLLT<sup>40,41</sup> or PBM.<sup>20,42</sup> PBM is performed with near-infrared laser light and laser-parameters similar to ours, thus with 165- to 200-mW average power and radiant exposures between 1350 and 3272 J/cm<sup>2</sup>,<sup>19,40,43</sup> using macroscopic observation by endoscopy and microscopic observation, e.g., hair cell counting or scanning electron microscopy for assessing the biocompatibility. However, for PBM and LLLT, cw lasers are applied and consequently, the biocompatibility results are hard to compare to the effects of pulsed nanosecond lasers. Another noninvasive application analyzed the thermal thresholds at the TM for laser Doppler vibrometry. This study from Foth et al. presents the safe use of 633-nm cw laser for this application. It reveals a large difference between the power density of 80 W/cm<sup>2</sup> classically used in laser Doppler vibrometry and the experimental damage threshold of 7100 W/cm<sup>2</sup> for the irradiation of the pig TM analyzed with via hematoxylin & eosin (H&E).<sup>18</sup> In addition, the studies related to INS,<sup>3,8,44</sup> e.g., Goyal et al., analyzing the effect of infrared laser light at the cochlea could not find any significant effect within the electrophysiological signals generated in the inner ear after continuous irradiation below 30  $\mu$ J/pulse. Histologically, they did not observe any structural changes of the tissue while working with a diode laser at 1869 nm and with 100  $\mu$ s pulse length either.<sup>8</sup>

In our study, no significant effects of the irradiation on the hearing function could be demonstrated since any significant increase in hearing thresholds could be detected following the irradiation. The fact that we did not find any correlation between bigger areas with necrotic cells and an increase in hearing threshold after irradiation at the TM is most probably due to the distance from the TM to the sensory cells within the inner ear and therefore too far and insulated by surrounding structures to

be negatively influenced. No significant changes in amplitude values, after the irradiation at the umbo or at the *pars tensa*, could be identified either. This fact conflicted with the finding of higher latency values in one group, after the irradiation at the umbo with 99 mW. Since this effect is singular and has not been confirmed in our experiments in the mice groups irradiated with higher laser intensity, further analyzes need to be performed for a closer characterization of this presumed effect. The results within the negative control mice did demonstrate significantly higher latency values at +30 dB acoustic stimulation, indicating either possible anesthesia-induced effects or physiological changes during the incubation/ irradiation time that need to be taken in account to the cumulative results as well.

The results of the further control experiment analyzing the effects 3 h after the laser exposure did show a nonsignificant trend for higher threshold values. One reason for this might be heat-induced edema formation in the middle ear or the alteration of the vibratory characteristics of the TM. The elasticity of the TM might be influenced by the laser irradiation because of the heat-formation, leading to altered vibrations and thus, changed sound perception to the middle ear and the inner ear. In addition, one should keep in mind the influence of free field stimulation on the contralateral ear and the possible underestimation of the ABR-measurements, which could lead to minor, nonsignificant effects. These possible confounding effects between the ears cannot be easily ruled out in the current presented experimental set. We see the best solution for this in improving our future experimental design regarding this and planning experiments using an animal model that has an increased inter-aural difference.

## 5 Conclusion

We established a new method to analyze the biocompatibility of light application at the mouse TM. The optoacoustic stimulation at least up to 50 mW was demonstrated to be safe in our experiments. Above 89 mW, the irradiated areas demonstrating cells with affected viability increased with increasing average power. These effects could be due to a thermal effect and/or the absorption of green laser light by the surrounding blood vessels in the TM or by bony structures, such as the umbo or the surrounding *bulla* inducing a debilitating blood supply of the affected tissue. No clear relation between higher laser powers and increased hearing thresholds could be detected in these experiments. Although we did not find any significant negative effect of optoacoustic stimulation on the hearing of mice, we need to improve the used parameters based on the histology results as well as the experimental setup. Further studies are therefore forthcoming for the optimization of the applied laser parameters for a safe optoacoustic stimulation method of the hearing organ.

## Disclosures

The authors have no relevant financial interests in this article and no potential conflicts of interest to disclose.

## Acknowledgments

This research has been funded by the European Research Council under the European Union's Seventh Framework Program (FP/2007-2013)/ERC Grant, LaserHearingAids: 311469.

## References

1. World Health Organization, "Deafness and hearing loss," 2018, <https://www.who.int/news-room/fact-sheets/detail/deafness-and-hearing-loss> (accessed 7 December 2018).
2. P. Stahn et al., "Frequency-specific activation of the peripheral auditory system using optoacoustic laser stimulation," *Sci. Rep.* **9**(1), 4171 (2019).
3. A. D. Izzo et al., "Laser stimulation of the auditory nerve," *Lasers Surg. Med.* **38**(8), 745–753 (2006).
4. T. Moser, "Optogenetic stimulation of the auditory pathway for research and future prosthetics," *Curr. Opin. Neurobiol.* **34**, 29–36 (2015).
5. G. I. Wenzel et al., "Green laser light activates the inner ear," *J. Biomed. Opt.* **14**(4), 044007 (2009).
6. A. D. Izzo et al., "Laser stimulation of auditory neurons: effect of shorter pulse duration and penetration depth," *Biophys. J.* **94**(8), 3159–3166 (2008).
7. H. K. Young et al., "Target structures for cochlear infrared neural stimulation," *Neurophotonics* **2**(2), 025002 (2015).
8. V. Goyal et al., "Acute damage threshold for infrared neural stimulation of the cochlea: functional and histological evaluation," *Anat. Rec.* **295**(11), 1987–1999 (2012).
9. R. U. Verma et al., "Auditory responses to electric and infrared neural stimulation of the rat cochlear nucleus," *Hear. Res.* **310**, 69–75 (2014).
10. G. I. Wenzel, T. Lenarz, and B. Schick, "Welche Farben könnten wir hören?" *HNO* **62**(2), 82–87 (2014).
11. N. Kallweit et al., "Optoacoustic effect is responsible for laser-induced cochlear responses," *Sci. Rep.* **6**(1), 28141 (2016).
12. M. Schultz et al., "Nanosecond laser pulse stimulation of the inner ear: a wavelength study," *Biomed. Opt. Express* **3**(12), 3332–3345 (2012).
13. V. H. Hernandez et al., "Optogenetic stimulation of the auditory nerve," *J. Visual Exp.* (92), e52069 (2014).
14. W. Guo et al., "Hearing the light: neural and perceptual encoding of optogenetic stimulation in the central auditory pathway," *Sci. Rep.* **5**(1), 10319 (2015).
15. A. Fridberger and T. Ren, "Local mechanical stimulation of the hearing organ by laser irradiation," *Neuroreport* **17**(1), 33–37 (2006).
16. K. Zhang et al., "Optoacoustic induced vibrations within the inner ear," *Opt. Express* **17**(25), 23037–23043 (2009).
17. G. I. Wenzel et al., "Effects of green light application at ear drum and middle ear level," in *ARO Midwinter Meeting*, Baltimore (2010).
18. H. J. Foth et al., "Thermal damage threshold at 633 nm of tympanic membrane of pig," *Hear. Res.* **142**(1–2), 71–78 (2000).
19. C.-K. Rhee et al., "Effect of low-level laser treatment on cochlea hair-cell recovery after ototoxic hearing loss," *J. Biomed. Opt.* **18**(12), 128003 (2013).
20. T. H. Moon et al., "Safety assessment of trans-tympanic photobiomodulation," *Lasers Med. Sci.* **31**(2), 323–333 (2016).
21. D. J. Lim, "Human tympanic membrane," *Acta Otolaryngol.* **70**(3), 176–186 (1970).
22. D. J. Lim, "Structure and function of the tympanic membrane: a review," *Acta Otorhinolaryngol. Belg.* **49**(2), 101–115 (1995).
23. S. A. L. Schacht et al., "Laser-induced tissue remodeling within the tympanic membrane," *J. Biomed. Opt.* **23**(12), 121614 (2018).
24. L. Rüttiger et al., "The reduced cochlear output and the failure to adapt the central auditory response causes tinnitus in noise exposed rats," *PLoS One* **8**(3), e57247 (2013).
25. J. Engel et al., "Two classes of outer hair cells along the tonotopic axis of the cochlea," *Neuroscience* **143**(3), 837–849 (2006).
26. T. Schimmang et al., "Lack of Bdnf and TrkB signalling in the postnatal cochlea leads to a spatial reshaping of innervation along the tonotopic axis and hearing loss," *Development* **130**(19), 4741–4750 (2003).
27. D. L. Jewett and J. S. Williston, "Auditory-evoked far fields averaged from the scalp of humans," *Brain* **94**(4), 681–696 (1971).
28. J. J. Chuu, C. J. Hsu, and S. Y. Lin-Shiau, "Abnormal auditory brainstem responses for mice treated with mercurial compounds: involvement of excessive nitric oxide," *Toxicology* **162**(1), 11–22 (2001).
29. K. P. Hunter and J. F. Willott, "Aging and the auditory brainstem response in mice with severe or minimal presbycusis," *Hear. Res.* **30**(2–3), 207–218 (1987).
30. Q. Y. Zheng, K. R. Johnson, and L. C. Erway, "Assessment of hearing in 80 inbred strains of mice by ABR threshold analyses," *Hear. Res.* **130**(1–2), 94–107 (1999).

31. J. F. Willott, "Measurement of the auditory brainstem response (ABR) to study auditory sensitivity in mice," *Curr. Protoc.* **34**(1), 8.21B.1–8.21B.12 (2006).
32. L. Pillong et al., "Biocompatibility studies of optical stimulation via 532 nm-laser pulses on human fibroblasts," *Laryngo-Rhino-Otol.* **97**(S 02), S232 (2018).
33. A. G. Bell, "On the production and reproduction of sound by light," *Am. J. Sci.* **s3-20**(118), 305–324 (1880).
34. M. J. Colles, N. R. Geddes, and E. Mehdizadeh, "The optoacoustic effect," *Contemp. Phys.* **20**(1), 11–36 (1979).
35. G. Paltauf, H. Schmidt-Kloiber, and M. Frenz, "Photoacoustic waves excited in liquids by fiber-transmitted laser pulses," *J. Acoust. Soc. Am.* **104**(2), 890–897 (1998).
36. S. Thomsen, "Pathologic analysis of photothermal and photomechanical effects of laser-tissue interactions," *Photochem. Photobiol.* **53**(6), 825–835 (1991).
37. K. Zhang et al., "A contrastive analysis of laser heating between the human and guinea pig cochlea by numerical simulations," *Biomed. Eng. Online* **15**(1), 59 (2016).
38. B. L. Horecker, "The absorption spectra of hemoglobin and its derivatives in the visible and near infra-red regions," *J. Biol. Chem.* **148**, 173 (1943).
39. J. Behari, S. K. Guha, and P. N. Agarwal, "Absorption spectra of bone," *Calcif. Tissue Res.* **23**(1), 113–114 (1977).
40. Y. M. Park et al., "Trans-canal laser irradiation reduces tinnitus perception of salicylate treated rat," *Neurosci. Lett.* **544**, 131–135 (2013).
41. A. Tamura et al., "Low-level laser therapy for prevention of noise-induced hearing loss in rats," *Neurosci. Lett.* **595**, 81–86 (2015).
42. M. Y. Lee et al., "Photobiomodulation by laser therapy rescued auditory neuropathy induced by ouabain," *Neurosci. Lett.* **633**, 165–173 (2016).
43. C.-K. Rhee et al., "Effect of low-level laser treatment on cochlea hair-cell recovery after acute acoustic trauma," *J. Biomed. Opt.* **17**(6), 068002 (2012).
44. J. D. Wells et al., "Optically mediated nerve stimulation: identification of injury thresholds," *Lasers Surg. Med.* **39**(6), 513–526 (2007).

**Katharina Sorg** is a PhD student at Saarland University in the Department of Otolaryngology. She received her BS degree in 2013 and her MS degree at University Marburg in biomedical science in 2015. In 2016, she started her PhD. Her current research interests include the effects of optical stimulation on the ear and the development of innovative stimulation strategies for hearing impaired persons, based on the use of light energy.

Biographies of the other authors are not available.

## 2) Cytotoxicity studies of an optoacoustic stimulation strategy for the development of laser-based hearing aids

Lukas Pillong, Patricia Stahn, Marius Hinsberger, Katharina Sorg, Bernhard Schick, Gentiana I. Wenzel

Contribution of the authors:

Lukas Pillong designed and performed the experiments, analyzed the data, and composed the manuscript. Patricia Stahn developed and programmed the software used to perform the experiments and assisted during the experiments, as Marius Hinsberger also did. Katharina Sorg assisted during the experiment preparations, as well as, with the design, the composition of the manuscript and with scientific discussions. Bernhard Schick assisted during manuscript preparation and with scientific discussions. Gentiana I. Wenzel worked on the study conception, assisted with the study design, data analysis, during manuscript preparation and with scientific discussions.

# Cytotoxicity studies of an optoacoustic stimulation strategy for the development of laser-based hearing aids

Lukas Pillong,\* Patricia Stahn, Marius Hinsberger, Katharina Sorg,  
Bernhard Schick, and Gentiana I. Wenzel\*

Saarland University, Department of Otorhinolaryngology, Faculty of Medicine,  
Homburg, Germany

## Abstract

**Significance:** Worldwide, ~460 million people suffer from disabling hearing impairment. Many of these patients are still not sufficiently supplied with currently available auditory technologies. Optical stimulation of the hearing organ offers a promising alternative for a new generation of auditory prostheses.

**Aim:** To assess the biocompatibility margins of our laser pulse amplitude strategy *in vitro*, we designed a protocol and present the effects on normal human dermal fibroblasts, human chondrocytes, and human osteoblasts.

**Approach:** Laser pulses of 532 nm were applied over 120 s using our laser pulse amplitude modulation strategy. We then assessed cell viability and cytotoxicity through fluorescence staining and quantitative polymerase chain reaction-analysis regarding 84 key player-genes for cytotoxicity and stress response.

**Results:** The first *in vitro* biocompatibility margins for our stimulation parameters applied to cells of the peripheral hearing organ were between 200 and 223 mW (3348 J/cm<sup>2</sup>). After irradiation with a subphototoxic laser power of 199 mW (2988 J/cm<sup>2</sup>), only the fibroblasts showed a significant upregulation of GADD45G.

**Conclusion:** Further studies are underway to optimize parameters for the optoacoustic stimulation of the auditory system. Our protocol and results on laser–tissue interactions can be useful for translational laser applications in various other irradiated biological tissues.

© The Authors. Published by SPIE under a Creative Commons Attribution 4.0 Unported License. Distribution or reproduction of this work in whole or in part requires full attribution of the original publication, including its DOI. [DOI: [10.1117/1.JBO.25.6.068002](https://doi.org/10.1117/1.JBO.25.6.068002)]

**Keywords:** biocompatibility; 532 nm; laser; optoacoustic stimulation; human fibroblasts; osteoblasts; chondrocytes; hearing impairment.

Paper 200066R received Mar. 14, 2020; accepted for publication Jun. 5, 2020; published online Jun. 23, 2020.

## 1 Introduction

Approximately 460 million people worldwide are suffering from disabling hearing impairment. Factors such as growing global population, longer mean life expectancies, and increased exposure to environmental noise contribute to a growing hard of hearing population. Untreated hearing impairment not only leads to a decreased quality of life and social isolation, but also poses an economic burden with annual global costs of ~750 billion international dollars.<sup>1</sup>

Despite the rapid technological progress and innovations within the field of auditory prostheses, a large number of hard of hearing people are still not sufficiently supplied with the currently available technologies. In addition, many patients who have received conventional hearing aids do not use them regularly or at all. Reasons for this lack of compliance are, for example, insufficient frequency-specific gain, especially in a noisy environment, deficient wearing comfort, feedback and occlusion effects, and recurrent inflammations of the outer ear canal.<sup>2</sup>

---

\*Address all correspondence to Lukas Pillong, E-mail: [lukas.pillong@uks.eu](mailto:lukas.pillong@uks.eu); Gentiana I. Wenzel, E-mail: [gentiana.wenzel@uks.eu](mailto:gentiana.wenzel@uks.eu)

Consequently, new stimulation strategies are required to more specifically address the needs of the hard of hearing population. Photons could provide a fast, specific, and contactless energy transfer into vibratory structures of the hearing organ giving rise to a new generation of light-driven hearing aids.

The first local mechanical stimulation of the hearing organ using laser light was reported in 2006 by Fridberger and Ren.<sup>3</sup> In 2009, Wenzel et al. demonstrated a controlled, contact-free activation of the vibratory structures within the inner ear (Wenzel et al. 2009<sup>4</sup> and Zhang et al. 2009<sup>5</sup>) and one year later demonstrated the possibility to use this method for the application at different loci, from the tympanic membrane to the inner ear.<sup>6</sup> However, for frequency specific activation of the hearing organ using optoacoustic stimulation at the eardrum level, a coding strategy based on laser pulse amplitude modulation had to be designed.<sup>7</sup>

To achieve this within the developmental work, we have to take into account the fact that biocompatibility is a fundamental requirement for any medical device. To date, there is only poor knowledge about the effects of 532-nm laser light on human cells and none with the modulation parameters as used in the stimulation strategy described by Stahn et al.<sup>7</sup> Therefore, in this study, we proposed to establish an *in vitro* cell-culture-based model that would enable us to investigate the effects of our optoacoustic laser amplitude modulation strategy on human cells in parallel to our *in vivo* studies in a mouse model.<sup>8</sup> These two studies together were planned to define a first biologically safe power range keeping in mind its application for a laser-based hearing aid.

The tympanic membrane is a complex, oval shaped, trilaminar structure, consisting of an outer layer of squamous cell epithelium, a middle layer (lamina propria) formed by fibroblasts and collagen fibers, and an inner layer of mucosal epithelium. The distribution of collagen fibrils in the lamina propria contributes to the elastic properties of the eardrum.<sup>9</sup> This membrane is anchored and spanned to a fibrocartilage ring along the circumference of the outer ear canal and connected to the bony structure of the malleus at the tympanic side. This architecture enables the tympanic membrane to move in complex vibration modes to transmit energy to the middle and inner ears. The inhomogeneous structure of this tissue with various absorption characteristics at different locations exhibits the potential for complex laser–tissue interactions. For these reasons, we needed to establish a method to assess the cytotoxicity thresholds for our optoacoustic stimulation with 10-ns 532-nm laser pulses in an *in vitro* model using human fibroblasts, chondrocytes, and osteoblasts as three representative cell types for the irradiated tissue.

## 2 Materials and Methods

### 2.1 Cells, Culture Conditions, and Media

In our studies, we used three different adherent human primary cell types to mimic natural conditions as closely as possible: normal human dermal fibroblasts (NHDF), human chondrocytes (HCH), and human osteoblasts (HOB). The cells were cultured in phenol red-free media [fibroblast basal medium 2 (phenol red-free)/chondrocyte basal medium (phenol red-free)/osteoblast basal medium] and the corresponding supplement mix (Promocell, Heidelberg, Germany) to avoid absorption by the media at a wavelength of 532 nm. Adherent cells were seeded out in a 96-well flat-bottom microtiter plate (glass) (Viewplate 96-F, PerkinElmer, Rodgau-Jügesheim, Germany) and covered with 100- $\mu$ l phenol red-free medium. The cells were incubated at 37°C with 5% CO<sub>2</sub> for 48 h until the monolayer culture had reached confluence.

### 2.2 Laser Setup

We used a pulsed 532-nm neodymium-doped yttrium orthovanadate laser system (INCA, Xiton Photonics GmbH, Kaiserslautern, Germany). The parameters for the laser amplitude modulation (Fig. 1) were generated as described before<sup>7</sup> on a personal computer (PC) (Hewlett-Packard Company /HP Inc., Palo Alto, California, USA). The laser system was operated with a predetermined laser pulse rate (LPR) of 50 kHz. We transferred a MATLAB® (R2014a, MathWorks Inc., Natick, Massachusetts, USA) that generated a continuous sinusoid signal to a waveform generator (33500b Waveform Generator, Agilent Technologies, Santa Clara, California, USA)

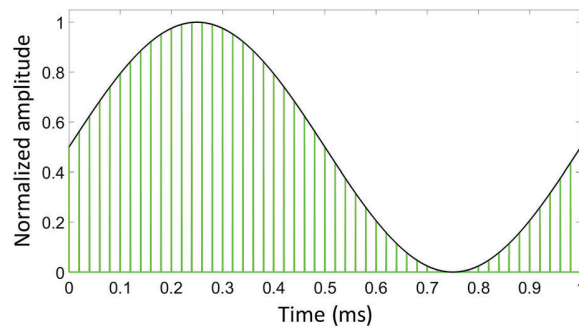


**Fig. 1** Our laser amplitude modulation strategy with a laser modulation rate of 1 kHz and laser repetition rate of 50 kHz (green vertical lines). (Figure modified from Sorg et al.<sup>8</sup>)

as an arbitrary file via a Virtual Instrument Software Architecture interface. This sinusoid laser signal was sent to the input of the acousto-optic modulator (AOM) (Xiton Photonics GmbH, Kaiserslautern, Germany). The laser pulses were then delivered to the target well using the laser fiber ( $\varnothing 365 \mu\text{m}$ ) that was connected to the AOM.

Before irradiation, the culture medium was removed from two wells: (1) the well that was going to be irradiated and (2) the corresponding untreated control well. The culture plate was placed on a platform with the irradiated well positioned above a pinhole in the bearing surface (Fig. 2). The laser fiber was positioned in the center of the well at a distance of about 1.5 mm from the surface of the well bottom, allowing the laser spot to cover  $\sim 0.8 \text{ mm}^2$  of the monolayer. The fiber tip pointed in a right angle toward the bottom of the well and was positioned manually with the help of a micromanipulator (Narishige, Tokyo, Japan). Underneath the pinhole, we positioned a mirror at a 45-deg angle to divert the laser beam in a 90-deg angle, accomplishing a one-way passage of the photons through the irradiated surface. The reflected laser beam was then projected onto a screen that allowed us to assess the shape and homogeneity of the laser spot online. Cells were irradiated for 120 s with our laser pulse amplitude modulation strategy (Fig. 1) that would induce a sinusoid of 1 kHz using an LPR of 50 kHz.

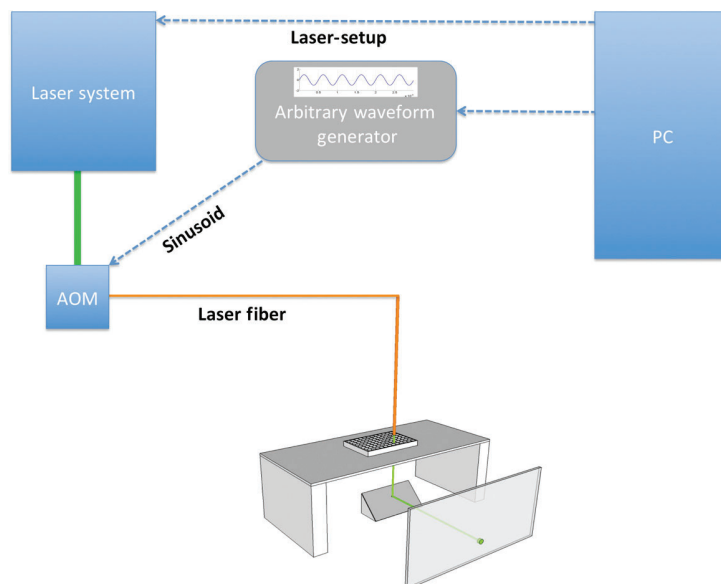


**Fig. 2** Experimental set up. Laser parameters were defined on a PC via MATLAB<sup>®</sup>. Information concerning the laser power sent to the laser system and the sinusoid signal generated by the MATLAB<sup>®</sup> was transferred to an arbitrary wave generator and sent to the AOM. A laser fiber connected to the AOM delivered the laser pulses to the target structure.

**Table 1** Laser parameters used in our experiments regarding average power, energy per pulse, average radiant exposure, and average power density.

Average power (mW)	Energy per pulse ( $\mu$ J)	Average radiant exposure ( $J/cm^2$ )	Average power density ( $W/cm^2$ )
177	3.5	2652	22.1
199	4	2988	24.9
223	4.5	3348	27.9
250	5	3756	31.3
281	5.6	4212	35.1
315	6.3	4728	39.4
354	7	5316	44.3
397	8	5952	49.6
500	10	7500	62.5

The laser parameters used in our studies are shown in Table 1. After irradiation, the cells in the irradiated group as well as the controls were supplied with 100  $\mu$ l of fresh culture medium and the plate was incubated at 37°C with 5% CO<sub>2</sub> for the following steps of the experiment.

### 2.3 Fluorescence Staining and Microscopy

To assess the cytotoxicity margins of laser irradiation, we performed fluorescence staining using an Apoptotic/Necrotic/Healthy cells detection kit (Promokine, Heidelberg, Germany). The kit uses fluorescein isothiocyanate (FITC)-labeled Annexin-V, Ethidium homodimer III, and Hoechst 33342 as fluorescence markers. Membrane-permeable, minor groove-binding deoxyribose nucleic acid (DNA) stain Hoechst 33342 is used for blue-fluorescent ( $\lambda_{abs}/\lambda_{em} = 350/461$  nm) staining of the entire cell population.

Ethidium homodimer III has a high affinity to DNA staining of the nuclei of necrotic cells red ( $\lambda_{abs}/\lambda_{em} = 528/617$  nm), but cannot enter into healthy cells. Annexin-V is a phospholipid protein with a high affinity to phosphatidylserine, which is present on the outer membrane layer during apoptosis. Apoptotic cells are consequently stained green by FITC-labeled Annexin-V (FITC;  $\lambda_{abs}/\lambda_{em} = 492/514$  nm) (Fig. 3).

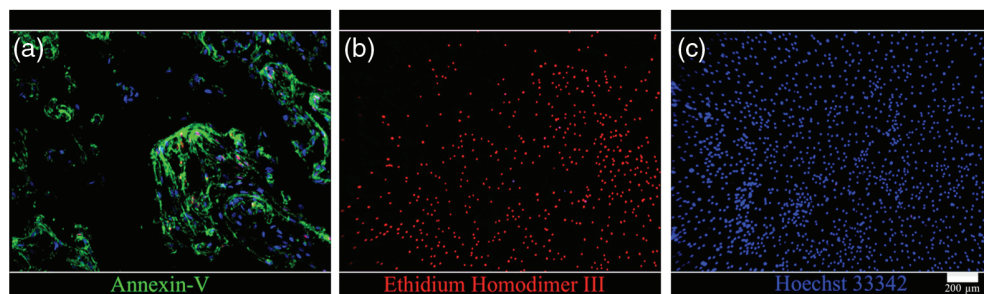


**Fig. 3** (a) A positive control for apoptosis was established using staurosporine. Apoptotic cells are stained green with FITC-Annexin-V binding to the outer membrane leaflet of apoptotic cells. (b) A positive control for detection of necrotic cells was achieved using a black filter that was placed under the glass bottom of the well being irradiated. Nuclei of necrotic cells are stained red with Ethidium Homodimer III. (c) Hoechst 33342 as a membrane-permeable probe stains the nuclei of the entire cell population. However, only healthy cells are stained blue. The scale bar represents 200  $\mu$ m.

After irradiation with different laser powers, the cells were washed with a binding buffer. The staining solution was prepared by adding 5  $\mu\text{l}$  of the FITC-Annexin-V, 5  $\mu\text{l}$  of Ethidium Homodimer III, and 5  $\mu\text{l}$  of Hoechst 33342 to the binding buffer. The cells were then covered with the staining solution and incubated for 15 min at room temperature and protected from light. Following another washing step, the samples were analyzed using a fluorescence microscope (Olympus BX61, Olympus Deutschland GmbH, Hamburg, Germany).

## 2.4 Cytotoxicity Assays

### 2.4.1 Lactate dehydrogenase assay

Lactate dehydrogenase (LDH) is an enzyme located in the cytosol of many different cell types. A loss of plasma membrane integrity during cell death leads to a release of LDH into the extracellular space. Thus, measuring the LDH activity in the culture medium can be used as a marker for cell death. With the LDH assay, we chose an enzymatic approach to assess the possible cytotoxicity of the laser treatment in every sample. In addition, although the fluorescence staining method required several washing steps associated with the loss of nonadherent cells, the LDH assay provided information about cell lysis in the entire investigated well.

After irradiation, cells were cultured for 24 h at 37°C with 5% CO<sub>2</sub>. LDH activity in the culture media was determined using an LDH Cytotoxicity Assay Kit (Pierce LDH Cytotoxicity Assay Kit; Fisher Scientific, Schwerte, Germany) correcting for spontaneous LDH release and intrinsic serum-LDH activity in the culture medium.

We compared every irradiated sample with the corresponding untreated control using a paired *t*-test. Taking into account multiple comparisons, we used the Bonferroni correction method.

In addition, we performed a baseline correction, i.e., subtracting the calculated cytotoxicity in the untreated control group from the cytotoxicity of the irradiated group.

### 2.4.2 Water-soluble tetrazolium salt-1 assay

We chose to perform this assay to assess the potential cytostatic effects induced through laser irradiation within the wells.

Following the laser treatment, 10  $\mu\text{l}$  of water-soluble tetrazolium salt (WST)-1 solution was added to 100  $\mu\text{l}$  of culture medium in every well. Cells were incubated at 37°C with 5% CO<sub>2</sub> for 2 h. The conversion of WST-1 to formazan by metabolically active cells was measured using an automated microplate reader (Tecan Infinite 200 Pro; Tecan, Männedorf, Germany) at a wavelength of 450 nm and a reference wavelength of 620 nm.

The results of the WST-1 assay were presented as a percentage of the control value obtained in untreated cells.

## 2.5 RT<sup>2</sup> Profiler™ PCR Array

The effects of laser irradiation in cell cultures were assessed by quantitative polymerase chain reaction (qPCR)-array analysis for the expression of 84 genes related to stress and toxicity pathways using a real-time RT<sup>2</sup> Profiler™ PCR Array: Human Stress and Toxicity Finder™ (Qiagen, Hilden, Germany; Ref. PAHS-003Z).

The array included five housekeeping genes (ACTB, B2M, GAPDH, HPRT1, and PRLP0) as well as controls concerning the efficiency of the reverse transcription, the efficiency of the polymerase chain reaction itself, and the detection of genomic DNA contamination.

The cells were cultured, incubated, and treated as described above.

### 2.5.1 RNA isolation

After an incubation period of 2 h post laser irradiation, we performed total ribonucleic acid (RNA) extraction using the QiaShredder™ Column system and the RNeasy® Micro Kit (Qiagen, Hilden, Germany), including a genomic DNA elimination step. Isolated RNA was eluted in 14  $\mu\text{l}$  of RNase-free water and quantified using the Nanodrop ND-1000 spectrophotometer (NanoDrop Technologies Inc, Wilmington, Delaware, USA).

### 2.5.2 First-strand cDNA synthesis

We achieved first-strand complementary DNA (cDNA) synthesis using the RT<sup>2</sup> First Strand Kit (Qiagen, Hilden). Therefore, 600 ng of total RNA were reverse transcribed in a final volume of 20  $\mu$ l containing another genomic DNA elimination step. Reverse transcription was performed at 42°C for 15 min and stopped by heating the probe at 95°C for 5 min. The cDNA was diluted to 111  $\mu$ l final volume by adding RNase-free water and stored at -20°C until use.

### 2.5.3 PCR array

The PCR components mix was attained by mixing the cDNA with the RT2 SYBR green/ ROX qPCR master mix (SABiosciences, Frederick, Maryland, USA) and RNase-free water according to the manufacturer's instructions. Each well of the 96-well RT<sup>2</sup> Profiler array plate (Qiagen, Hilden, Germany; Ref. PAHS-003Z) containing predispensed specific primer sets was loaded with 25  $\mu$ l of the PCR components mix.

The qPCR reaction was performed for 10 min at 95°C for the activation of the Hot Start DNA Taq Polymerase followed by 40 cycles of 15 s at 95°C and 1 min at 60°C for fluorescence data collection with an ABI Step One Plus instrument (Applied Biosystems® Life Technologies, Darmstadt, Germany).

We analyzed data using the  $\Delta\Delta$ Ct-method. The  $\Delta$ Ct for each pathway focused gene in the array plate was calculated by subtracting the average Ct value of the housekeeping genes from the gene of interest's Ct value. Ct values >35 cycles were considered nondetectable. The  $\Delta\Delta$ Ct value was calculated according to the difference between the  $\Delta$ Ct of the laser irradiated group and one of the untreated control groups. The fold change was calculated by  $2^{(\Delta\Delta\text{Ct})}$  representing the expression level of the sample from the irradiated group in relation to the untreated control group. A fold change of  $\pm 1.5$  was chosen as a cutoff value to determine an expression level relevant for further investigation. Statistical analysis was performed using the Student's *t*-test with *p*-values <0.05 leading to the rejection of the null hypothesis. We did not perform any correction for multiple comparisons since the qPCR array was used as a screening method.<sup>10</sup>

## 3 Results

### 3.1 Fluorescence Staining

After irradiation of human fibroblasts with laser powers up to 199 mW (2988 J/cm<sup>2</sup>), no significant increase in the induction of necrosis or apoptosis in comparison to the nonirradiated group could be observed. Following irradiation with 223 mW (3348 J/cm<sup>2</sup>), discrete circular areas of necrotic cells could be detected beginning in the center of the irradiated spot and increasing with increasing laser power [Fig. 4(a)].

Similar behavior is demonstrated in the HCH and HOB. However, for the chondrocytes, a first upper margin could be determined between 223 mW (3348 J/cm<sup>2</sup>) and 250 mW (3756 J/cm<sup>2</sup>) [Fig. 4(b)] and for the osteoblasts, the first cytotoxic effects could be observed at 285 mW [Fig. 4(c)].

### 3.2 LDH Assay

After irradiation of the fibroblasts with laser powers up to 223 mW (3348 J/cm<sup>2</sup>), no significant cytotoxicity in comparison to the nonirradiated wells could be observed. Following the irradiation with 250 mW (3756 J/cm<sup>2</sup>), a significant difference from the control group (*p* < 0.0001), with a mean laser-irradiation-associated cytotoxicity of *circa* (ca.) 1.8% could be detected. With growing laser power, a significant increase in the cytotoxic response in the irradiated group with a mean of ca. 3.5% at 315 mW and ca. 10.4% at 500 mW [Fig. 5(a)] could be observed.

The chondrocytes demonstrated no significant changes regarding the LDH release after irradiation with 223 mW (*p* = 0.3948) and 250 mW (*p* = 0.2462). However, at 281 mW (4212 J/cm<sup>2</sup>), a significant cytotoxicity of ca. 2% could be detected (*p* < 0.0001) that increased with increasing laser power [Fig. 5(b)].

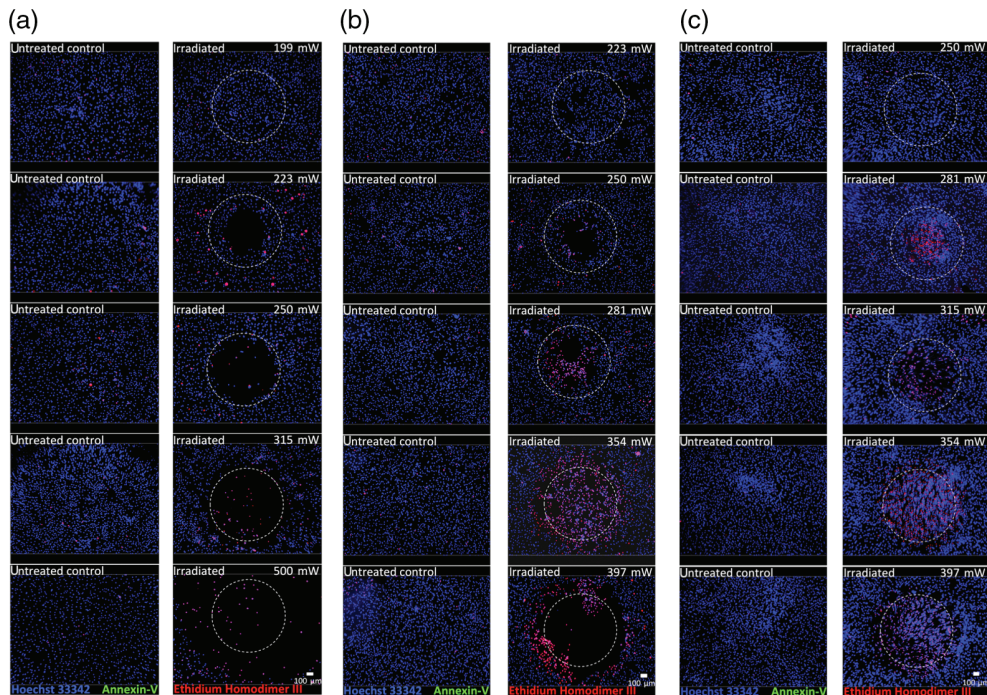


**Fig. 4** Fluorescence staining with the Apoptotic/Necrotic/Healthy cells detection assay (Promokine, Germany) after irradiation of the (a) fibroblasts (NHDF), (b) chondrocytes (HCH), and (c) osteoblasts (HOB) at different average laser powers (right side of each column) and the corresponding untreated control (left side of each column). The irradiated region is representatively marked as a white dotted circle in the right column. Dead cells are stained red (Ethidium Homodimer III), apoptotic cells are stained green (Annexin-V), and vital cells are stained blue (Hoechst 33342). The scale bar represents 100  $\mu\text{m}$ .

The irradiated osteoblasts demonstrated a significantly higher LDH release after application of 315 mW ( $p < 0.0001$ ) laser power in comparison to the nonirradiated controls, increasing as well with increasing laser power.

Interestingly, after the irradiation with a laser power of 250 mW ( $3756 \text{ J/cm}^2$ ), we found a significant lower LDH release in the irradiated culture ( $-1.28\%$ ;  $p = 0.0004$ ) when compared to the nonirradiated controls [Fig. 5(c)].

### 3.3 WST-1 Assay

After the irradiation of the fibroblasts with 199 mW ( $2988 \text{ J/cm}^2$ ) laser power, which was below our predetermined threshold for cytotoxic effects, no significant decrease in viability of the treated group in comparison to the untreated group could be detected. Following laser irradiation with a power of 223 mW ( $3348 \text{ J/cm}^2$ ), we observed a significant decrease in cell viability of ca. 4.2%, and after 250 mW ( $3756 \text{ J/cm}^2$ ) the decrease in cell viability was ca. 5.6%. After irradiation with 315 mW ( $4728 \text{ J/cm}^2$ ), the decrease in cell viability was ca. 8.7% and after 500 mW, the cell viability was ca. 18.5%. According to our prior observations, we noticed a trend for a decline in cell viability with increasing laser power [Fig. 6(a)]. This trend was also found in the chondrocytes and osteoblasts seeded wells.

The irradiation of the chondrocytes with 354 mW induced a significant decrease in viability of ca. 10.9% ( $p < 0.0001$ ) and the irradiation with 397 mW caused a viability loss of ca. 11.1% ( $p < 0.0001$ ). After irradiation of the chondrocytes with laser powers of up to 281 mW ( $4212 \text{ J/cm}^2$ ), we did not find a significant decline in viability [Fig. 6(b)].

In the wells with HOB, we noticed a first significant loss of viability after the irradiation with 281 mW ( $4212 \text{ J/cm}^2$ ), compared to the untreated control, of ca. 4.6% ( $p = 0.0007$ ).

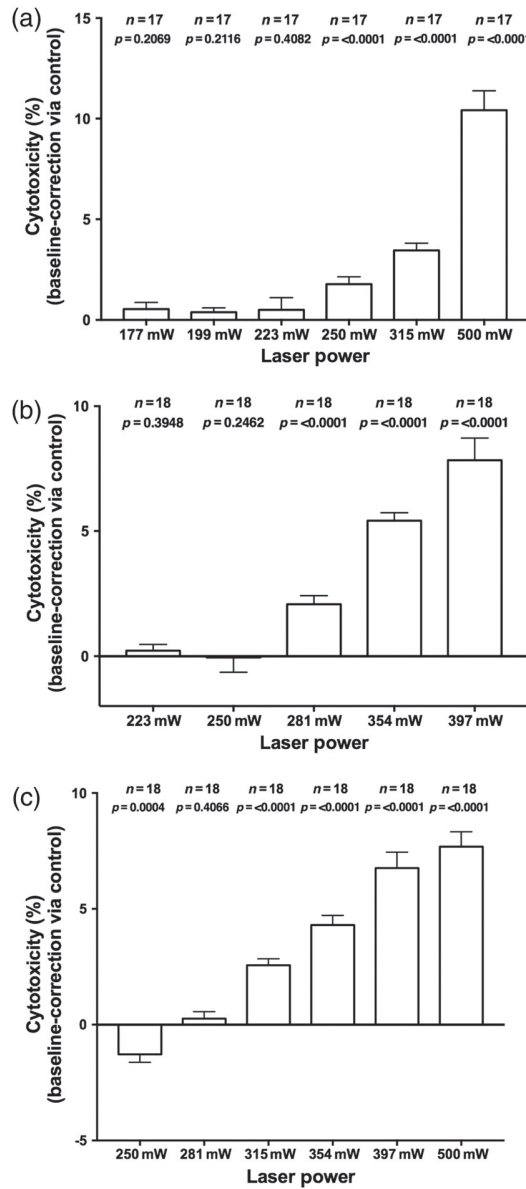


**Fig. 5** Results of the LDH assay displayed as the cytotoxicity in % after irradiation of the (a) fibroblasts (NHDF), (b) chondrocytes (HCH), and (c) osteoblasts (HOB) at different average laser powers. Error bars represent the standard error of the mean (SEM). Adjusted level of significance after Bonferroni correction: (a) and (c)  $p^* = 0.008$  and (b)  $p^* = 0.01$ .

After the irradiation with 250 mW ( $3756 \text{ J/cm}^2$ ), no significant loss of metabolic activity of the osteoblasts could be detected [Fig. 6(c)].

### 3.4 qPCR Analysis

To develop a better understanding about the cellular processes playing a role in the changes observed after irradiation, we performed qPCR analysis for the expression of 84 key player genes known to be involved in cytotoxicity and stress response. We, therefore, irradiated cells, as described above, with laser powers below and above the cytotoxic threshold determined through our experiments and performed qPCR analysis after irradiation.

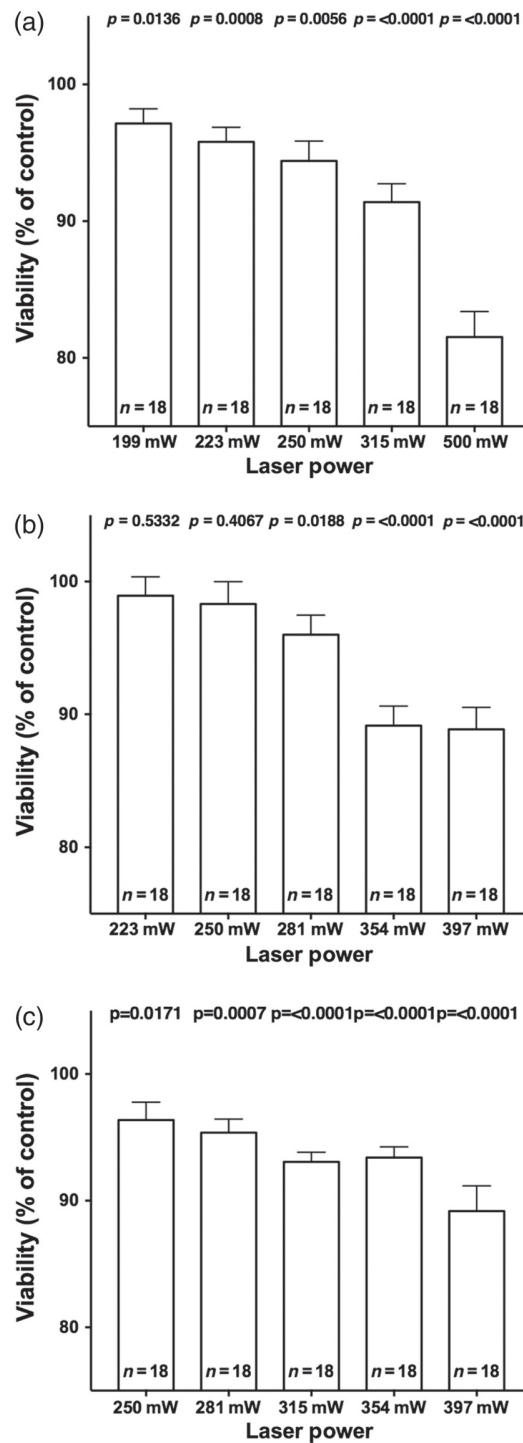


**Fig. 6** Results of the WST-1 assay displayed as the viability in % of an untreated control group after irradiation of the (a) fibroblasts (NHDF), (b) chondrocytes (HCH), and (c) osteoblasts (HOB) at different laser powers. Error bars represent the SEM. Adjusted level of significance after Bonferroni correction:  $p^* = 0.01$ .

### 3.4.1 Normal human dermal fibroblasts

After irradiation with 500 mW, we found 21 of the 84 genes significantly upregulated exceeding the fold change cutoff of 1.5. The upregulated genes derived from different pathways, such as DNA-damage response (GADD45A, XPC, NBN, and CDKN1A), oxidative stress (FTH1,

SQSTM1, and TXNRD1), heat shock response (HSPA4, ATF6B, and BBC3), inflammatory response (CD40LG), hypoxia (SERPINE1 and EPO), and autophagy (ULK1, FAS, ATG7, ATG5, and ATG12). A significant relative downregulation of genes in this panel could not be observed [Fig. 7(a)].

Interestingly, following irradiation with a laser power of 199 mW (2988 J/cm<sup>2</sup>), which was below the predetermined cytotoxic threshold, we found only one of the 84 genes significantly upregulated: GADD45G. A significant downregulation could not be identified [Fig. 7(b)].

### 3.4.2 Human chondrocytes

The irradiation of chondrocytes with a laser power of 500 mW led to a significant upregulation of genes from the heat shock protein (HSP) response and unfolded protein response (BBC3), DNA-damage response (GADD45A), and hypoxia signaling-pathway (VEGFA) with a fold change >1.5. A significant downregulation of genes could not be demonstrated [Fig. 7(c)].

Following the irradiation with a laser power of 199 mW (2988 J/cm<sup>2</sup>), we could find neither a significant upregulation nor downregulation of the genes in the panel [Fig. 7(d)].

### 3.4.3 Human osteoblasts

The irradiation of the HOB with a laser power of 500 mW led to an upregulation of genes associated with osmotic stress response (AQP1), as well as HSP response/unfolded protein response (HSPA4), autophagy (ATG5), cell cycle arrest, and DNA-repair pathway (CHEK2).

Only AQP1 displayed a fold change of 1.78 while HSPA4, ATG5, and CHEK2 demonstrated fold change values below 1.5. A significant downregulation was not observed [Fig. 7(e)].

After the irradiation of the osteoblasts with a laser power of 199 mW (2988 J/cm<sup>2</sup>), we found an upregulation of TLR4 with a fold change of 1.38 and a downregulation of IFNG with a fold change of -1.44, both genes referring to inflammatory response pathways [Fig. 7(f)].

## 4 Discussion

We developed an experimental setup that enabled us to define the first *in vitro* biocompatibility margins for our optoacoustic stimulation within different cell types that can be found in the peripheral hearing organ.

The fluorescence staining, the LDH assay, and the WST-1 assay could confirm a safe application of our stimulation strategy with 532-nm laser pulses *in vitro* with laser powers of up to 199 mW (2988 J/cm<sup>2</sup>), suggesting the first biocompatibility margin for our stimulation parameters to be 200 to 223 mW (3348 J/cm<sup>2</sup>) in our experimental setup. As expected, we found a trend of an increase in cytotoxicity with rising laser powers in all three cell types with different thresholds among them.

Although first cytotoxic effects could be detected in the fibroblasts after irradiation with an average laser power of 223 mW (3348 J/cm<sup>2</sup>), the chondrocytes showed similar effects after irradiation with 250 mW (3756 J/cm<sup>2</sup>) and the osteoblasts with 281 mW (4212 J/cm<sup>2</sup>). These observations imply a difference in vulnerability of the different cell types to the irradiation with the parameters as described above.

There are many studies proposing specific cellular molecules as the key photoacceptors at different wavelengths. Van Breugel and Bär<sup>11</sup> reported several absorption peaks in human fibroblasts around 420, 445, 470, 560, 630, 690, and 730 nm, suggesting several cellular molecules serving as photoacceptors in the visible spectrum. Karu<sup>12</sup> discussed different primary mechanisms of light effects, proposing the terminal respiratory chain oxidase (cytochrome c oxidase) as the main photoacceptor molecule for red-to-near-infrared radiation, such as flavoproteins in the violet-to-blue spectral field. Furthermore, it was suggested that the different oxidation states of all cytochrome c oxidase have different absorption spectra and that the photoacceptor, after its electronic excitation, can be affected by changes in its redox properties leading to an acceleration of electron transfer.<sup>13,14</sup> The biochemical activity could be induced by transient heating of the absorbing chromophore.<sup>15</sup>

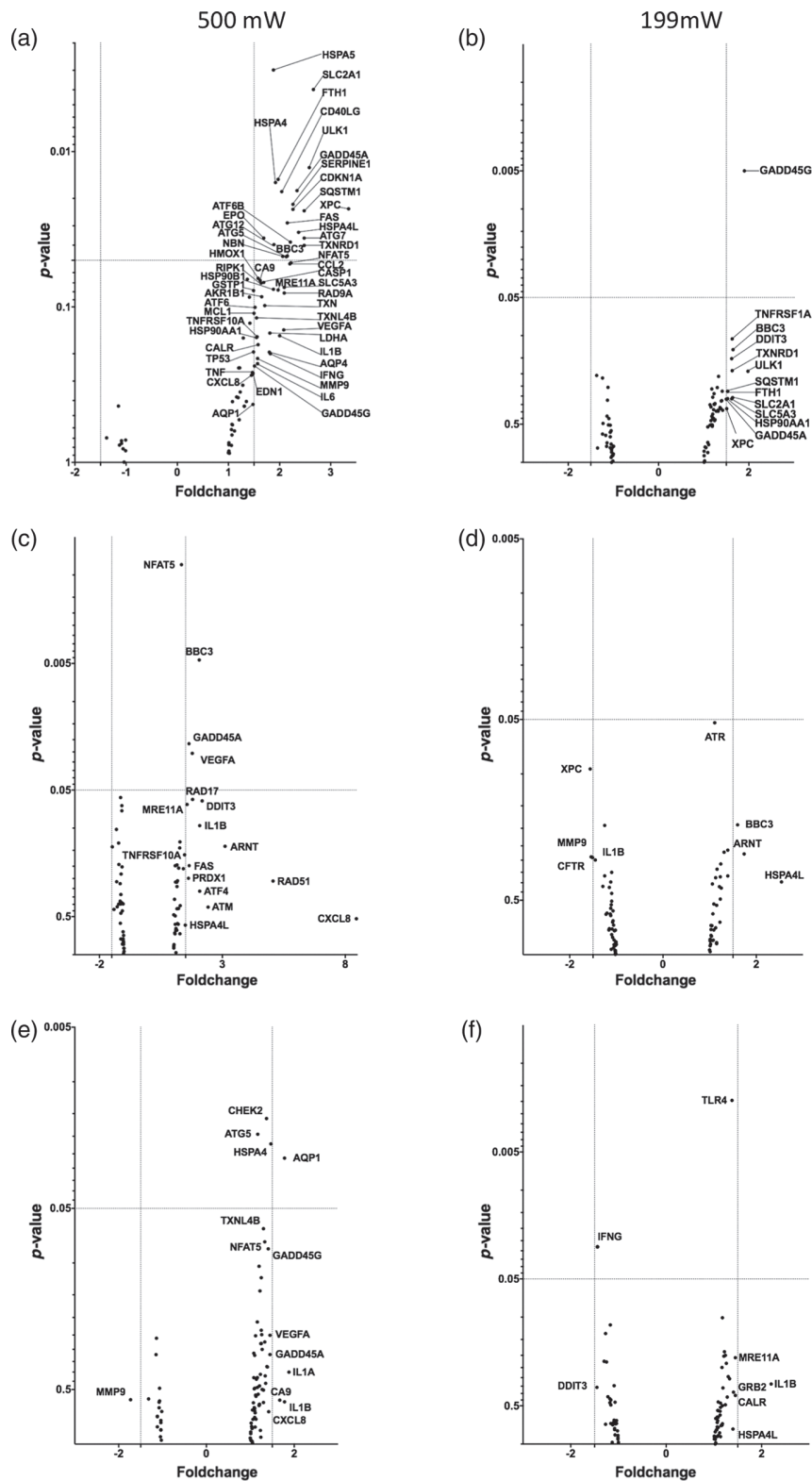


**Fig. 7** Results of the qPCR analysis displayed as volcano plots after irradiation of the (a) and (b) fibroblasts (NHDF), (c) and (d) chondrocytes (HCH), and (e) and (f) osteoblasts (HOB) with a laser power of 500 mW, which is above the cytotoxic threshold [(a), (c), and (e)] and at a laser power of 199 mW, which is below the cytotoxic threshold [(b), (d), and (f)].

Studies addressing the effects of light–tissue interaction on a molecular level are mainly in the optical window from 600 to 1400 nm, but there is only poor information about the effects of green laser light in fibroblasts, chondrocytes, and osteoblasts. Kassák et al. reported that irradiation of Chinese hamster ovarian cells with a wavelength of 532 nm and 30 mW, corresponding to an average radiant exposure of 1146 J/cm<sup>2</sup>, led to a significant increase in the mitochondrial transmembrane potential. The observations were explained with the occurrence of protoporphyrin IX as the key photoacceptor at 532 nm being part of the heme molecule, for example, in cytochrome c.<sup>16,17</sup> Disregarding the differences in the laser modulation modes between our experiments and the setup described by Kassák et al., effects on the mitochondrial function and absorption of the laser light by parts of the respiratory chain should be taken into consideration. The primary underlying effects for the different sensitivities for laser irradiation between the cell types were not addressed further in this study. Our observations could be explained through varying concentrations of the photoacceptor molecules between the different cell types used or by differences in the growth patterns, respectively. Considering the fact that the extent of the affected area was not only laser power- but also time-dependent, as observed in previous experiments (data not shown), the assumption of potential thermal effects as a major damage mechanism seemed the most possible in this set of experiments.

This hypothesis was also supported by the qPCR data demonstrating multiple responses from different stress and toxicity pathways after irradiation above the safety threshold, such as DNA-damage response, oxidative stress, heat shock and inflammatory response, hypoxia, and autophagy.

References for the induction of DNA-damage response pathways following laser irradiation at a wavelength of 532 nm have been reported in the human liver cell line HepG2<sup>18</sup> and hamster fibroblasts.<sup>19</sup> However, the comparability of our results to these studies is very limited due to the use of a 532-nm laser with picosecond pulses and differences concerning the average radiant exposure and power density (Obringer et al.<sup>18</sup>: average radiant exposure: 46.7 J/cm<sup>2</sup> and Leavitt et al.<sup>19</sup>: average power density: 30 GW/cm<sup>2</sup>).

A laser-associated induction of the heat shock response could be observed by Bowman.<sup>20</sup> Human keratinocytes pretreated with the HSP-inductor Herbimycin A showed an increased viability following laser irradiation. Hence, the induction of the HSP response was interpreted as a cytoprotective mechanism.

Khan et al.<sup>21</sup> observed an increased sensitivity of laser-irradiated cells pretreated with an HSP inhibitor, thus supporting the hypothesis of a cytoprotective effect by HSP upregulation. Furthermore, they found evidence for an interrelation between the endoplasmic reticulum-stress response and HSP upregulation after laser irradiation.

Lepock et al.<sup>22</sup> stated that the nuclear matrix reacts as a thermolabile cell structure, creating a link to HSP- and DNA-repair pathways. The knockout of ATF-4 led to a diminished HSP activity and autophagy response, while ATF-4 overexpression resulted in a reduced laser-associated toxicity.

An increased autophagy response following irradiation with 532 nm at a laser power of 2 W over an exposure time of 30 s (average radiant exposure: 477.5 J/cm<sup>2</sup>) was observed by Krmpot et al. using a rat glioma cell line. Similar to our findings, the extent of laser-induced cytotoxicity was laser power dependent. After irradiation with cytotoxic laser powers evidence for a laser-mediated induction of autophagy response was demonstrated. Cells treated with an autophagy inhibitor after irradiation showed an increased cytotoxicity. From this observation, they concluded that autophagy was induced as a cytoprotective response mechanism.<sup>23</sup>

Interestingly, the experimental setup was very similar to the one used in our presented *in vitro* study. However, a cytotoxicity of 50% was already observed after applying 477.5 J/cm<sup>2</sup>, while necrosis and total destruction of cell structures were found after irradiation with 1910 J/cm<sup>2</sup>. These different cytotoxic thresholds might be due to a higher vulnerability or altered response mechanisms to the laser irradiation in the glioma cell line used in their study.

The qPCR analysis and the induction of the multiple stress and toxicity pathways do not explain the genesis of the cytotoxic effects, but provide some important information about potential underlying effects and their interrelation.

We only found a significant upregulation of the stress response gene GADD45G following irradiation of the fibroblasts with a laser power of 199 mW (2988 J/cm<sup>2</sup>), which is below the predetermined cytotoxic threshold within our experiments.

Interestingly, the degree of metabolic activity impairment 2 h after irradiation often exceeded the amount of LDH release measured after 24 h. Considering our findings that the key player in the cell cycle arrest<sup>24</sup> GADD45G was upregulated, these observations could be explained as a potential induction of growth arrest after irradiation with subphototoxic laser powers. This finding is in consensus with Kim et al.<sup>25</sup> who observed a protective mechanism induced by an upregulation of GADD45A after irradiation with visible red light.

In addition, an interesting side effect could be noticed in the osteoblasts after irradiation with a laser power below the predetermined cytotoxic threshold 250 mW (3756 J/cm<sup>2</sup>) demonstrating a significantly lower LDH release than the nonirradiated control group.

Several studies in the field of low-level laser therapy (LLLT) report that light of different wavelengths can have stimulating effects on cell proliferation, recovery, and metabolic activity. Stein et al.<sup>26</sup> demonstrated that LLLT of 632.8 nm and 10 mW for 3 s (0.43 J/cm<sup>2</sup>) could significantly promote proliferation and differentiation of HOB *in vitro*. Similar observations were reported by Fujihara et al.,<sup>27</sup> who found an increased proliferation rate of rat calvarial osteoblast-like cells after irradiation with 780 nm and an average radiant exposure of 3 J/cm<sup>2</sup>. An increased fibroblast proliferation could also be observed after irradiation with light-emitting diodes at 950, 660, and 570 nm at average radiant exposures ranging from 0.1 to 1 J/cm<sup>2</sup> and the highest proliferation rate occurred after exposure to green light.<sup>28</sup> Anwer et al. observed an increased proliferation and mitochondrial activity after irradiation of adipose tissue-derived stem cells with a wavelength of 532 nm and a laser power of 30 mW. These effects were mainly found after exposure times of 30 and 45 s corresponding to radiant exposures of 5 and 6.8 J/cm<sup>2</sup>. They explained their findings with an increasing activity of respiratory chain components serving as photoacceptors at a wavelength of 532 nm.<sup>29</sup> However, comparing these results with our findings is very difficult, since the experimental setup such as cell type and irradiation modalities (wavelength and continuous wave mode application) was different from ours. In addition, the radiant exposures used in our experiments are much higher than in these studies. Nevertheless, our observations could implicate this additional positive effect of our stimulation strategy on human cells using laser powers below the cytotoxic threshold. Although biostimulatory effects were not the focus of this study, findings from the field of LLLT should be regarded as important clues for a better understanding of underlying photochemical effects and further applications.

Last but not least, our previously published *in vivo* studies in mice (Sorg et al.<sup>8</sup>), which we performed in parallel to the *in vitro* studies, demonstrated no significant damage of the irradiated area of the tympanic membrane at an average laser power of 50 mW corresponding to an average radiant exposure of 3000 J/cm<sup>2</sup>. First circular lesions could be observed after irradiation of the tympanic membrane with an average laser power of 89 mW and an average radiant exposure of 5340 J/cm<sup>2</sup>. Considering the differences in irradiation geometry between the *in vivo* performed by Sorg et al. and our *in vitro* studies, the average power density or the average radiant exposure is a more appropriate parameter for a comparison of the safety margins found for our stimulation strategy. In our *in vitro* studies, the upper limit could be found after treatment with a radiant exposure of 2988 J/cm<sup>2</sup>. These results display a good correlation between the upper thresholds for no significant cytotoxic effects in our *in vitro* as well as in the *in vivo* study by Sorg et al.

In our previously published *in vivo* studies (Sorg et al.<sup>8</sup>), a limiting factor for a very short distance between the fiber tip and the irradiated area was the conical shape and tilted angle of the mouse eardrum. However, we could accomplish a better fine-tuning regarding the limits for first cytotoxic effects in our *in vitro* model due to the flat surface of the cell cultures. In addition, we used three different adherent human primary cell types to mimic natural conditions as closely as possible.

The differences in the cytotoxicity thresholds observed in the cell types used in this study might be due to a variability in the distribution of photoacceptor molecules among the different cell types. Although the position of the fiber and the distance from the irradiated surface could be controlled with a higher precision than in the *in vivo* studies, minor variations concerning power density and homogeneity of the beam profile should be considered.

Additionally, our *in vitro* model represents only a monolayer culture. The tympanic membrane is, however, an epithelial structure consisting of different cell types and connective tissues organized in layers. It contains bone, cartilage, and blood vessels. Therefore, it creates a more complex absorption pattern for laser light when compared to the monolayer cell culture. However, this

*in vitro* model offers the great advantage of analyzing the sensitivity for each cell type separately giving additional insight into the different sensitivity patterns of irradiated structures.

## 5 Conclusion

We successfully established an *in vitro* cell culture system for the cytotoxicity thresholds of the optoacoustic stimulation of the hearing organ. Our data suggest that the first *in vitro* biocompatibility margin for our stimulation parameters can be found between 200 and 223 mW (3348 J/cm<sup>2</sup>). After irradiation with a subphototoxic laser power of 199 mW (2988 J/cm<sup>2</sup>), only the qPCR analysis of the fibroblast culture revealed a significant upregulation of GADD45G. This could be a clue for cell cycle control mechanisms as a response to laser irradiation with sublethal laser powers. Further studies are necessary to analyze laser-irradiation-associated thermal and photochemical effects and define the optimal parameters for the optoacoustic stimulation.

## Disclosures

The authors have no relevant financial interests in this article and no potential conflicts of interest to disclose.

## Acknowledgments

This research was funded by the European Research Council under the European Union's Seventh Framework Program (FP/2007-2013/ERC Grant, LaserHearingAids: 311469).

## References

1. World Health Organization, "Deafness and hearing loss," 2018, <https://www.who.int/news-room/fact-sheets/detail/deafness-and-hearing-loss> (accessed 7 December 2018).
2. A. McCormack and H. Fortnum, "Why do people fitted with hearing aids not wear them?" *Int. J. Audiol.* **52**, 360–368 (2013).
3. A. Fridberger and T. Ren, "Local mechanical stimulation of the hearing organ by laser irradiation," *Neuroreport* **17**, 33–37 (2006).
4. G. I. Wenzel et al., "Green laser light activates the inner ear," *J. Biomed. Opt.* **14**, 044007 (2009).
5. K. Y. Zhang et al., "Optoacoustic induced vibrations within the inner ear," *Opt. Express* **17**, 23037–23043 (2009).
6. G. I. Wenzel et al., "Effects of green light application at ear drum and middle ear level," in *ARO Midwinter Meeting*, Baltimore (2010).
7. P. Stahn et al., "Frequency-specific activation of the peripheral auditory system using optoacoustic laser stimulation," *Sci. Rep.* **9**, 4171 (2019).
8. K. Sorg et al., "First biocompatibility margins for optical stimulation at the eardrum via 532-nm laser pulses in a mouse model," *J. Biomed. Opt.* **24**, 085003 (2019).
9. B. M. Teh et al., "Tissue engineering of the tympanic membrane," *Tissue Eng. Part B Rev.* **19**, 116–132 (2013).
10. K. J. Rothman, "No adjustments are needed for multiple comparisons," *Epidemiology* **1**, 43–46 (1990).
11. H. H. van Breugel and P. R. Bär, "Power density and exposure time of He–Ne laser irradiation are more important than total energy dose in photo-biomodulation of human fibroblasts *in vitro*," *Lasers Surg. Med.* **12**, 528–537 (1992).
12. T. Karu, "Basics of the action of monochromatic visible and near IR (laser) radiation on cells," in *Proc. 2nd Int. Conf. Bioelectromagnetism*, IEEE, pp. 125–126 (1998).
13. T. I. Karu et al., "Absorption measurements of cell monolayers relevant to mechanisms of laser phototherapy: reduction or oxidation of cytochrome c oxidase under laser radiation at 632.8 nm," *Photomed. Laser Surg.* **26**, 593–599 (2008).

14. T. I. Karu, "Multiple roles of cytochrome c oxidase in mammalian cells under action of red and IR-A radiation," *IUBMB Life* **62**, 607–610 (2010).
15. T. Karu, "Primary and secondary mechanisms of action of visible to near-IR radiation on cells," *J. Photochem. Photobiol. B* **49**, 1–17 (1999).
16. P. Kassák et al., "Mitochondrial alterations induced by 532 nm laser irradiation," *Gen. Physiol. Biophys.* **24**, 209–220 (2005).
17. C. K. Lim et al., "Isolation and characterization of protoporphyrin glycoconjugates from rat Harderian gland by HPLC, capillary electrophoresis and HPLC/electrospray ionization MS," *Biochem. J.* **347**, 757 (2000).
18. J. W. Obringer, S. Phipps, and M. D. Johnson, "High energy, ultrashort pulse green laser-light exposure of cultured human cells yields evidence of DNA damage," Defense Technical Information Center (1999).
19. J. Leavitt et al., "Mutagenic activity of high-energy 532 nm ultra-short laser pulses," *Radiat. Res.* **147**, 490 (1997).
20. P. D. Bowman and T. S. Steven, "In vitro models of laser induced injury: pathophysiology and cytoprotection" (2007).
21. I. Khan, E. Tang, and P. Arany, "Molecular pathway of near-infrared laser phototoxicity involves ATF-4 orchestrated ER stress," *Sci. Rep.* **5**, 10581 (2015).
22. J. R. Lepock et al., "The nuclear matrix is a thermolabile cellular structure," *Cell Stress Chaperones* **6**, 136–147 (2001).
23. A. J. Krmpot et al., "Protective effect of autophagy in laser-induced glioma cell death in vitro," *Lasers Surg. Med.* **42**, 338–347 (2010).
24. M. Vairapandi et al., "GADD45b and GADD45g are cdc2/cyclinB1 kinase inhibitors with a role in S and G2/M cell cycle checkpoints induced by genotoxic stress," *J. Cell. Physiol.* **192**, 327–338 (2002).
25. Y. J. Kim et al., "A protective mechanism of visible red light in normal human dermal fibroblasts: enhancement of GADD45A-mediated DNA repair activity," *J. Invest. Dermatol.* **137**, 466–474 (2017).
26. A. Stein et al., "Low-level laser irradiation promotes proliferation and differentiation of human osteoblasts in vitro," *Photomed. Laser Surg.* **23**, 161–166 (2005).
27. N. A. Fujihara, K. Hiraki, and M. M. Marques, "Irradiation at 780 nm increases proliferation rate of osteoblasts independently of dexamethasone presence," *Lasers Surg. Med.* **38**, 332–336 (2006).
28. E. M. Vinck et al., "Increased fibroblast proliferation induced by light emitting diode and low power laser irradiation," *Lasers Med. Sci.* **18**, 95–99 (2003).
29. A. G. Anwer et al., "Visible 532 nm laser irradiation of human adipose tissue-derived stem cells: effect on proliferation rates, mitochondria membrane potential and autofluorescence," *Lasers Surg. Med.* **44**, 769–778 (2012).

**Lukas Pillong** is working as a resident in the Department for Otorhinolaryngology, the University Medical Center Homburg, Germany. He earned his medical degree in 2017 and since 2016, he has been a member of the research group "Laser Hearing Aids" led by Prof. Dr. Gentiana Wenzel. His research interests focus on light-tissue/cell-interaction and biocompatibility as the basis for the development of light-driven hearing aids using the optoacoustic effect.

Biographies of the other authors are not available.

### 3) Optoacoustically induced auditory brainstem responses in the mouse model enhanced through an absorbing film

Katharina Sorg, Larissa Heimann, Gabriela Moreira Lana, Achim Langenbacher, Bernhard Schick, Eduard Arzt, Gentiana Ioana Wenzel

Contribution of the authors:

This work was prepared as shared first authorship between Katharina Sorg and Larissa Heimann who both designed and performed the experiments and composed the manuscript. Both were also equally involved in data analysis. Gabriela Moreira Lana produced and characterized the films used in the study and assisted in manuscript preparation. Achim Langenbacher and Bernhard Schick assisted during manuscript preparation and with scientific discussions. Gentiana I. Wenzel worked on the study conception, assisted with the study design, data analysis, during manuscript preparation and with scientific discussions.

# Optoacoustically induced auditory brainstem responses in the mouse model enhanced through an absorbing film

Katharina Sorg<sup>Ⓜ, a, †</sup> Larissa Heimann<sup>Ⓜ, a, †</sup> Gabriela Moreira Lana<sup>Ⓜ, b, c</sup>  
Achim Langenbacher,<sup>d</sup> Bernhard Schick,<sup>a</sup> Eduard Arzt,<sup>b, c</sup>  
and Gentiana Ioana Wenzel<sup>a, \*</sup>

<sup>a</sup>Saarland University Medical Center, Department of Otorhinolaryngology,  
Homburg, Germany

<sup>b</sup>INM Leibniz Institute for New Materials, Saarbrücken, Germany

<sup>c</sup>Saarland University, Department of Materials Science and Engineering,  
Saarbrücken, Germany

<sup>d</sup>Saarland University, Department of Experimental Ophthalmology,  
Homburg, Germany

## Abstract

**Significance:** Optoacoustic stimulation offers an alternative stimulation strategy for the hearing organ. To serve as the base for a novel auditory prosthesis, the optoacoustic stimulation must be biocompatible and energy-saving.

**Aim:** Enhancing the efficiency of optoacoustic stimulation while reducing the energy input in a suited animal model.

**Approach:** Optoacoustically induced auditory brainstem responses (oABRs) were recorded after the pulsed laser irradiation of the tympanic membrane (TM) in mice. The results were compared with the ABRs induced through acoustic click stimulation. In addition, self-adhesive absorbing films were applied on the TM before the optoacoustic stimulation to investigate their effect on the resulting ABRs.

**Results:** Using an absorbing film on the TM during optical stimulation led to considerably enhanced oABR wave I amplitude values compared with the stimulation of the bare TM. When using our stimulation strategy, we induced oABR waves in the 50% to 60% range of the acoustical stimulation reached with 80-dB SPL click stimuli.

**Conclusions:** The mouse model can be used for certain developmental work for an optoacoustic auditory prosthesis. Using absorbing films on the TM during optical stimulation considerably enhances oABR wave I amplitude. Optimization of the stimulation strategy could further enhance the efficiency within biocompatibility margins.

© The Authors. Published by SPIE under a Creative Commons Attribution 4.0 Unported License. Distribution or reproduction of this work in whole or in part requires full attribution of the original publication, including its DOI. [DOI: [10.1117/1.JBO.26.9.098001](https://doi.org/10.1117/1.JBO.26.9.098001)]

**Keywords:** optoacoustic; laser; auditory brainstem responses; silicone elastomers; optoacoustically induced auditory brainstem responses.

Paper 210173R received Jun. 10, 2021; accepted for publication Aug. 17, 2021; published online Sep. 3, 2021.

## 1 Introduction

Optoacoustics is applied in the fields of, e.g., imaging, spectroscopy, and quantification of molecules. The result of the absorption of pulsed light in an absorber medium inducing a thermal expansion and contraction of the substrate and, therefore creating a sound source, represents the

---

\*Address all correspondence to Gentiana Ioana Wenzel, [gentiana.wenzel@uks.eu](mailto:gentiana.wenzel@uks.eu)

†Shared first authors

optoacoustic effect. This effect can be used to stimulate the hearing organ by inducing vibrations of the irradiated structures. Since optoacoustic stimulation could be applied on every stimulation target in the peripheral hearing system, which could vibrate, e.g., the eardrum or the otic capsule, it offers the potential for use in the development of a new generation of auditory prostheses.

The optoacoustic-induced vibrations are transmitted through the auditory pathway and activate the central auditory system. This activation can be analyzed by recording auditory brainstem responses (ABRs) to the optoacoustic stimuli. ABRs are electroencephalographic signals recorded through peripheral electrodes detecting voltages generated by neural activity throughout the brain, including the auditory brainstem and the eighth cranial nerve.<sup>1</sup> ABR waves can either be induced by acoustical (aABR), electrical (eABR), or optoacoustic (oABR) stimulation and are a well-established method to analyze the hearing function for different basic and advanced research purposes.<sup>2-6</sup> In 2009, Wenzel et al.<sup>7</sup> first demonstrated that optoacoustic stimulation in the peripheral hearing system induces ABR waves in guinea pigs, resembling the form of acoustically induced waves. In a further study, we were able to demonstrate a novel stimulation strategy to induce frequency-specific optoacoustic vibrations in the tympanic membrane (TM), demonstrated by evoked activities in the inferior colliculus in guinea pigs.<sup>8</sup> Recently, we demonstrated that the effectiveness of optoacoustically induced vibrations of the guinea pig TM depends on the laser wavelength, most probably through dissimilar absorption characteristics of the TM tissues for different wavelengths.<sup>9</sup> However, one main work package that needs to be performed, before considering the design of a hearing device, is the optimization of the stimulation method to achieve higher activation intensities within biocompatibility margins. We, therefore, sought to assess if the induced vibrations can be amplified by the application of highly absorbing material on the target-irradiated structure in an animal model.

So far, biocompatibility studies have been performed in mice<sup>10</sup> due to better availability of suited immunostaining antibodies on the market for this animal model compared with bigger mammals, e.g., gerbils or guinea pigs. Electrophysiological studies for optoacoustic stimulation have been, however, performed in guinea pigs.<sup>7,8</sup> To directly use the safety margins defined in our previous biocompatibility report,<sup>10</sup> we decided for the herein presented set of experiments to use mice and needed therefore to establish as well our stimulation strategy for the murine TM as well.

For the highly absorbing material, we chose at this stage silicone elastomers that are promising biomaterials with a broad range of applications.<sup>11-14</sup> Among the different silicones, a subclass of poly-(dimethylsiloxane) (PDMS) elastomers, the pressure-sensitive adhesives present interesting properties for applications such as skin adhesives.<sup>12-15</sup> They adhere steadily after a short contact time and with low applied pressure on biological surfaces. As they have a low elastic modulus, they can adapt to the surface and reach high adhesion through Van der Waals interface interactions, dismissing the use of adhesive glues or any chemical fixation.<sup>16</sup> Recently, we were able to introduce soft skin adhesive (SSA) as a promising material for wound scaffolding with high cellular biocompatibility, good adhesion on rough surfaces, such as human skin, and gentle peel-off characteristics, without damaging the tissue. The gentle attachment and detachment are essential for the application onto sensitive tissues, e.g., the TM.<sup>17,18</sup> PDMS grafts were successfully used in the treatment of human TM perforations<sup>19</sup> and demonstrated to have similar basic acoustic properties in the higher frequency range that replicate the human TM motion.<sup>20</sup>

Therefore, to further improve the optoacoustic stimulation, we analyzed herein these silicone elastomers, further named films, as the absorbing material. To analyze the electrophysiological effects of this stimulation method, we assessed, to our knowledge for the first time in literature, the optoacoustic-induced auditory brainstem responses (oABR) in a mouse model.

## 2 Materials and Methods

### 2.1 Animal Model

We used 4- to 12-weeks old female CBA/J mice (Janvier Labs, France) weighing 18 to 23 g in our experiments (14 animals in total in this study). The studies were performed according to the guidelines of the Animal Care and Use Committee of Saarland by qualified persons, approved by

the Animal Welfare Agency under the State Office for Consumer Protection of Saarland. All animals were initially anesthetized intraperitoneally with 100 mg/kg ketamine (Ketaset, Zoetis, Berlin; Germany) 10 mg/kg xylazine (Rompun, Bayer, Leverkusen; Germany). The anesthesia was maintained by injection of  $\frac{1}{4}$  to  $\frac{1}{2}$  of the initial dose intraperitoneally every 30 min. To keep the body temperature constant at 37°C, the animals were positioned on an electrical heating pad throughout the experiment and were supplied with additional oxygen. To expose the TM of mice for film application and subsequent irradiation, the outer ear canal had to be prepared. Therefore, the hair around the outer ear canal was trimmed and a vertical incision beginning at the incisura intertragica expanding along the cartilaginous outer ear canal was made. The TM was exposed by fixing the edges of the incision with sutures.

## 2.2 Film Application

The films (Fig. 2) were punched with a suction tube manually to  $\sim 1$  mm diameter under microscope control and applied carefully with forceps, with the adhesive side in contact to the TM centrally over the umbo [Fig. 1(b)]. We covered the TM with films of different constitutions: (i) transparent (nonabsorbing) films, (ii) absorbing films, and compared the results to (iii) mice that were irradiated without the use of any film (control). The absorbing films were covered with an additional layer of sputtered silver that was then stained with black color (permanent marker, edding International GmbH, Ahrensburg, Germany) to ensure increased laser light absorption. The silver coating is meant to ensure the total reflection of light that could otherwise pass through the absorbing layer. The films were placed on both TM's of the animal: one side for the irradiation and the other side served as a control.

## 2.3 Laser Irradiation

The laser irradiation was always performed on the left ear of the mice. We used a 532-nm pulsed neodymium-doped yttrium orthovanadate (Nd:YVO<sub>4</sub>) laser (Xiton Photonics GmbH, Kaiserslautern, Germany) as the light source. The pulsed laser light was applied through a glass fiber (365  $\mu\text{m}$  diameter, FG365LEC-CUSTOM, Thorlabs GmbH, Munich, Germany) directed with a micromanipulator (Narishige, Tokyo, Japan) under microscope control vertically to the surface and in the center of the absorbing film or TM [Fig. 1(a)]. The distance to the irradiated structure was  $\sim 300$  to  $500$   $\mu\text{m}$ . Therefore, the calculated irradiation spot diameter was  $\sim 590$   $\mu\text{m}$ , whereas the laser spot was either positioned centrally over the absorbing or nonabsorbing film or

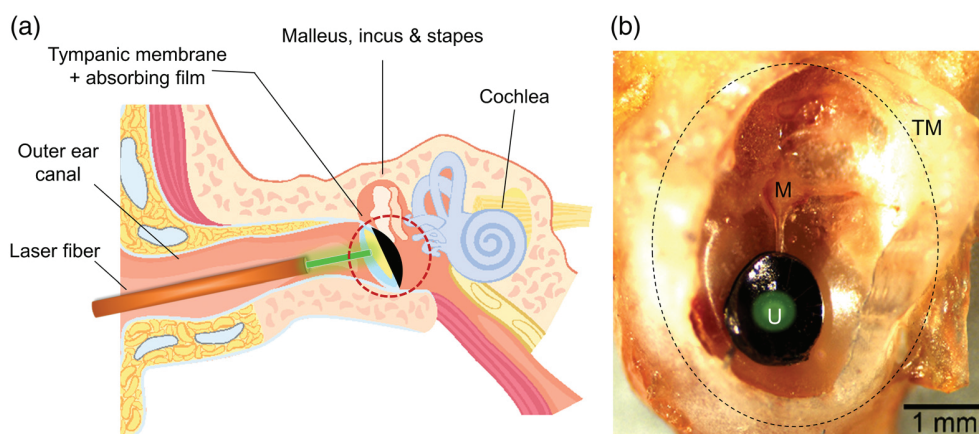


**Fig. 1** Schematic drawing for the position of the laser fiber inside the outer ear canal (a) centrally over the absorbing patch attached to the TM. (b) Detailed information of the red circled area in (a) showing the absorbing film applied on an explanted murine TM (black dotted circle) with a graphical illustration of the green laser spot in the center of the absorbing film (round black structure) covering the umbo (U) the deepest point of the malleus (M). The scale bar in (b) represents 1 mm. The image in (a) was purchased and edited from iStock.com/iLexx.

the native TM at the umbo [Fig. 1(b)]. The laser irradiation parameters were chosen to replicate our self-designed stimulation strategy creating a sinusoid signal at the targeted frequency, the laser-modulation rate (LMR). We irradiated the selected area for 5 ms and paused for 95 ms with average laser powers of 2, 3, 5, 8, 12, 20, 31, 50, and 79 mW with the laser repetition rate (LPR) of 50 kHz and LMRs of 1, 8, and 10 kHz. Afterward, the laser power was calibrated using a power meter (Uno, Gentec Electro-Optics, Inc., Québec, Canada).

## 2.4 Electrophysiology: aABR and oABR

Before and after the patch application, as well as after the laser irradiation, click auditory brainstem response (click ABR) recordings were performed to assess the hearing function of the mice and serve as controls for the effectiveness of optical stimulation. The recording of ABRs was performed in the same way as previously reported.<sup>3,21–23</sup> We recorded ABRs using subcutaneous needles: one on the mastoid, one at the vertex (reference), and one at the base of the tail (ground). The click stimuli were generated with a digital signal processing system (Agilent 33500 B Series True form Waveform Generator, Keysight Technologies GmbH, Germany) and were delivered through a free field speaker (custom made from a DT-911, Beyerdynamic GmbH & Co. KG, Germany<sup>3</sup>) placed in a 5-cm distance in front of the left ear (the irradiated ear). The recorded signals were then amplified through the biosignal amplifier (g.USBamp, g.tec medical engineering GmbH, Austria), digitized at 19.2 kHz, and filtered to obtain the frequencies from 300 to 2500 Hz. The stimulus intensities ranged from 0 to 80 dB SPL, increased in 10 dB steps. The stimulus repetition rate was 20 Hz, and 500 trials were averaged. The speaker output was calibrated periodically. The hearing thresholds were determined visually during the recording as well as offline and were defined by the lowest intensity where the Jewett's wave complex was identifiable. The Jewett complex was first described by Jewett and Williston in 1971.<sup>24</sup> In mice, it typically consists of five vertical positive waves between 1 and 6 ms.<sup>25–27</sup> During the laser irradiation, we recorded ABR signals that were generated by laser-induced stimulation (oABR) from 2 to 79 mW for each LMR. We analyzed wave I amplitude [Fig. 4(a)] after acoustic (aABR) and after laser stimulation (oABR). The amplitude was determined as the absolute value between the first negative ( $I_n$ ) and first positive ( $I_p$ ) values of the first wave [Fig. 4(a)]. We normalized the resulting oABR amplitudes at the respective laser stimulation levels to the maximum reached aABR amplitude at 80 dB SPL of each animal and averaged the resulting data between the animals in the three different groups. To analyze the o- and aABR signals at different energy levels of the stimulus, the measured values were fitted with a sigmoidal function. Information about data fitting is included in the [Supplementary Material](#).

## 2.5 Production and Characterization of the Silicon Films

The silicone films used in this study consisted of multilayer samples, prepared as follows [see Fig. 2(a)]. First, a polydimethylsiloxane (PDMS, Elastomer kit Sylgard 184, Dow Silicones, Midland, Michigan) film was manufactured on a polyethyleneterephthalat (PET) foil by the doctor blade technique using an automatic film applicator (MSK-AFA-IV, MTI Corporation, Richmond, California) set with a gap of 100  $\mu\text{m}$ . The film was then cured at 95°C for 1 h. Subsequently, on the cured Sylgard 184 film, a second layer was prepared, of SSA MG7-1010 (Dow Silicones, Midland, Michigan), also using a doctor blade, set for 200 or 300  $\mu\text{m}$  in total (cured Sylgard + SSA). The double-layer sample was removed from the PET foil and placed on a fluorosilicone release foil (3M<sup>TM</sup> Scotchpak<sup>TM</sup> 9709 Release Liner) with the SSA surface (adhesive side) on the foil for further use. Two different designs of samples were prepared [Fig. 2(b)]: (i) pristine patches without any absorbing layer and (ii) patches covered with a thin Ag layer on the PDMS side and a layer of black ink above that. For the second design, a thin Ag layer was deposited on the Sylgard surface (JEOL-1300 Auto fine coater) under vacuum using 30 mA for 180 s. Covering the Ag layer, a black film was prepared using, as described before, a black marker (permanent marker, edding International GmbH, Ahrensburg, Germany) [Fig. 2(b)]. For further characterization, the thickness of the polymer films was measured using an optical microscope (Eclipse LV100ND, Nikon, Tokyo, Japan), and the transmission spectrum of the samples was recorded by UV-Vis spectrometry (Cary 5000 UV-Vis-NIR, Agilent, Santa Clara,

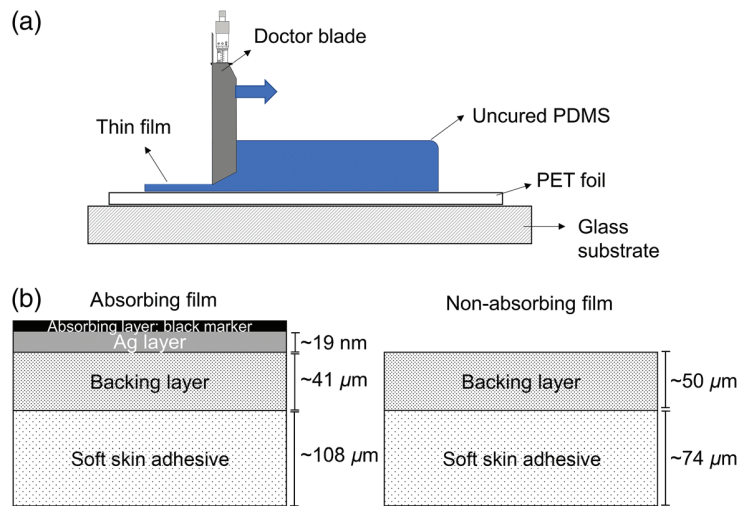


**Fig. 2** (a) The films were produced using the doctor blade technique as double layer design of SSA and backing layer. (b) Two types of patches were produced: (i) absorbing films with an Ag layer and an absorbing layer of black marker on top of the backing layer, having a total thickness of  $\sim 150 \mu\text{m}$  and (ii) pristine patches without any absorbing layer, with a total thickness of  $\sim 125 \mu\text{m}$ .

California) in the range from 200 to 1300 nm. To determine the thickness of the Ag layer, ellipsometric spectroscopy (J.A. Woollam Co., Lincoln, Nebraska) was used, varying the incidence angle from 65 deg to 75 deg in 5 deg steps, and averaging 50 measurements. The following data analysis was performed according to the Cauchy Model with the Software WVASE32 from Woollam.

## 2.6 Statistical Analysis

For statistical analysis, OriginPro 2020 software was used (OriginLab Corp., Northhampton, Massachusetts). The Shapiro-Wilk-test was applied to verify the normal distribution of the data followed by a Levene's test for variance homogeneity. For the analysis of aABR amplitude before and after patch application, we performed paired *t*-tests at each acoustical stimulation level.

## 3 Results

### 3.1 Production and Characterization of the Silicon Patches

First, the absorbing film, containing the Ag and the black absorbing layers, as well as the non-absorbing sample, the pristine PDMS-SSA double layer, were measured regarding its dimensions, light transmission, and absorbance. For the nonabsorbing film, the SSA portion was  $74.16 \pm 2.06 \mu\text{m}$  thick, and the PDMS backing layer was  $49.82 \pm 1.35 \mu\text{m}$ . The absorbing film consisted of an SSA film of  $108.26 \pm 16.42 \mu\text{m}$ , a PDMS backing layer of  $41.53 \pm 1.79 \mu\text{m}$ , and the Ag thin film of 19.9 nm thickness, covered by the black absorbing surface. As described in Sec. 2.1.1, the films were punched with a suction tube in circular patches and positioned on the TM [Fig. 1(b)]. The transmission and reflection spectra obtained from UV-Vis spectrometry are shown in Fig. 3(a), in which the transmission of the nonabsorbing samples demonstrated a plateau of  $\sim 94\%$  for wavelength values above 300 nm, being 93.72% at 532 nm. The absorbing structure, on the other hand, demonstrated a constant behavior of low transmission, being about 0.24% at 532 nm. This behavior was attributed to the combination of the black and silver layers. Measurements of the silver layer before staining the film black demonstrated partially blocking the transmission of the incident irradiation. The silver layer combined with the absorbing layer could achieve even lower transmission (under 0.5%), as shown in Fig. 3(a), minimizing the transference to the TM. The reflection of the absorbing patch is also presented and lies at

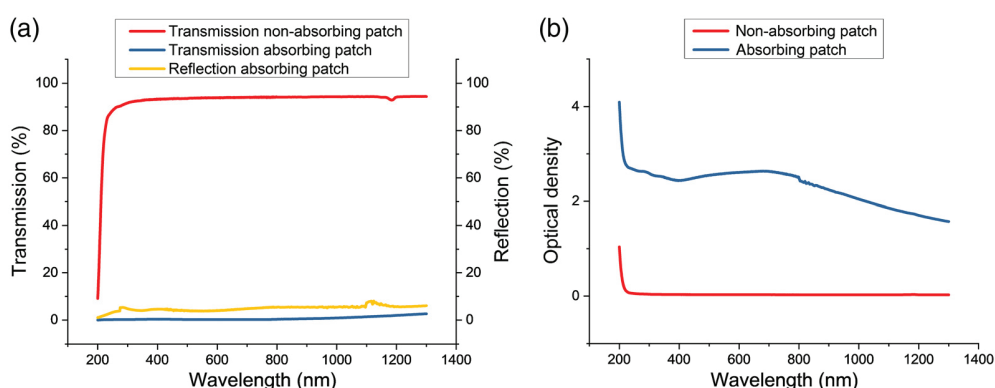


**Fig. 3** (a) Transmission, reflection, and (b) optical density spectra of absorbing and nonabsorbing films between 200 and 1300 nm.

~5% or less over the measured wavelength range, being 3.843% at 532 nm. The optical density of these samples at the different wavelengths [Fig. 3(b)] was calculated as  $Abs = \log(1/T)$  and was at 532 nm 2.574 for the stained absorbing structure and 0.028 for the control film. These values take into account both absorption as well as the reflection of the samples. Considering the incident radiation as the sum of absorption, reflection, and transmission, we obtained absorption values of the absorbing film of ~95%.

### 3.2 oABR

To examine whether the application of absorbing films influences (i) the generation of optically induced ABR waves itself and (ii) the form of the resulting waves, we compared optically induced ABR waves after stimulation with 79 mW average laser powers at 1, 8, and 10 kHz LMR with acoustically induced ABR waves after stimulation with 80 dB SPL (Fig. 4). In this study, three different groups were investigated. The first group ( $n = 3$ ) served as a control and was stimulated on the bare TM. The second group ( $n = 5$ ) with a nonabsorbing film demonstrated the impact of the film on the stimulation. The third group ( $n = 6$ ) using an absorbing film displayed the effect of an extra absorbing layer.

We were able to induce oABR waves in all groups. The oABR waves of the control group without the use of any film [Fig. 4(a)] demonstrated clearly identifiable signals with five positive peaks, resembling the Jewett wave complex<sup>25–27</sup> when stimulated with 8 and 10 kHz LMR; however, with considerably lower amplitudes when compared with the activation induced through acoustic stimulation. At 1 kHz LMR, a periodical oscillation with a frequency of 1 kHz could be detected demonstrating five waves as well, however, resembling the shape of the stimulus. The signal level was further reduced in animals that had a nonabsorbing film [Fig. 4(b)] attached to the TM, meaning that just signals at 1 kHz were identifiable. As presumed, the oABR wave complex significantly increased after the application of an absorbing film on the TM of those mice [Fig. 4(c)]. In this group of mice, the oABR wave complex was clearly identifiable after stimulation with all LMRs and the signal form and amplitude resembled that of the aABR after click stimulation with 80 dB SPL.

To analyze these differences in the signal formation, we analyzed wave I of all oABRs and compared its amplitude with the generated aABR signals in all groups. The click aABR amplitudes (Fig. 5, outer column, 0 to 80 dB SPL) followed the shape of a sigmoidal function (Fig. S1 in the [Supplementary Material](#)). The oABR stimulation (mostly 2 to 79 mW) demonstrated increasing amplitudes for rising laser power (Fig. 5). Amplitudes measured for stimulation of native TM increased linearly within the applied laser power values. Applying a nonabsorbing film reduced the amplitudes at 79 mW to ~33% of the amplitudes recorded from the laser stimulation on a native TM. The optical stimulation of TMs with an absorbing film led to a logarithmic growth of the amplitude being 6.8 times higher at 79 mW and 1 kHz LMR, 4 times higher at 8 kHz, and 3.5 times higher at 10 kHz than the amplitudes after stimulation onto the native TM (Fig. 5).

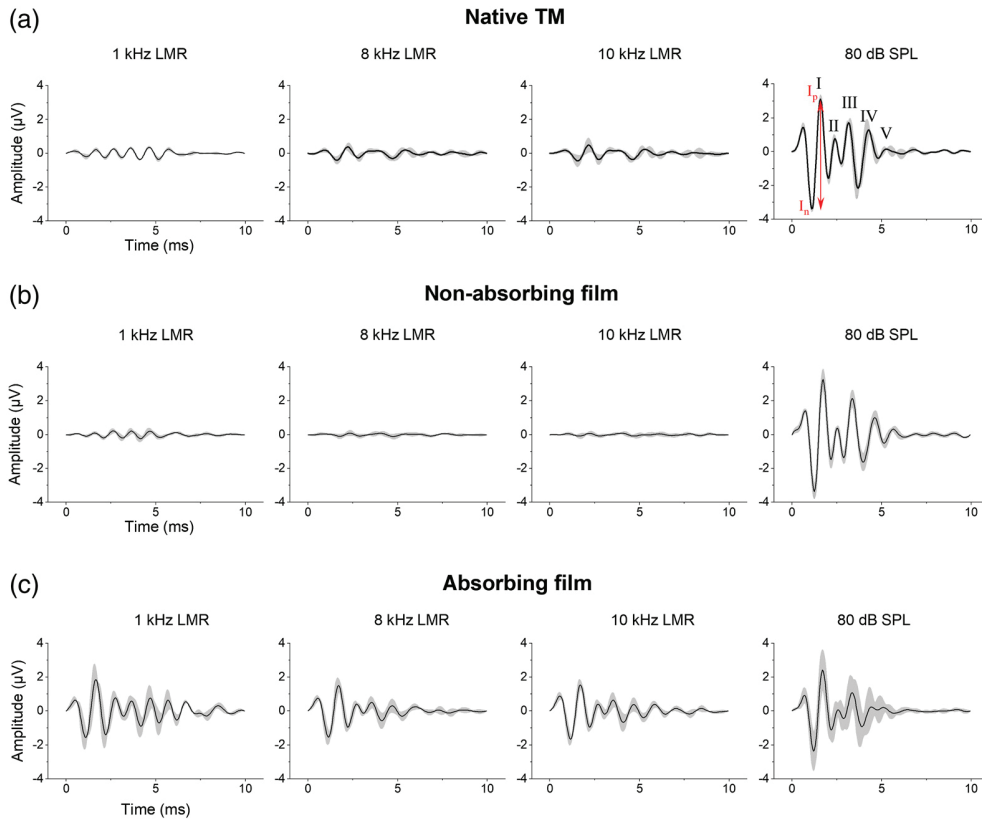


**Fig. 4** Resulting averaged oABR waves after stimulation with 79 mW average laser power (a) without a film, (b) with a nonabsorbing film, or (c) an absorbing film with 1, 8, and 10 kHz LMR in comparison to the aABR waves at 80 dB SPL acoustical stimulation (outer column), respectively. In the outer column in (a), the Jewett wave complex of wave I to V is illustrated exemplarily for all ABR waves. Wave I amplitude was analyzed from the first negative (In) to the first positive (Ip) peak [red arrow, (a) outer column]. All waves are illustrated as averaged between all replicas in the respective groups with the standard deviation. The number of replicas was (a)  $n = 3$ , (b)  $n = 5$ , and (c)  $n = 6$  animals.

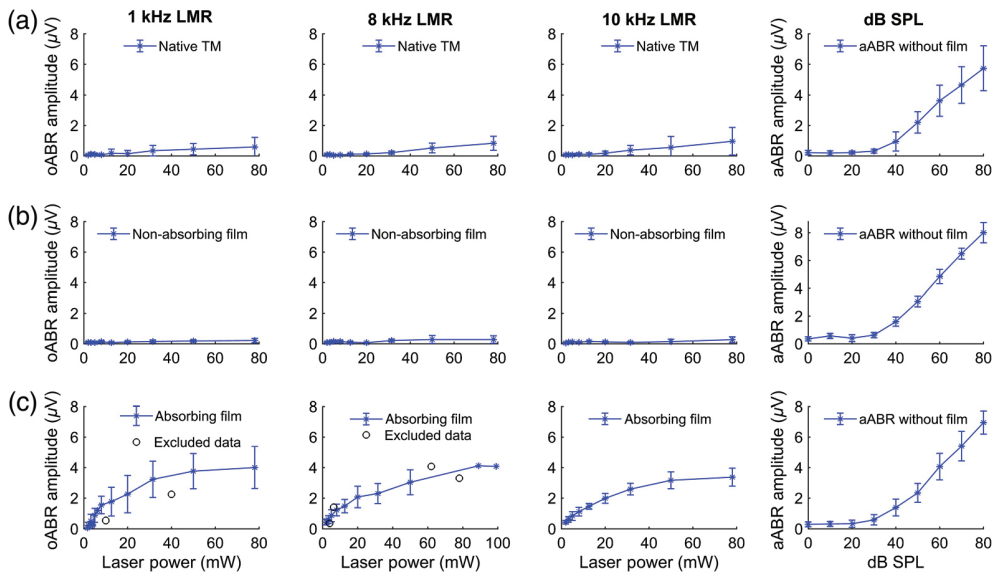


**Fig. 5** Averaged oABR amplitudes (a) without a film, and with (b) a nonabsorbing film, (c) or an absorbing film with 1, 8, and 10 kHz LMR in comparison to the averaged click stimulated aABR amplitudes (right column) of the respective group.

Since the aABR amplitudes without the film represented the individual hearing ability (Fig. 6) and the aABR amplitude recorded with a film attached to the TM represents the hearing ability affected by the weight of the film, both curves in Fig. 6 demonstrated the classical growth behavior known for click ABR waves. At all stimulation levels, the amplitude values were significantly lower in the group recorded with a film added to the TM. To analyze the impact of the animal's individual hearing ability, the measured oABR amplitudes from each animal were normalized to its aABR amplitude at 80 dB SPL. To analyze this effect further and to avoid incorrect analysis of oABR recordings, we normalized the oABR wave I amplitudes to both different aABR levels (with and without film) and compared the resulting growth curves (Fig. 7). Since without absorbing film application or using a nonabsorbing film, only low intensity oABR waves could be induced, we focused in the following analysis on oABR waves after application of an absorbing film.

Following the results of the averaged wave I aABR amplitudes of all groups (Fig. 7), the wave I amplitudes normalized to the wave I aABR amplitude recorded for stimulation with 80 dB SPL after patch application demonstrated slightly higher amplitudes and smaller error bars in comparison to the oABR amplitude normalized to the aABR amplitude recorded for

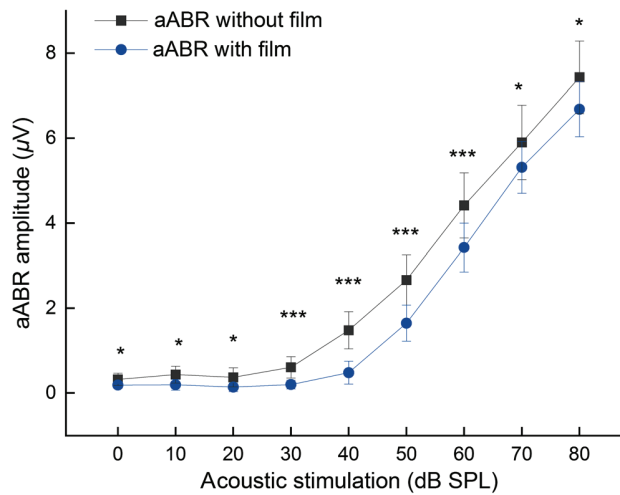


**Fig. 6** Averaged aABR amplitudes before and the lower averaged aABR amplitudes after ( $n = 11$ ) film application. The error bars represent the standard deviation. \* indicates  $p < 0.05$ ; \*\*\* indicates  $p < 0.001$ .

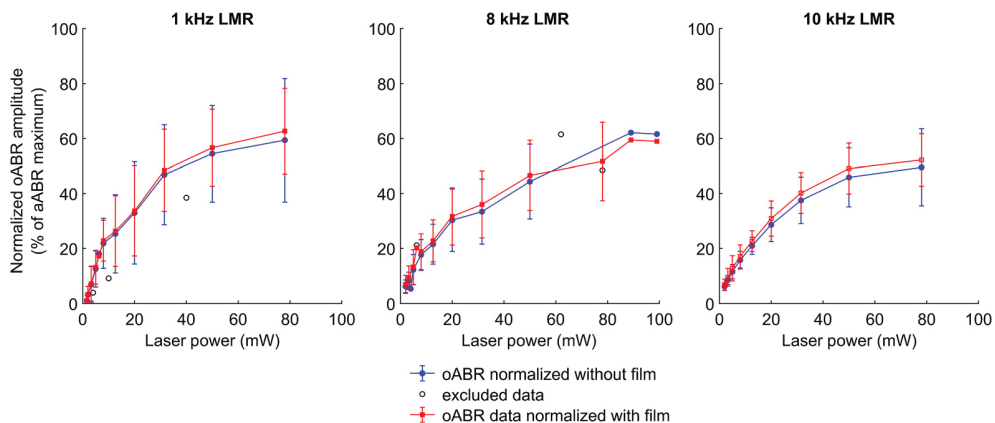


**Fig. 7** Averaged oABR amplitudes at 1, 8, and 10 kHz LMR normalized to the aABR amplitude at 80 dB SPL measured without film (blue lines) and with film (red lines) demonstrating a growth behavior with a sharp slope followed by saturation. The error bars represent the standard deviation ( $n = 6$ ) of the mean.

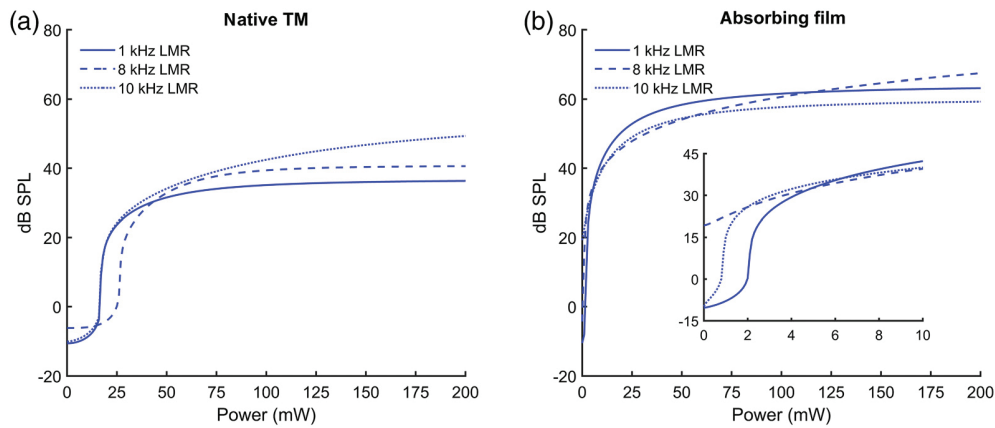


**Fig. 8** IO function [Eq. (3), [Supplementary Material](#)] calculated for the averaged data measured with (a) native TM and (b) the absorbing film for 1, 8, and 10 kHz LMR, respectively, demonstrating the sigmoidal growth behavior adopted from physiological acoustic stimulation. The absorbing film IO function is zoomed in from 0 to 10 mW.

stimulation with 80 dB SPL before patch application. However, the difference between the amplitude values normalized with the two normalization methods in the amplitude values was <5%. Based on our data, we demonstrated that single frequency stimulation with laser power of 79 mW reached 60% of the wave I aABR amplitude level at 80 dB SPL for 1 kHz LMR, and ~50% for 8 and 10 kHz LMR in this animal model with our current stimulation paradigm (Fig. 7).

### 3.3 Comparison of oABR and aABR Amplitudes

To determine the theoretical laser power and SPL values inducing the same amplitude values, the averaged oABR and aABR amplitudes of the two groups, absorbing film, and native TM were fitted and set equal ([Supplementary Material](#)). The dynamic range of the IO function of the absorbing film was close to 70 dB SPL and, therefore, 20 dB SPL higher than the dynamic range of data recorded from irradiated native TM (Fig. 8). The turning point of the functions calculated for the group absorbing film was between 1 and 2 mW and for native TM 17 mW (1 and 10 kHz) and 27 mW (8 kHz).

## 4 Discussion

Short, pulsed laser light irradiating a medium, the TM, in this case, induces ultrasonic vibrations arising from photon absorption causing a thermal expansion and contraction of this medium.<sup>28</sup> These ultrasound-induced mechanical vibrations can be used to stimulate the hearing organ at different loci.<sup>5-9</sup> Therefore, the idea to work with this stimulation method to specifically influence the auditory activation suggests the design of a new generation of hearing prosthesis. A stimulation strategy based on a single laser wavelength for frequency-specific stimulation has already been demonstrated by Stahn et al.<sup>8</sup> The modulation of the stimulation intensity was the next step of our research and the focus for this report.

Since we planned to explore this in the same animal model in which we performed the first biocompatibility studies<sup>10</sup> to build upon those results, as a proof-of-principle study, we had first to assess if the induction of optoacoustic ABR waves is possible in mice as well since these mammals have a very transparent TM.<sup>21</sup> To increase the absorption of photons additionally, we explored the effects of the application of our self-designed light-absorbing PDMS film onto the TM and investigated whether such materials could optimize the optical stimulation effects.

The detection of ABR waves is a well-established method to monitor the neural response to the stimulation of the auditory system and includes the impact of the cochlear amplifier. oABR waveform and growth behavior analysis helps to characterize the light-induced activation of the

auditory pathway. Growth behavior as a function of irradiation power gives therefore an insight into the efficiency of the stimulation method represented herein by the laser irradiation. Wenzel et al. demonstrated optoacoustic stimulation-induced oABR waves in guinea pigs and used wave V growth behavior to compare the efficiency of optic stimulation in comparison to acoustic stimulation. Thereby, wave V increased with increasing laser intensities and reached a saturation plateau around  $15 \mu\text{J}/\text{pulse}$  for a 10-Hz repetition rate. The shape of wave V growth function was similar for the optoacoustic and acoustic stimulation. In our presented study, we performed optoacoustic stimulation in normal-hearing mice. Although oABRs recorded in mice were described earlier associated with optogenetic stimulation<sup>29</sup> or infrared neuronal stimulation,<sup>30</sup> we demonstrated, to the best of our knowledge for the first time in the literature, optoacoustically induced oABRs in mice.

Using pulsed green laser light applied on the TM, the induced ABR waves resembled, in their shape and amount of positive and negative peaks, the aABR signals. We were able to generate oABR signals with different levels on three tested conditions: applying laser light on (i) the native TM, (ii) covered TM with a nonabsorbing film, and (iii) using an absorbing film. These findings were reproducible applying different LMRs (8 and 10 kHz) (Fig. 4). At 1 kHz the auditory function in these mice was very limited and no signals should be recordable. The shape of the recorded signal at 1 kHz LMR can be compared to cochlear microphonics (CM) mimicking the stimulus [Figs. 4(a) and 4(b)].<sup>31</sup> However, CMs result from the activation of the cochlea and therefore cause overlaying ABR signals as well. The excitation of the hearing system leading to a broad activation of the cochlea could also be induced by harmonics originating from irradiation of the structure behind the TM of mice, e.g., the otic capsule. This might be induced especially during stimulation without an absorber as the native murine TM or the non-absorbing film is nearly transparent. Interestingly, oABR signals at 1-kHz LMR and an absorbing film having the classic Jewett wave shape could be detected even though, physiologically mice prove low hearing ability at this frequency. This effect might be induced through the modulation or damping of the vibration characteristics of the TM by the attached absorbing film. Further planned experiments will give more insight in this regard, specifically considering the frequency-specific activation by optoacoustic stimulation in the mouse model. In addition, the studies exploring the vibratory characteristics of the film-membrane complex, e.g., with laser Doppler vibrometry would give more insight into the sound conduction characteristics of this new stimulation method.

We used the sigmoidal growth function of wave I, the most prominent wave in murine ABR signals<sup>1,4,32,33</sup> as a marker determining the intensity of a stimulus, to analyze the efficiency of optoacoustic stimulation. The optoacoustic stimulation depends on the absorption of light energy and is, therefore, a function of the absorption coefficient. The film demonstrated good light-absorbing properties (Fig. 3) and therefore increased the efficiency of the optoacoustic stimulation. This was demonstrated by the wave I amplitudes, which were enhanced by factors of 6.8, 4, and 3.5 in comparison to the irradiation of native TM. The different maximum amplitudes of the LMRs occur through the characteristic of our stimulation paradigm. By varying the LMR and keeping the LPR constant at 50 kHz fewer pulses are included in one sine period of the LMR at higher frequencies. In addition, a higher absorption coefficient does not automatically lead to higher oABR amplitudes. In their study, Kallweit et al.<sup>34</sup> described an absorption coefficient optimum and a negative correlation between optoacoustic signal amplitude and absorption coefficient beyond this optimum *in vitro*.<sup>34</sup> Therefore, we hypothesized and demonstrated herein that an extra absorbing layer is a solution to increase the induced activation of the auditory system.

To analyze the effectiveness of our stimulation method further, oABR amplitude values were normalized to aABR values at 80 dB SPL click stimuli. We then analyzed the impact of the film application on the wave I amplitude in aABR and found significantly reduced amplitude values when using a film attached to the TM. This finding is most likely due to the additional mass and damping induced through it on the TM, reducing therefore the sound transduction and damping the vibrations.

As a comparison, we used both aABRs, recorded with and without absorbing film, to normalize the resulting oABR wave I amplitudes (Fig. 7) and the difference was only 5%. Therefore, the impact of the conformation of the film on the interpretation of the results was for this set of experiments negligible.

The optoacoustic stimulation at 79 mW average laser power and 1-kHz LMR led to amplitude values of ~60% of the level that could be reached with 80 dB SPL acoustic click stimulation. At this point, one should consider as well that the click activates multiple frequencies inducing a stronger ABR signal due to the summation of activated potentials in comparison to the single frequencies activated with a frequency-specific stimulation strategy (S2). Nevertheless, we opted for this method of normalizing our data to be in line with research protocols reported by other groups.<sup>29,35–37</sup> Using 8- and 10-kHz LMR, the resulting level was only 50% of the click stimulation while keeping in mind that the number of pulses in one period is lower the higher the LMR. Therefore, the comparison of the oABR data with an adapted acoustic stimulus is not perfect at this point and will be optimized in future experiments.

For biocompatibility reasons with these particular laser parameters,<sup>10</sup> the irradiation level was limited to 79 mW, so higher laser values and the resulting level of reached amplitude levels were simulated by fitting the resulting growth curves. Thereby, we could detect a dynamic range of 50 dB SPL when irradiating the native TM and 70 dB SPL when using an absorbing film. The fitted data also demonstrated that using our actual stimulation method, a saturation level would be reached at 80 mW, inducing amplitudes around 60 dB SPL acoustic click stimulation depending on the used LMR. Further work to optimize the optoacoustic stimulation is therefore planned. Experiments regarding the frequency-specific activation of the hearing function in mice are also intended for the future.

The self-adhesive property of the light-absorbing film and its ability to amplify the optoacoustically induced vibrations make it a promising candidate for enhancing stimulation on different application loci, e.g., TM, middle ear. The light transmission measurements demonstrated that our self-designed film would be applicable for other wavelengths as well. The tight contact between the film and the TM allows the transfer of vibrations directly to the vibrating structure, e.g., TM. Although the weight of the film on the membrane dampens the vibrations in comparison to a native TM (Fig. 6), this influence was minor regarding the effectiveness of the optoacoustic stimulation. The double-layer silicone-based design was developed to provide a structure with both good adhesion and stability. The SSA surface allows for reliable adhesion to the TM without damaging the tissue.<sup>18</sup> On the other hand, the Sylgard portion provides support for the soft SSA film and creates stability during handling and application. The transmission measurements indicate how much of the applied laser energy is transmitted to the TM, which needs to be considered in the biocompatibility studies.<sup>10</sup> The low transmission of the absorbing film confers increased safety while using it during optoacoustic stimulation since a very low amount of the irradiation energy would be transmitted to deeper layers, e.g., in this experimental design the middle and/or inner ear. In addition, the absorption spectrum of the two films was measured and indicates, for the absorbing film, good absorption properties for all wavelengths from 200 to 1300 nm. In contrast, the nonabsorbing film demonstrated no significant absorption and reflection from which it can be concluded that the optoacoustic effect occurs indeed in the absorbing layer of the film.

Fischer et al. demonstrated that PDMS films securely adhere on rough surfaces and even on human skin.<sup>17,38,39</sup> Since our absorbing films could be manufactured in every conceivable design and structure, also other application loci, e.g., the ossicles or the otic capsule (the cochlea wall) within the middle ear, would be imaginable to serve as stimulation loci and adapt therefore to the different pathologies of the hard of hearing patients (e.g., malformed middle ears or having changed anatomy due to infections, cholesteatomas, and/or surgeries). In these cases, the optoacoustic stimulation could be applied on the residual ossicles or the inner ear wall, the otic capsule, directly. Since the optical energy in the form of laser light can be applied very focused on the targeted structure, the optoacoustic stimulation offers a very precise activation method that can be applied according to the individual needs without the very impairing occlusion effect as in conventional hearing devices or a tight contact to the vibratory structure as in bone conduction hearing devices or middle ear implants. As in a future clinical application, gains of up to 75 dB or above for people with profound hearing loss would have to be accomplished by an optoacoustic hearing aid, further strategies to optimize the stimulation strategy are needed, within biocompatibility margins.

Further design optimizations of the absorbing film are possible. For example, a completely pigmented patch could achieve even better results. In addition, the absorbing films have thermal

insulating properties, which make the stimulation less susceptible to heat transmission to the vibrating tissue, and therefore increasing the biocompatibility of the stimulation method. Determination of these properties, as well as long-term application of the absorbing films on the TM, is the subject of our further investigations.

## 5 Conclusion

The optoacoustic stimulation induces oABR waves in mice that are comparable in form and amplitude to acoustically induced waves. The amplitudes obtained were considerably improved by the application of light-absorbing PDMS films on the TM. Therefore, this method is a promising approach for the realization of optoacoustic auditory prostheses.

## Disclosures

The authors have no relevant financial interests in this article and have no potential conflicts of interest to disclose.

## Acknowledgments

This research has been funded by the European Research Council under the European Union's Seventh Framework Program (FP/2007-2013)/ERC Grant, LaserHearingAids: 311469. We further thank Klaus Kruttwig for his assistance in producing absorbable films and his support during manuscript preparation. Further, we acknowledge Isaac Ayala for his assistance in creating the graphical illustration of the mice TM in Fig. 1. The authors also acknowledge Patricia Stahn for her assistance during the manuscript preparation and her support in technical issues during the experiments.

## References

1. J. F. Willott, "Measurement of the auditory brainstem response (ABR) to study auditory sensitivity in mice," *Curr. Protoc. Neurosci.* **34**(1), 8.21B.1–8.21B.12 (2006).
2. L. Rüttiger, U. Zimmermann, and M. Knipper, "Biomarkers for hearing dysfunction: facts and outlook," *ORL* **79**(1–2), 93–111 (2017).
3. T. Schimmang et al., "Lack of Bdnf and TrkB signalling in the postnatal cochlea leads to a spatial reshaping of innervation along the tonotopic axis and hearing loss," *Development* **130**(19), 4741–4750 (2003).
4. A. Zuccotti et al., "L-type CaV1.2 deletion in the cochlea but not in the brainstem reduces noise vulnerability: implication for CaV1.2-mediated control of cochlear BDNF expression," *Front. Mol. Neurosci.* **6**, 20 (2013).
5. K. Zhang et al., "Optoacoustic induced vibrations within the inner ear," *Opt. Express* **17**(25), 23037–23043 (2009).
6. M. Schultz et al., "Nanosecond laser pulse stimulation of the inner ear: a wavelength study," *Biomed. Opt. Express* **3**(12), 3332–3345 (2012).
7. G. I. Wenzel et al., "Green laser light activates the inner ear," *J. Biomed. Opt.* **14**(4), 044007 (2009).
8. P. Stahn et al., "Frequency-specific activation of the peripheral auditory system using optoacoustic laser stimulation," *Sci. Rep.* **9**(1), 4171 (2019).
9. L. Heimann et al., "Wavelength-specific optoacoustic-induced vibrations of the guinea pig tympanic membrane," *J. Biomed. Opt.* **26**(3), 038001 (2021).
10. K. Sorg et al., "First biocompatibility margins for optical stimulation at the eardrum via 532-nm laser pulses in a mouse model," *J. Biomed. Opt.* **26**(8), 085003 (2019).
11. M. K. Kwak, H.-E. Jeong, and K. Y. Suh, "Rational design and enhanced biocompatibility of a dry adhesive medical skin patch," *Adv. Mater.* **23**(34), 3949–3953 (2011).

12. G. P. Duck et al., "Development of flexible self adhesive patch for professional heat stress monitoring service," in *Annu. Int. Conf. IEEE Eng. Med. and Biol. Proc.*, Vol. 7, pp. 3789–3792 (2005).
13. S. H. Jeong et al., "PDMS-based elastomer tuned soft, stretchable, and sticky for epidermal electronics," *Adv. Mater.* **28**(28), 5830–5836 (2016).
14. S. Baik et al., "Bioinspired adhesive architectures: from skin patch to integrated bioelectronics," *Adv. Mater.* **31**(34), 1803309 (2019).
15. A. S. Nittala et al., "Like a second skin: understanding how epidermal devices affect human tactile perception," in *Conf. Hum. Factors Comput. Syst. Proc.* (2019).
16. C. Creton, "Pressure-sensitive adhesives: an introductory course," *MRS Bull.* **28**(6), 434–439 (2003).
17. S. Boyadzhieva et al., "Thin film composite silicon elastomers for cell culture and skin applications: manufacturing and characterization," *J. Vis. Exp.* **2018**(137), 57573 (2018).
18. S. Boyadzhieva et al., "A self-adhesive elastomeric wound scaffold for sensitive adhesion to tissue," *Polymers* **11**(6), 942 (2019).
19. M. Farhadi et al., "Collagen-immobilized patch for repairing small tympanic membrane perforations: *in vitro* and *in vivo* assays," *J. Biomed. Mater. Res. A* **100**(3), 549–553 (2011).
20. E. D. Kozin et al., "Design, fabrication, and *in vitro* testing of novel three-dimensionally printed tympanic membrane grafts," *Hear. Res.* **340**, 191–203 (2016).
21. S. A. L. Schacht et al., "Laser-induced tissue remodeling within the tympanic membrane," *J. Biomed. Opt.* **23**(12), 121614 (2018).
22. L. Rüttiger et al., "The reduced cochlear output and the failure to adapt the central auditory response causes tinnitus in noise exposed rats," *PLoS One* **8**(3), e57247 (2013).
23. J. Engel et al., "Two classes of outer hair cells along the tonotopic axis of the cochlea," *Neuroscience* **143**(3), 837–849 (2006).
24. D. L. Jewett and J. S. Williston, "Auditory-evoked far fields averaged from the scalp of humans," *Brain* **94**(4), 681–696 (1971).
25. J.-J. Chuu, C.-J. Hsu, and S.-Y. Lin-Shiau, "Abnormal auditory brainstem responses for mice treated with mercurial compounds: involvement of excessive nitric oxide," *Toxicology* **162**(1), 11–22 (2001).
26. Q. Y. Zheng, K. R. Johnson, and L. C. Erway, "Assessment of hearing in 80 inbred strains of mice by ABR threshold analyses," *Hear. Res.* **130**(1–2), 94–107 (1999).
27. K. P. Hunter and J. F. Willott, "Aging and the auditory brainstem response in mice with severe or minimal presbycusis," *Hear. Res.* **30**(2–3), 207–218 (1987).
28. A. A. Karabutov, N. B. Podymova, and V. S. Letokhov, "Time-resolved laser optoacoustic tomography of inhomogeneous media," *Appl. Phys. B* **63**(6), 545–563 (1996).
29. V. H. Hernandez et al., "Optogenetic stimulation of the auditory pathway," *J. Clin. Invest.* **124**(3), 1114–1129 (2014).
30. X. Tan et al., "Auditory neural activity in congenitally deaf mice induced by infrared neural stimulation," *Sci. Rep.* **8**(1), 388 (2018).
31. K. R. Henry, "Cochlear microphonics and action potentials mature and decline at different rates in the normal and pathologic mouse cochlea," *Dev. Psychobiol.* **17**(5), 493–504 (1984).
32. B. Fell et al., " $\alpha 2\delta 2$  controls the function and trans-synaptic coupling of cav1.3 channels in mouse inner hair cells and is essential for normal hearing," *J. Neurosci.* **36**(43), 11024–11036 (2016).
33. X. Zhou et al., "Auditory brainstem responses in 10 inbred strains of mice," *Brain Res.* **1091**(1), 16–26 (2006).
34. N. Kallweit et al., "Optoacoustic effect is responsible for laser-induced cochlear responses," *Sci. Rep.* **6**(1), 28141 (2016).
35. T. Mager et al., "High frequency neural spiking and auditory signaling by ultrafast red-shifted optogenetics," *Nat. Commun.* **9**(1), 1750 (2018).
36. J. Wang et al., "Performance analysis of the beam shaping method on optical auditory neural stimulation *in vivo*," *Lasers Med. Sci.* **30**(5), 1533–1540 (2015).
37. R. U. Verma et al., "Auditory responses to electric and infrared neural stimulation of the rat cochlear nucleus," *Hear. Res.* **310**, 69–75 (2014).

Sorg et al.: Optoacoustically induced auditory brainstem responses in the mouse model enhanced...

38. S. C. L. Fischer et al., "Adhesion and relaxation of a soft elastomer on surfaces with skin like roughness," *J. Mech. Behav. Biomed. Mater.* **80**, 303–310 (2018).
39. S. C. L. Fischer et al., "Adhesion and cellular compatibility of silicone-based skin adhesives," *Macromol. Mater. Eng.* **302**(5), 1600526 (2017).

**Katharina Sorg** is a PhD student in the Department of Otolaryngology at Saarland University. She received her BS degree in 2013 and her MS degree in biomedical science from the University Marburg in 2015. In 2016, she started her PhD. Her current research interests include the effects of optical stimulation on the ear and the development of innovative stimulation strategies for hearing impaired persons, based on the use of light energy.

**Larissa Heimann** is a PhD student at Saarland University. She received her German diploma in biophysics from the University of Kaiserslautern in 2018. Her current research interests include optoacoustic stimulation of the hearing organ and the development of a light-based hearing device.

**Gentiana Ioana Wenzel** is apl. Professor and consultant at the University of Saarland, Department of Otorhinolaryngology. Being fascinated by the auditory system, she works on solving therapeutic issues in this field. Currently, she is performing her research work on the development of a new generation of hearing aids based on light energy in parallel to her clinical activities. In addition, she is interested in the development of new materials for medical purposes.

Biographies of the other authors are not available.

#### 4) Self-adhesive silicone microstructures for the treatment of tympanic membrane perforations

Gabriela Moreira Lana, Katharina Sorg, Gentiana Ioana Wenzel, Dietmar Hecker, René Hensel, Bernhard Schick, Klaus Kruttwig, Eduard Arzt

Contribution of the authors:

This work was prepared as shared first authorship between Gabriela Moreira Lana and Katharina Sorg who both performed experiments and composed the manuscript. Gabriela Moreira Lana manufactured the adhesive structures and investigated their characteristics as well as the adhesion on rough indenters and the roughness measurements. Katharina Sorg and Klaus Kruttwig performed the *in vivo* experiments for hearing analysis and analyzed the resulting data. The *ex vivo* adhesion measurements were performed by Katharina Sorg and Gabriela Moreira Lana in equal parts. Gentiana I. Wenzel, Dietmar Hecker, René Hensel, Bernhard Schick and Eduard Arzt were involved in conceptualization, data analysis, manuscript preparation and scientific discussion.

# Self-Adhesive Silicone Microstructures for the Treatment of Tympanic Membrane Perforations

Gabriela Moreira Lana, Katharina Sorg, Gentiana Ioana Wenzel, Dietmar Hecker, René Hensel, Bernhard Schick, Klaus Kruttwig, and Eduard Arzt\*

Inspired by the gecko foot, polymeric microstructures have demonstrated reliable dry adhesion to both stiff objects and sensitive surfaces such as skin. Microstructured silicone patches are proposed, herein, for the treatment of tympanic membrane perforations with the aim of serving as an alternative for current surgical procedures that require anesthesia and ear canal packing. Sylgard 184 PDMS micropillars of 20  $\mu\text{m}$  in diameter and 60  $\mu\text{m}$  in length are topped by a Soft Skin Adhesive (SSA) MG7-1010 terminal layer, of about 25  $\mu\text{m}$  thickness. The adhesion is evaluated by specially designed tack tests against explanted murine eardrums and, for comparison, against a rigid substrate. Functional effects are evaluated using auditory brainstem responses (ABRs) and distortion product otoacoustic emissions (DPOAE). The adhesion strength of the microstructure and unstructured controls to explanted murine tympanic membranes is comparable (typically 12 kPa), but the microstructured patches are easier to handle by the surgeon. For the first time, partial recovery of hearing performance is measured immediately after patch application. The novel patches adhere without the need for further fixation, removing the need for ear canal packing. The proposed material design holds great promise for improving clinical treatments of tympanic membrane perforations.

## 1. Introduction

Micropatterning of polymeric materials is a powerful sustainable strategy for enhancing adhesion without the use of chemicals.<sup>[1]</sup> Such self-adhesive structures allow gentle and reversible adhesion in industrial robotics applications<sup>[2]</sup> and have been proposed for improved adhesive contact to human skin.<sup>[3–5]</sup> The principle is derived from the attachment organs of geckos, which can reversibly attach to vertical walls and ceilings.<sup>[6–9]</sup> Their adhesion is based on van der Waals interaction strongly enhanced by a compliant microfibrillar (“hairy”) structure. The main advantage of such dry adhesives lies in their chemical-free adhesive function, which would allow biomedical application without the need for further attachment agents.

Our research has focused on developing microstructured adhesives specifically for contact with human skin. Depending on many factors, e.g., location, age, and strain, skin can exhibit different roughness features. Trojahn and coauthors measured in four different skin areas,  $R_a$  ranging from 13.9 to 16.2  $\mu\text{m}$  and  $R_z$  from 61.5 to 71.9  $\mu\text{m}$  (where  $R_a$  is the arithmetic mean deviation from the center line and  $R_z$  is the mean roughness depth).<sup>[10,11]</sup> Roughness is the main factor reducing adhesion due to insufficient molecular contact between the surfaces.<sup>[12]</sup> To achieve good adhesion under these circumstances, several materials strategies are available: 1) the dimensions of elastomeric micropillars can be chosen to optimize adhesion to a specific roughness;<sup>[13]</sup> 2) a compliant polymer film, when thinner than a critical thickness, can sufficiently conform to the surface irregularities to create reliable adhesion;<sup>[14]</sup> and 3) composite micropillars with very soft terminal layers can accommodate roughness of the countersurface.<sup>[8]</sup> Strategies (2) and (3) can be combined by designing a film-terminated structure in which arrays of micropillars are bridged at their terminal ends by a continuous compliant top layer. The mechanics of such film-terminated designs was discussed in detail by Glassmaker et al.<sup>[15]</sup> and Noderer et al.,<sup>[16]</sup> who attributed their superior adhesion to a crack-trapping mechanism: the interfacial crack “feels” the spatial modulation of the local compliance and is pinned in the space between the pillars, where the energy release rate to drive crack propagation is reduced. Such a microstructure can additionally adhere to

G. Moreira Lana, Dr. R. Hensel, Dr. K. Kruttwig, Prof. E. Arzt  
INM – Leibniz Institute for New Materials  
Campus D2 2, Saarbrücken 66123, Germany  
E-mail: eduard.arzt@leibniz-inm.de

G. Moreira Lana, Prof. E. Arzt  
Department of Materials Science and Engineering  
Saarland University  
Campus D2 2, Saarbrücken 66123, Germany

K. Sorg, Prof. G. I. Wenzel, Dr. D. Hecker, Prof. B. Schick  
Department of Otorhinolaryngology  
Saarland University Medical Center  
Homburg 66421, Germany

 The ORCID identification number(s) for the author(s) of this article can be found under <https://doi.org/10.1002/anbr.202100057>.

© 2021 The Authors. Advanced NanoBiomed Research published by Wiley-VCH GmbH. This is an open access article under the terms of the Creative Commons Attribution License, which permits use, distribution and reproduction in any medium, provided the original work is properly cited.

DOI: 10.1002/anbr.202100057

surfaces of different degrees of roughness<sup>[17]</sup> as the real contact area is increased due to the adaptation of the soft top layer and the compliant micropillars.<sup>[17–19]</sup>

The application proposed here for such microstructured films is the treatment of perforated tympanic membranes (TMs). Currently, tympanic membrane perforations (TMPs), especially in persistent or chronic cases, are treated by costly surgical procedures under anesthesia, involving the packing of the outer ear canal until the healing process is completed. This therapy impairs the patient's hearing and could implicate surgery complications.<sup>[20]</sup> Due to these risks of TMP treatments, biomaterials research started to look for promising therapeutic alternatives for TM regeneration, especially for the treatment of large or persistent perforations. Even when perforated membranes heal spontaneously, the repaired membranes can be malformed, acoustically suboptimal, and susceptible to re-perforations.<sup>[20]</sup> The time of healing and the closure rate of TMPs strongly depend on the type (acute or chronic) and size.<sup>[21,22]</sup> Recurring and chronic perforations can cause, in addition to hearing loss,<sup>[23–25]</sup> severe health issues due to the risk of infections and of cholesteatoma formation.<sup>[26]</sup> A fast and mechanically reliable closure of the perforation is therefore indicated.

The TM has an important role in sound transmission to the ossicles and in protecting the middle ear. By collecting vibrations from the incoming sound waves and transforming into mechanical waves as vibrations, the TM is an important factor of the acoustic impedance system. Disturbances in this mechanical system lead to hearing impairment. This can be quantified by recording the auditory brainstem response (ABR) and by measuring the distortion product otoacoustic emissions (DPOAEs). ABR signals generated in the auditory cortex can be detected by peripheral electrodes using a standard method for diagnostic purposes in humans and research purposes in laboratory animals, often along with DPOAEs.<sup>[27,28]</sup> The latter is an important frequency-specific method to detect the functional effects of middle ear disorders, such as otitis media, TMPs, and discontinuity of the ossicular chain.<sup>[29–31]</sup> DPOAE measurements are a very sensitive tool to analyze mechanical alterations in the middle ear, among other things, and therefore can also be used to obtain information about the healing process of the perforated tympanic membrane.<sup>[32]</sup>

In the clinic, acute clean TMPs that are not very large and present no other complications, e.g., large destruction of the edges or involvement of the ossicular chain, are treated by unrolling, subtle correction of their edges, and overlaying a film, which should protect the middle ear and support the healing process. For larger or persistent TMPs, a surgical procedure called myringoplasty, or tympanoplasty, is needed as was first described by Zöllner<sup>[33]</sup> and Wullstein.<sup>[34]</sup> An autologous film (perichondrium, cartilage, or fascia) is positioned underneath the perforation with freshly cleaned margins. For both medical treatments, the newly introduced material needs to be kept in position by packing the outer ear canal, e.g., with a layer of silicon stripes and finally with antibiotic-impregnated gel foam. As an alternative procedure, simple silicone foils can be used to sustain the healing process, reducing the risk of ear infections and possibly improving hearing abilities for small and medium TMPs.<sup>[35,36]</sup> In a clinical study, polydimethylsiloxane (PDMS) films, in combination with immobilized collagen, were used to treat small TMPs with a

success rate of 70%.<sup>[37]</sup> We previously proposed the soft skin adhesive SSA MG7-9800 for this purpose due to its reliable but gentle self-adhesion to tissues, enabling secure adherence and atraumatic removal.<sup>[38,39]</sup> Patching perforated eardrums with self-adhesive materials in humans could therefore improve the treatment for the affected patients and has however, to our knowledge, not been reported so far.

We designed a novel self-adhesive patch in the form of film-terminated microstructured silicone film. For the micropillars, PDMS Sylgard 184 was chosen, whereas the top layer consisted of a soft skin adhesive (SSA MG7-1010). The patches were evaluated, in comparison to nonstructured control samples, regarding adhesion to rigid rough substrates and to explanted murine eardrums. In addition, the functional properties for restoring hearing after closing of TMPs by the adhesive patches were evaluated by click ABR and DPOAE measurements. The resulting properties of the novel patch were extremely encouraging and suggest finalizing the preparations for clinical studies.

## 2. Results

### 2.1. Film-Terminated Microstructured and Control Samples

Film-terminated microstructures consist of a pillar array microstructure topped by a soft skin adhesive layer. Pillars were fabricated by replica molding of Sylgard 184 and subsequently integrated to the SSA layer. **Figure 1a** shows the film-terminated microstructured architecture is schematically illustrated. The scanning electron micrograph presented in **Figure 1b** shows that the actual aspect ratio of the pillars supporting the top layer was somewhat smaller than the designed value 3 because the dipping process required for integration of the MG7-1010 top had created some overlap. Among all sets fabricated, thickness values of the film-terminated microstructures were  $43.2 \pm 1.9 \mu\text{m}$  for the backing layer,  $44.7 \pm 3.0 \mu\text{m}$  for the micropillars, and  $24.9 \pm 3.3 \mu\text{m}$  for the top layer, in total,  $\approx 112 \mu\text{m}$  (**Figure 1c**). The unstructured controls consisted of a  $58.9 \pm 2.3 \mu\text{m}$ -thick Sylgard 184 layer and a  $24.1 \pm 1.9 \mu\text{m}$ -thick MG7-1010 top layer, with a total thickness of  $\approx 85 \mu\text{m}$ . The mass per area was  $\approx 0.08 \text{ mg mm}^{-2}$  for the two specimen types.

### 2.2. Roughness

To define the roughness of the murine tympanic membrane, replicas were produced by imprinting with a room-temperature fast-curing silicone, applied through the outer ear canal on the exposed tympanic membrane. Subsequently, the roughness was determined from the silicone replicas using confocal scanning microscopy. The arithmetic mean height ( $R_a$ ) of the replicas of explanted TMs was  $0.14 \pm 0.04 \mu\text{m}$ . In comparison, the arithmetic mean height ( $R_a$ ) of the epoxy substrate used in the adhesion measurements carried out in laboratory was  $0.41 \pm 0.01 \mu\text{m}$ . Mean peak to valley roughness ( $R_z$ ) values were  $1.18 \pm 0.42 \mu\text{m}$  for the TM replicas and  $2.5 \pm 0.08 \mu\text{m}$  for the epoxy substrate. Root mean square (RMS) roughness values were  $90 \pm 31$  and  $12 \pm 1 \mu\text{m}$ , respectively.

Exemplary surface scans of the TM replicas and the epoxy substrate are shown in **Figure 2**. The two measurements of the TM replicas (**Figure 2b,c**) show some differences, which illustrate the

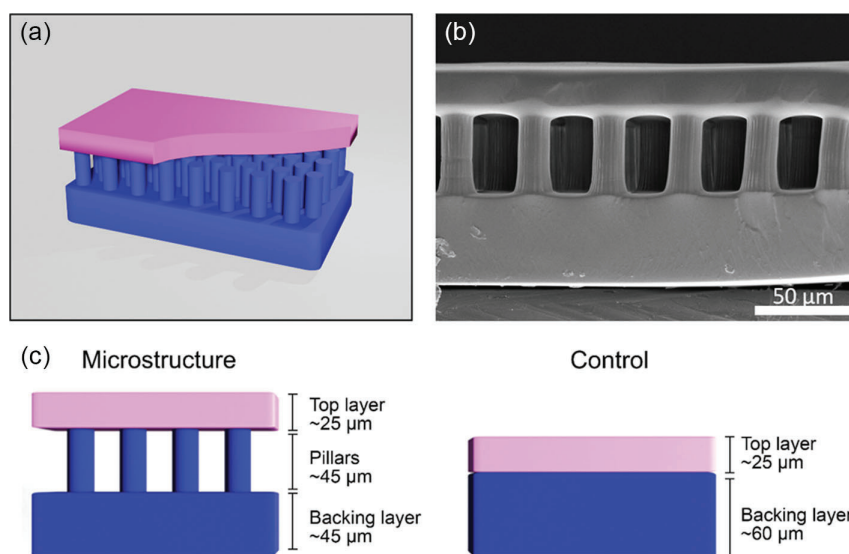


**Figure 1.** Film-terminated microstructure proposed for repair of tympanic membranes. a) 3D representation of the film-terminated design, Sylgard 184 in blue and soft skin adhesive SSA MG7-1010 in pink. b) Scanning electron micrograph of an actual microstructure, side view. c) Schematic illustration showing the approximate dimensions of the top layer, pillar portion, and backing layer for film-terminated samples in contrast to the top layer and backing layer in the unstructured control sample.

large deviation between different measurements and will reflect on deviations in adhesion measurements, described later. The scan of the epoxy substrate is shown in Figure 2d.

### 2.3. Pull-Off Stress Against Epoxy

First, the adhesion of the microstructured and control patches was measured against the rigid epoxy substrate of roughness  $R_z$  of 2.5  $\mu\text{m}$ . **Figure 3** shows that the microstructured adhesive had a significantly higher adhesion to epoxy than the unstructured control sample: after applying a compressive prestress of 11 kPa, the microstructures detached at  $72.7 \pm 9.4$  kPa and the control samples at  $39.4 \pm 16.5$  kPa; the improvement factor was 1.89 ( $p$ -value 0.001). For a prestress of 23 kPa, the microstructures exhibit similar adhesion values, but the improvement factor went down to 1.27 ( $p$ -value 0.03). This was due to the strong increase in the unstructured control samples by 56 % at the higher prestress, presumably due to better conformation to the substrate roughness.

### 2.4. Adhesive Strength Against Murine TMs Using Ex Vivo Tests

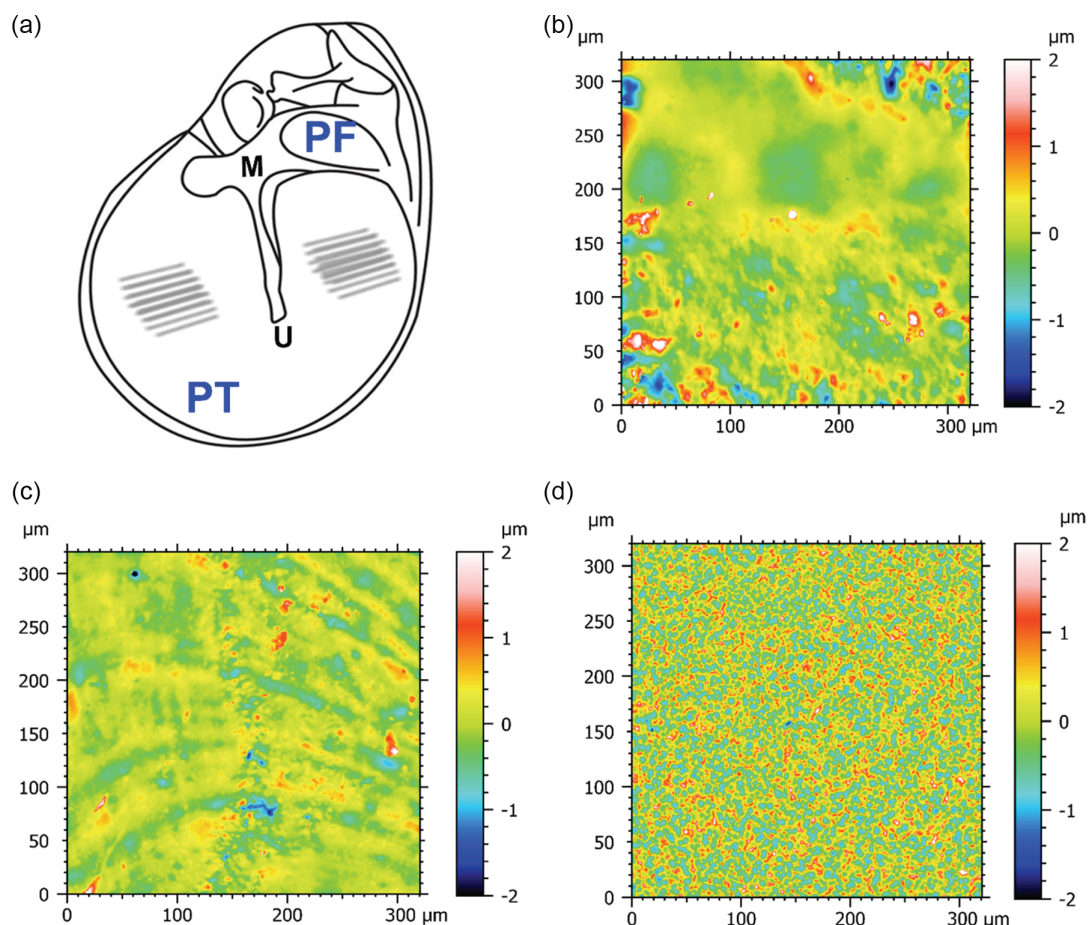
To evaluate the adhesion of the patches closer to real conditions, adhesion measurements were carried out on intact and perforated, explanted tympanic membranes of mice. **Figure 4a** shows an explanted murine petrosal bone with the TM exposed. Three different adhesive patches were tested: 1) film-terminated microstructures, 2) control films with its adhesive side (MG7-1010 layer) adhered to the TM, and 3) control films with nonadhesive backside (Sylgard 184 layer). The custom-made sample holder was used to align the explanted TM in a 90° angle to the patch applicator, as shown in Figure 4b,c. As shown in

Figure 4a, the patches were positioned to fully cover the perforation. Care was taken that the patch had still enough overlap with the remaining membrane to ensure its adhesion. The size of an average perforation was about  $700 \times 500 \mu\text{m}^2$ ; this amounted to roughly 10% of the total area of the murine tympanic membrane (with typical dimensions of  $2 \times 2 \text{mm}^2$ ) and  $\approx 40\%$  of the patch area (1 mm diameter).

Exemplary stress versus time curves (Figure 4d) for measurements on intact (blue) and perforated (green) TMs demonstrate the gradual increase in the compressive prestress up to a set value of  $\approx 25$  kPa. To conduct the experiments in the shortest time possible and avoid therefore changing in the membrane's properties, we limited the compressive preload condition to one value. The position was held for 10 s, which was accompanied by some slight relaxation possibly due to the soft top layer. Upon retraction, patches detached at various tensile loads. The detachment is typical for tack measurements of soft materials.<sup>[40]</sup>

Our results on intact TMs (**Figure 5a**) demonstrated that the adhesive strength of the film-terminated microstructure patches was significantly higher compared with the nonadhesive, unstructured control ( $p = 0.002$ ) but not higher than the adhesive side of the control sample. The mean pull-off stress of microstructured patches was  $14.5 \pm 8.8$  kPa, with a maximum of 32.3 kPa and a minimum of 5.7 kPa. Mean value for the adhesive control was  $13.3 \pm 7.2$  and  $5.7 \pm 4.6$  kPa for the nonadhesive control. The mean pull-off stress of the film-terminated microstructured patches was  $\approx 9\%$  higher, but not statistically significant, compared with the adhesive control ( $p = 1$ ). An explanation for the large deviation probably relates to large variations of the explanted TMs and the conditions of the ex situ adhesion measurements.

On the perforated TM (Figure 5b), the pull-off stress values were overall reduced compared with the intact condition. In



**Figure 2.** Surface roughness of murine TMs and epoxy substrate. a) Measurement locations in the pars tensa (PT), which is separated by the malleus (M) with its lowest part at the umbo (U). PF is pars flaccida. b,c) Inverse topography scans of tympanic membrane measured on silicone replicas. d): Topography scan of the epoxy substrate. Roughness measurements were obtained from 14 replicas of 7 TMs measured in three different positions of the PT, and for epoxy substrates in three independent positions.

the adhesive and nonadhesive control sample, adhesion decreased by 43% and 49%, which is comparable with the loss of contact area due to the perforation; by contrast, microstructured patches suffered only a 17% reduction. The adhesion of the film-terminated microstructure ( $p$ -value 0.002) and the adhesive, unstructured control ( $p$ -value 0.006) was significantly higher than the nonadhesive control. The difference between the microstructured adhesive patches and the adhesive control samples were higher than before (14.5–13.3 vs 12.1–7.6 kPa), but again not statistically significant ( $p = 0.14$ ).

## 2.5. Physiological Effects on the Hearing Performance

To gain information about the overall hearing function, ABR recordings were carried out as a standard method to determine auditory function in vivo. Thereby, the hearing threshold under three conditions was analyzed: 1) on intact TM; 2) perforated TM; and 3) after applying a patch on the perforation.

The results of the click ABR recordings demonstrated that the hearing threshold significantly increased after perforation from 12 dB SPL to 34 dB SPL in both groups, which translates into an

increase of 283% ( $p$ -value 0.003 and 0.01, respectively). Covering the perforation with patches led to a statistically nonsignificant decrease in the threshold in both groups with microstructured patches as well as unstructured control patches (Figure 6a,b).

The click-ABR is testing, however, the cumulative hearing activation overlapping the induced activation of all frequencies included in the click applied. The technique is therefore not sufficiently sensitive for judging the hearing improvement at individual frequencies through patch application. Therefore, to analyze the effects of closing the perforation in a more sensitive and frequency-specific manner, DPOAE recordings were carried out after ABR measurements. The results of the in vivo DPOAE measurements in anesthetized mice with intact and perforated TM were compared after the closure of the perforation with the two different patches, i) the film-terminated microstructured patch and ii) the unstructured adhesive control (Figure 7a,b). Through this, a difference between the lower frequencies (10–15 kHz) and the higher frequencies (15–18 kHz) could be measured.

The averaged DPOAEs between 10 and 15 kHz demonstrated an improvement after applying microstructured patches (Figure 7c). Here, the DPOAE signals dropped from

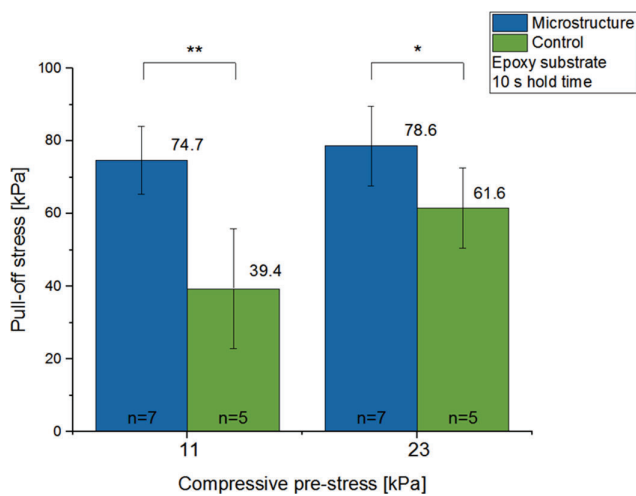


**Figure 3.** Adhesion of film-terminated microstructures and unstructured controls as determined by tack tests against epoxy substrates. The compressive prestress was varied from 11 (left) to 23 kPa (right). The hold time at prestress was 10 s. The data are presented as mean ± SD. The mean values are labeled above each graph. Number of experiments: seven measurements for film-terminated microstructures and five measurements for control samples, *p*-values are calculated using two-sided *t* test. \* characterizes *p* < 0.05 and \*\* indicates *p* < 0.01.

26.4 ± 2.3 dB in intact condition, by ≈34%, to 17.5 ± 3.8 dB after perforation (*p* = 1.27 × 10<sup>-6</sup>). The application of film-terminated microstructure led to a highly significant increase to 21.8 ± 2.9 dB (Figure 7c) corresponding to + 25 % (*p* = 0.006). By contrast, in the group treated with control adhesives (Figure 7d), the same proportional decrease was followed by an increase by ≈21% to 21.2 ± 4 dB, which is statistically not significant (*p* = 0.06). In the higher-frequency range, from 15.5 to 18 kHz (Figure 7e,f), the DPOAE signals decreased after perforation by ≈24% from 30.1 ± 3.3 to 23 ± 2.8 dB for the microstructure and by ≈28% from 30.7 ± 2.4 to 22.1 ± 4.9 dB for the control group. The application of the film-terminated microstructure led to a non-significant improvement from 23 to 23.2 dB being ≈+0.7 % of the DPOAEs (*p* = 1), whereas the application of control films led to a significant increase by about 10% from 22.1 to 24.5 dB (*p* = 0.02). In none of these measurements, full recovery of the DPOAE levels to intact levels was achieved by patching in the acute herein presented conditions.

As mass and damping are essential parameters to be considered in analyzing the vibratory characteristics of a structure, we also investigated the effects of applying microstructured and control patches (in the thin and additionally coarser dimensions ≈300 μm total thickness) on the intact membrane and gained more information on the influence of patching on the sound conduction

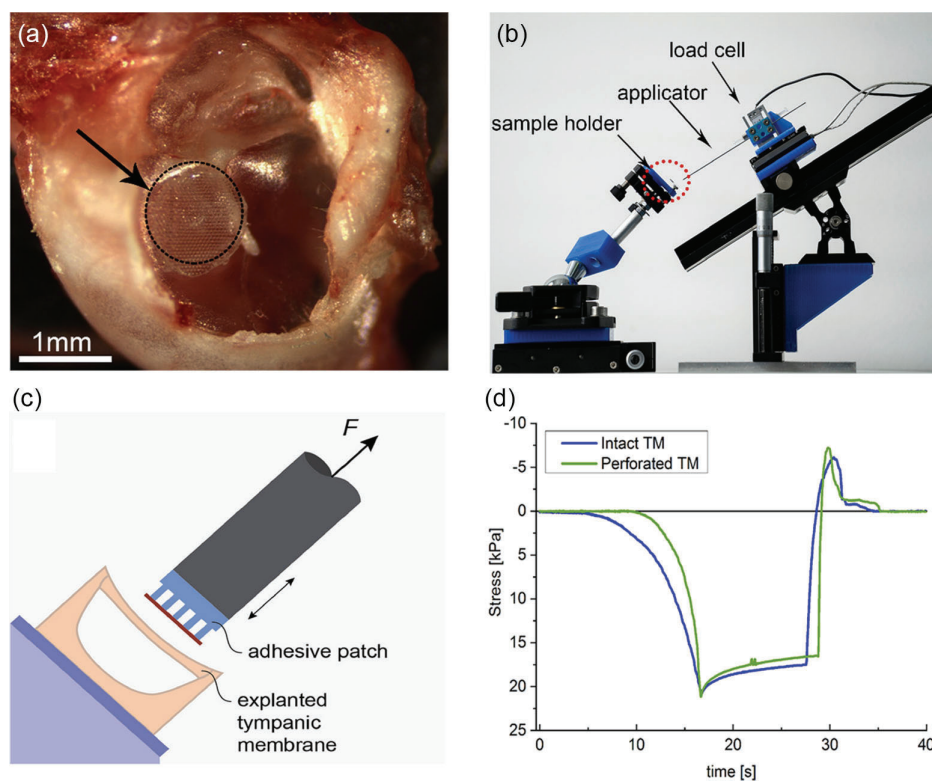


**Figure 4.** Ex vivo adhesion tests on intact and perforated murine TMs. a) Photograph of a film-terminated microstructured patch (indicated by the black arrow + dotted line) covering a perforation in the upper posterior quadrant of the murine TM. b) The measurement setup consisting of an adjustable sample holder to fix the explanted tympanic membrane and the adhesive patch mounted on a motorized applicator equipped with a load cell. c) Illustration of the test procedure indicated in b) as red dotted circle: TMs with petrosal bone mounted on a glass substrate was contacted by the adhesive patch, ensuring parallel contact. d) Exemplary stress versus time curve: The compressive prestress of ≈25 kPa was held for 10 s and the patch detached completely from the intact (blue line) or perforated (green line) TM at stresses of about 8 kPa. Positive values indicate compressive stress, and negative indicate tensile stress.

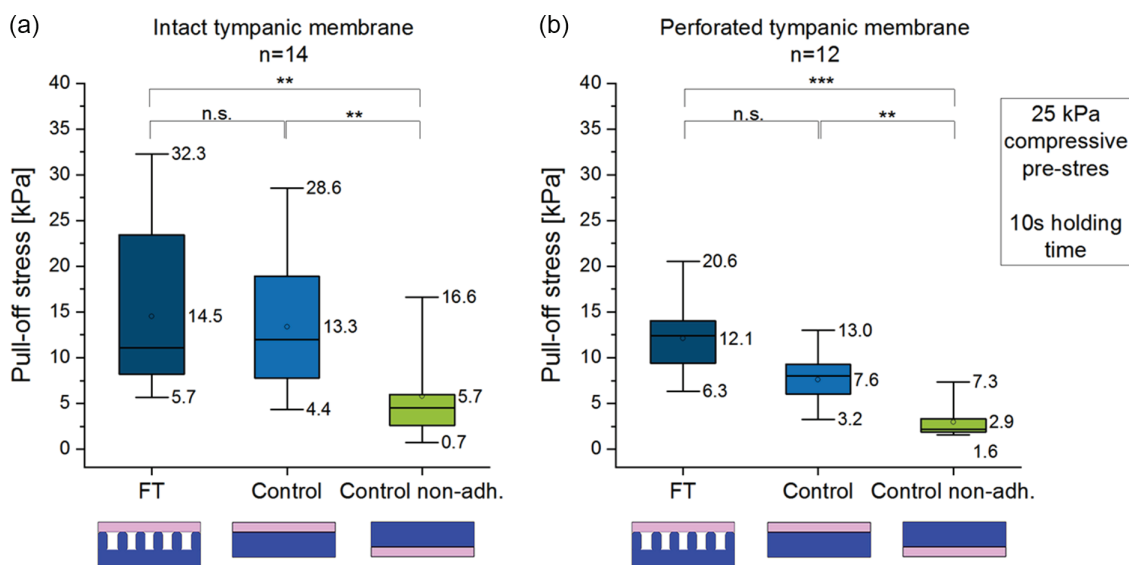


**Figure 5.** Pull-off stress for a) intact and b) perforated explanted TMs. Samples were film-terminated microstructures (FT, dark blue boxes) and unstructured control films with their adhesive side (control, light blue boxes) and their nonadhesive (nonadh., green boxes) side in contact. In the box and whisker plots, each box represents the range from the first quartile to the third quartile. The median is indicated by a line inside the box, the mean is indicated by a dot. The whiskers represent the ranges from the minimum to the maximum value of each group. Mean, minimum, and maximum values are also labeled with their values beside the boxes. Number *n* indicates independent measurements for a) *n* = 14, b) *n* = 12. *p*-Values are calculated using Kruskal–Wallis test followed by Dunn’s test posthoc analysis for pairwise comparisons \*\* indicates *p* < 0.01.\*\*\* indicates *p* < 0.001; n.s. = nonsignificant.

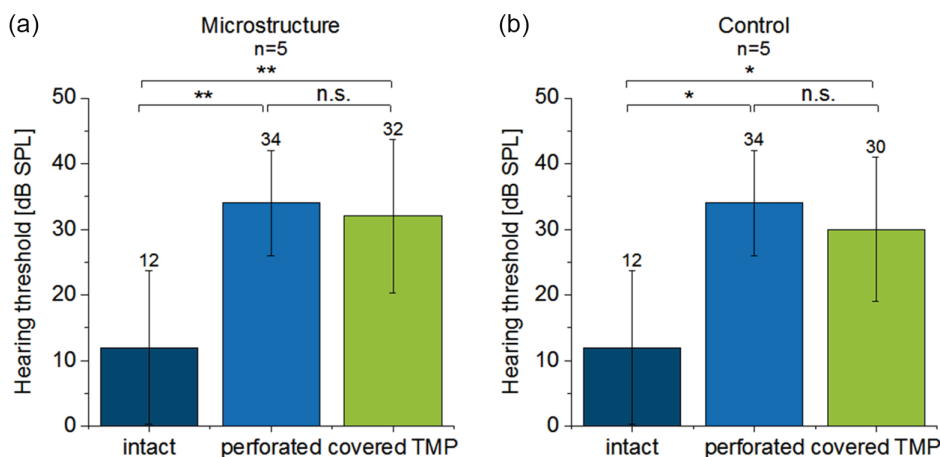


**Figure 6.** Analysis of the effects of perforation and covering of the TMP with a) microstructured or b) control patches on the hearing threshold, recorded by click–ABR in contrast to intact condition. The hearing threshold significantly increased after perforation from 12 to 34 dB SPL in both cases. a) After applying microstructured patches, the threshold decreased non-significantly to 32 dB SPL. b) After applying control patches, the threshold decreased nonsignificantly to 30 dB SPL. The data are presented as mean ± SD. The mean values are labeled above each graph, *n* = 5, *p*-values are calculated using one-way ANOVA with repeated measures followed by Bonferroni-test for pairwise comparison. \* indicates *p* < 0.05 \*\* indicates *p* < 0.01; n.s.= nonsignificant.

of the TM (Figure S1, Supporting Information). In all cases, the DPOAE signals were significantly reduced after patch application, especially for the coarser, more massive patches. When applied on the perforated membrane (Figure S2, Supporting Information), the coarser patches had no significant effect on the hearing function in comparison with the perforated condition.

From the surgeon’s perspective, handling and application of the microstructured patches was more precise than for the controls, possibly because the pressure was more easily distributed

through the more compliant structure onto the thin TM. In addition, the microstructure adhered less to the thin forceps allowing easier adjustments of its position.

### 3. Discussion

In an attempt to improve current therapeutic strategies for surgical interventions on ruptured tympanic membranes, we

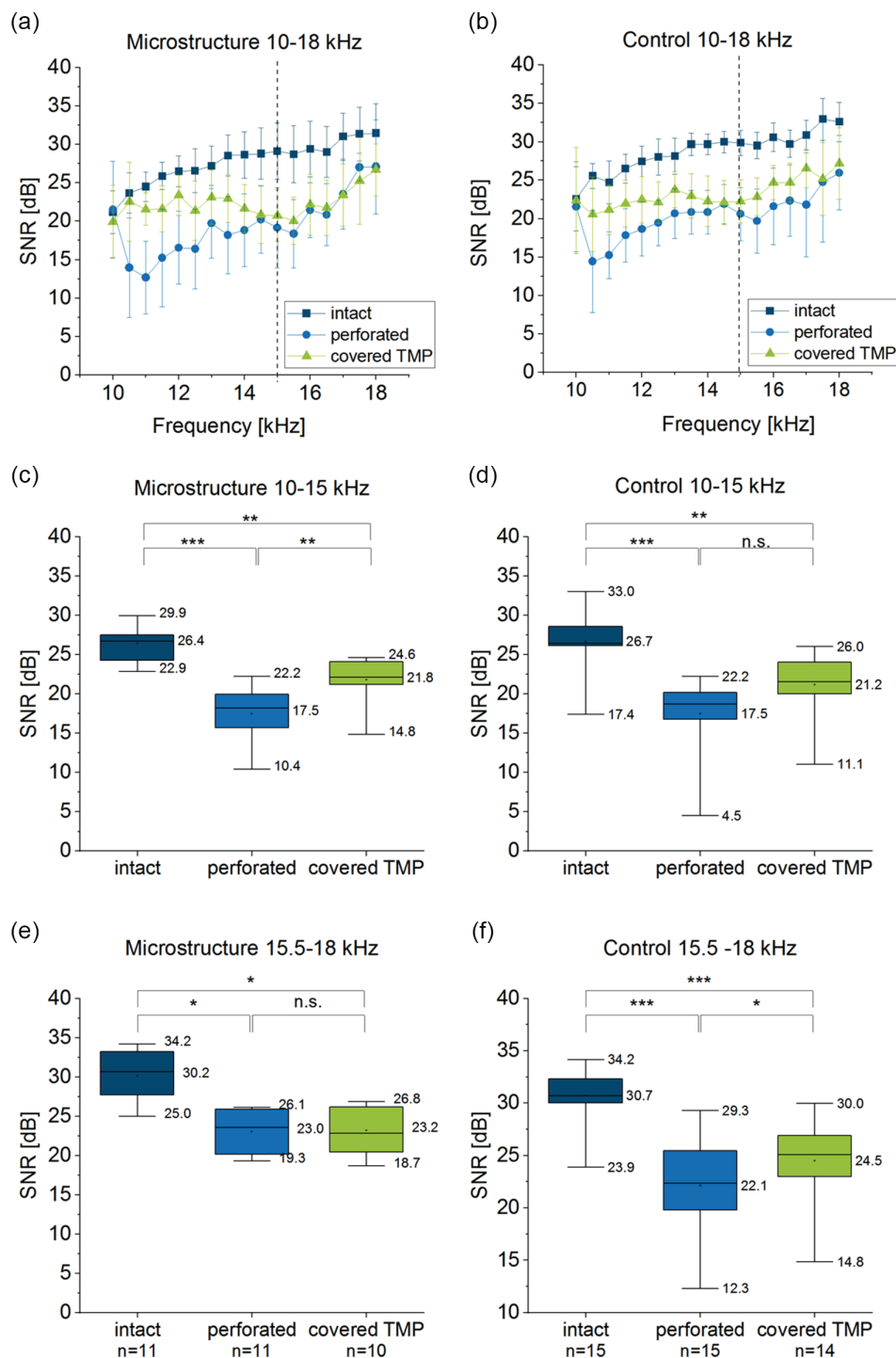


**Figure 7.** Hearing function in intact, perforated, and patched condition as measured by DPOAE. DPOAEs after treatment with microstructured patches (a, green data) showed an increase in the lower-frequency range, whereas the control (b) enhanced all frequencies compared with the perforated condition. c,d) Averaged SNRs point to a significant increase in DPOAE signals after patching compared with the untreated perforated TM between 10 and 15 kHz using the microstructure patches (c). d) Averaged SNRs were not significantly enhanced after applying control patches. e,f) Averaged SNRs in between 15.5 and 18 kHz. e) Microstructure patches led to a nonsignificant increase in SNRs, whereas in this frequency range, f) the application of control patches led to a significant increase in SNRs. Data are represented in a,b) as mean  $\pm$  SD. In the box and whisker plots, in c–f) each box represents the range from the first quartile to the third quartile. The median is indicated by a line inside the box, the mean is indicated by a dot. The whiskers represent the ranges from the minimum to the maximum value of each group. Mean, minimum, and maximum values are also labeled with their values beside the boxes. In c,f), *p*-values are calculated using ANOVA with repeated measures with Bonferroni test for pairwise comparisons and in e,d) with a Friedman–ANOVA with Dunn’s test for pairwise comparisons. \* indicates  $p < 0.05$ , \*\* indicates  $p < 0.01$ , and \*\*\* indicates  $p < 0.001$ , n.s. = nonsignificant. The number of replicates is indicated below the plots in e,f.

investigated a novel silicone microstructured patch in experiments with artificial surfaces and in a mouse model. Three main aspects will be discussed in turn: roughness of the tympanic membrane, adhesive properties of the patch, and its effect on hearing performance.

### 3.1. Roughness Characterization of the Murine TM

Aiming the development of an adhesive patch for application at the eardrum and considering the roughness as the first challenging factor against adhesion due to reduction of contact between two surfaces, we first evaluated this parameter of the tympanic membrane and the proposed model surface.

The height profiles in Figure 2b,c are, to our knowledge, the first reported roughness data for tympanic membranes of mice. The eardrum replicas are believed to closely match the conditions of the real murine membrane although slight material shrinkage could have affected the results.<sup>[14]</sup> The data showed relatively smooth surfaces for the TM ( $R_a \approx 0.14 \mu\text{m}$  and  $R_z \approx 1.18 \mu\text{m}$ ), in comparison, for example, to the roughness of human skin reported in literature ( $R_a \approx 13\text{--}16 \mu\text{m}$  and  $R_z \approx 61\text{--}71 \mu\text{m}$ ).<sup>[10]</sup> It should however be noted that singular values of  $R_a$  or  $R_z$  are insufficient descriptors of complex rough surfaces; a full analysis of the surface roughness using a power spectrum, as was carried out for skin, e.g., by Kovalev et al., was beyond the scope of this article.<sup>[41]</sup>

As a model surface, we chose an epoxy replica of frosted glass, whose roughness profile was comparable but did not fully match that of the eardrum. The epoxy exhibited a more homogeneously distributed roughness than the tympanic membrane, with higher  $R_z$  roughness values.

### 3.2. Adhesion Properties of the Patches

Against the epoxy model surface, our film-terminated microstructures demonstrated, for all tested parameters, higher adhesion in comparison with unstructured controls (Figure 3). This very likely reflects the previously studied crack trapping mechanism,<sup>[15,16]</sup> possibly in combination with the reduced effective modulus which facilitates adaptation to surface roughness. The advantage of the microstructure was especially pronounced (almost by a factor 2) for the smaller prestress value (11 kPa). For the larger prestress (23 kPa), on the other hand, the improvement was only about 27%. A possible explanation is the very soft top layer, which adapts to the surface topography leading to complete contact and a maximum pull-off stress when the prestress is sufficiently high.<sup>[17,42]</sup> The high adhesion for small prestress could be beneficial for future application in humans, as smaller forces exerted by the surgeon will lower the likelihood of damaging the TM.

As a next step, we evaluated the adhesion of the films on explanted tympanic membranes of mice as self-adhesion is an essential aspect for our novel designed films for eardrum perforation treatment. This characteristic gives them the advantage over the commercially available, nonadherent films, to not require packing of the outer ear canal with the consequent additional hearing impairment during the healing time. This experiment was carried out, to our best knowledge, for the first time in

the literature and required the design of a dedicated ex vivo measurement set-up. First, it was found that the adhesion values were generally lower for the perforated TM compared with the intact TM, presumably due to the reduction in actual contact area. An additional effect could be the reduced tension of the pars tensa (PT) after perforation, which would lead to a less defined contact and make the countersurface more compliant.<sup>[43]</sup>

Second, the adhesion performances of the microstructure and the control were very similar, the difference was not statistically significant for both the intact and the perforated condition.

A third observation is the generally lower adhesion to the eardrum than to the epoxy model surface. This is not surprising as the two substrate materials differ greatly in elastic modulus and geometric complexity (i.e., the concave curvature of the eardrum versus a nominally flat epoxy surface). A related aspect was that the two test setups used differed in stiffness. Still our approach follows common practice in standardized testing of medical adhesives, where adhesion is measured against steel substrates and empirical correlations to skin adhesion are assumed.<sup>[44,45]</sup>

In more quantitative terms, the top layer thickness necessary to accommodate the roughness characterized by  $R_z$  can be estimated. Following Davis et al.<sup>[46]</sup> and Fischer et al.,<sup>[14]</sup> adhesion will be insensitive to roughness above a critical film thickness given approximately by

$$h_{\text{crit}} \approx R_z^2 \cdot \frac{E_{\text{eff}}}{W_{\text{ad}}} \quad (1)$$

where  $E_{\text{eff}}$  is the effective modulus and  $W_{\text{ad}}$  the work of adhesion, assumed to be  $50 \text{ mJ m}^{-2}$ . For a film made of MG7-1010 with a Young's modulus of  $250 \text{ kPa}$ <sup>[47]</sup> on the tympanic membrane ( $R_z = 1.18 \mu\text{m}$ ),  $h_{\text{crit}} \approx 7 \mu\text{m}$ , which is well below the thickness of the top layer ( $\approx 25 \mu\text{m}$ ). In contrast, for the rougher epoxy substrate,  $h_{\text{crit}} \approx 32 \mu\text{m}$ , which is close to the top layer thickness. These results indicate that the adhesion on the epoxy substrates must benefit from the compliance of the underlying microstructure, whereas that on the explanted TM is solely associated with accommodation by the soft top layer, as in the control sample. Although the present results for microstructured patches did not confirm improved adhesion to murine eardrums, microstructures are expected to benefit in clinical applications where adhesion must be ensured to rougher human TMs. Work along these lines is currently in progress. In addition to advantageous adhesion on the rougher TM, the microstructure could even be further optimized by varying the top layer and the pillars dimensions,<sup>[17,47]</sup> allowing for a tunable and more personalized design of the patches, according to the patient's needs. Thereby, the adhesion could be easily adapted to the specific pathological findings. For example, larger or longer persistent perforations might need stronger adhesion to stay attached longer, in comparison with small acute perforations that heal faster. Another important argument in favor of our microstructured patches is the experience gained in the animal experiments that indicated that these patches proved to be easier to apply to the murine TM. The microstructures allowed for better gripping, were easier to handle and less prone to rolling-up. This can be explained by comparing the bending stiffness of both samples (calculations shown in Supporting Information). The calculated value of bending stiffness is almost 2.3 times higher for the microstructure than

the control sample (see Figure S3 and Section 1, Supporting Information). Also, the more even distribution of the compressive prestress improves the integrity of the remaining TM and ensures homogeneous adhesion without causing macroscopic damage of the sensitive membrane during removal. The film-terminated design offers the advantage, over bare micropillars, of proper sealing of the perforation especially along the perforation margins. This restores, at least partially, the acoustic and protective properties of the TM.

One further advantage of the film-terminated microstructures could be the insertion of inflammation- and infection-suppressing agents, e.g., cortisone or antibiotics between the pillar portions. The porosity of the top layer would allow diffusion through the material directly to the desired target location. This could result in an engineered release system allowing drug application over a predetermined time.<sup>[48,49]</sup>

### 3.3. Functional Effects on Hearing Ability

To our knowledge, we report here for the first time that appropriately designed adhesive patches have a positive impact on the hearing ability during the healing phase. DPOAE signals were significantly improved immediately following application of microstructured or control patches (Figure 7). The hearing threshold using click-ABR remained largely unaffected (Figure 6) due to the characteristics of click tones used in ABRs containing a wide range of frequencies applied simultaneously.

The frequency-specific analysis of DPOAE demonstrated that microstructured patches enhanced especially the lower frequencies (up to 15 kHz), whereas control patches improved the higher frequency range (between 15.5 and 18 kHz) (Figure 7). After translation to the much thicker human eardrum (thickness  $\approx 120\ \mu\text{m}$  compared with  $\approx 5\ \mu\text{m}$  for the mouse), these damping effects are expected to be much reduced in the final clinical application. Overall, the results will need to be newly evaluated in humans due to different dimensions of the eardrum.

The patches cannot fully restore the function of the damaged eardrum in the mouse model. This is very likely due to the added mass, which influences the acoustic impedance and dampens sound conduction. This effect was proven by the reduction in DPOAE levels after applying patches to intact TMs (Figure S1, Supporting Information). In evaluating these effects, the correlation of DPOAE signals with the state of the TM requires further discussion. In general, the signal level is strongly dependent on the anterograde and retrograde middle-ear transmission and is hence influenced by mechanical changes in the outer ear and middle ear, such as increased mass or stiffness. As a result, the middle ear constitution influences the DPOAE quality twice, by affecting the incoming tones in the inward-direction and the returning DPOAE signals in the outward direction.<sup>[32]</sup> DPOAEs are therefore valuable in detecting not only sensorineural but also conductive hearing loss<sup>[30]</sup> and are routinely used in clinical diagnosis.<sup>[50–52]</sup> In their study on gerbils, Dong et al.<sup>[32]</sup> analyzed the effects of TM perforations and altered middle ear transmission conditions on the generation of DPOAEs. DPOAEs were found to be measurable up to perforation sizes covering about half the tympanic membrane. DPOAE thresholds were not totally restored to normal after 4 weeks of incubation, especially at

higher frequencies ( $>10\ \text{kHz}$ ). The fact that DPOAE signals did not totally recover even after closure of the TM perforation was ascribed to an incompletely restored middle ear transmission.

The immediate improvement of the auditory function in mice, as suggested by our study, would be advantageous for the treatment of patients, who would also benefit from a free ear canal during the healing phase. According to most studies of the healing time of TMs, we expect a retention time of more than 4 weeks of the patch on the perforated membrane.<sup>[53–55]</sup> To the best of our knowledge, most studies on TMP treatment use nonadhesive materials that require the packing procedure of the outer ear canal to keep the patch in position. In the study of Farhadi et al.,<sup>[37]</sup> collagen-covered PDMS patches applied to longstanding, small perforations in ten patients had an overall success rate of 70% after 1 month. These patches had to be fixated by gel foam, which led to an inevitable conductive hearing loss. Park et al. reported about the use of Steri-Strip patching, an adhesive material using for wound closure, in comparison with paper patch and spontaneous closure and reported decreased need for repeated patching procedures in the Steri-Strip group. On the other hand, in the Steri-Strip group, significantly increased rates of otorrhea occurred.<sup>[56]</sup> Further studies on adhesive patching, published by Aslan et al. 2011, reported on an immediate hearing improvement after patching with Steri-Strips except in the patients with chronic perforations.<sup>[57]</sup> Self-adhesive silicone elastomers offer the advantage to be applied and fixed without the need of chemical glues, as e.g., acrylic adhesives used in Steri-Strips. Combined with the positive effects on the hearing performance after patching, silicone elastomers offer a minimally invasive, cost-effective, time saving, and easy to use technique for closing TMPs.

For future medical treatments of TMPs, cell growth on our adhesives is an important factor. In previous studies, we successfully demonstrated that cells spread in functionalized MG7-9800,<sup>[39,58]</sup> which is a similar soft skin adhesive as the MG7-1010 used in our study. However, these studies have to be repeated for the current material before considering clinical trials. Although less quantifiable, the surgeon's experience with the microstructured patches will be an important factor in their clinical success. The generally positive perception with regard to ease of handling, coupled with the potential benefits to the patient during and after the healing period, enhances the chances of a successful translation of these novel microstructured patches into clinical practice.

## 4. Conclusions

We present, for the first time, the design and fabrication of microstructured, film-terminated silicone patches for application on tympanic membrane perforations. These structures were tested first on relatively rough artificial rigid surfaces, where they demonstrated higher pull-off stresses compared with the unstructured controls. The adhesion of both types of patches, tested on murine explanted tympanic membranes using a customized setup, was similar for both samples. We foresee, however, a positive effect of microstructured patches on human tympanic membranes, which exhibit greater roughness. In

addition, through the continuous top layer, the patches allow proper sealing of the perforation and may avoid the entrance of pathogens into the middle ear. In a living animal model, the hearing function, investigated by DPOAE signals, was partially restored immediately after patch application. The microstructured patches allowed for better gripping by the surgeon and were easier to handle. They offer great potential for future treatment of patients suffering from a TMP. Further studies of these novel silicone patches, regarding their effects on healing and long-time behavior, are underway to ensure safe and effective clinical treatment of TMPs.

## 5. Experimental Section

**Fabrication of Film-Terminated and Control Samples:** A new film-terminated microstructure was developed using pillars of  $\approx 20\ \mu\text{m}$  diameter and  $60\ \mu\text{m}$  height (aspect ratio 3), with hexagonal configuration and interpillar distance equal to their diameter. The pillar fabrication process consisted of two replication steps. First, a master structure with a  $0.5 \times 0.5\ \text{cm}^2$  pillar array was printed on a  $2.5 \times 2.5\ \text{cm}^2$  silicon wafer using a methacrylate-based resin (Nanoscribe IP-Q Resin) by two-photon lithography (Photonic Professional GT2, Nanoscribe, Eggenstein-Leopoldshafen, Germany). The master structure was cleaned with isopropanol and gently dried using nitrogen flow. The surface of the master structure was coated with (tridecafluoro-1,1,2,2-tetrahydrooctyl) trichlorosilane (AB111444, ABCR, 97%) upon activation in an air plasma (Atto low pressure plasma system, Electronic Diener, Ebhausen, Germany) for 5 min. Coating occurred via vapor deposition in reduced pressure of about 3 mbar for 15 min. A mold (negative) was thereafter replicated from the master by pouring PDMS (Elastomer kit Sylgard 184, Dow Silicones, Midland, MI, USA) onto the microstructure placed in a Petri dish. After curing for 1 h at  $95\ ^\circ\text{C}$ , the mold was gently peeled and silanized using the same process as described earlier. Sylgard 184 was poured on the mold and degassed for 5 min to properly fill the cavities. Then, the excessive polymer was removed by spinning the mold at 1000 rpm for 120 s (Spin coater Laurell WS 650 MZ-23NPPB, North Wales, Pennsylvania, USA). This resulted in a homogeneous backing layer, the base for the pillars. After curing at  $95\ ^\circ\text{C}$  for 1 h, the pillar array was gently removed from the mold and placed on a polyethyleneterephthalat (PET) film to stabilize the microstructure and facilitate handling. For film-termination, first a thin MG7-1010 (Dow Silicones, Midland, Michigan, USA) film was prepared on a fluorosilicone release liner (Siliconature, SILFLU S 75 M 1R88002 clear) at 7000 rpm for 120 s and subsequently cured at  $95\ ^\circ\text{C}$  for 1 h. On top of this film, a second layer of MG7-1010 was prepared, again using 7000 rpm. The microstructure was placed upside down onto the uncured film and subsequently cured. Upon peeling the entire structure from the release liner, the film-terminated microstructures were used without further treatments. It is to be noted that MG 7-1010 is a certified medical product. In accordance with the safety data sheet, skin absorption of hazardous substances is unlikely even after long-term exposure to skin.

The unstructured samples (to be referred to as “control sample”) were prepared by first fabricating a Sylgard film on a PET film using a doctor blade (AFA-IV, MTI Corporation, Richmond, CA, USA). The thickness of the Sylgard layer was chosen according to the amount of Sylgard used for the microstructured specimen to match the mass of the sample. The soft skin adhesive layer was added with the same procedure as the film-termination described earlier. All specimen dimensions were measured using an optical microscope (Eclipse LV100ND, Nikon, Tokyo, Japan) and a scanning electron microscope (FEI Quanta 400 ESEM, Thermo Fisher, USA). For the latter, specimens were sputter-coated with gold and analyzed under high vacuum, below  $3 \times 10^{-2}\ \text{Pa}$ , 7 kV voltage and a secondary electron detector.

**Roughness of Model Surfaces and Tympanic Membranes:** The roughness of the substrate surfaces made from epoxy was measured using a confocal microscope (MarSurf CM explorer, Mahr, Göttingen, Germany). Measurements were carried out at three positions using a  $50\times$  objective. The roughness of the murine TM was indirectly determined by measuring silicone replicas prepared prior to the ex vivo adhesion measurements (see Section 2.4). In total, 14 replicas of seven eardrums were measured, each of them at three different positions of the PT, using a  $50\times$  objective. The surface analysis was carried out using the software “Marsurf MFM Extended” on a surface of dimensions  $320 \times 320\ \mu\text{m}^2$ . The raw data were fitted with a Gaussian filter having a cut-off length of  $2.5\ \mu\text{m}$ , a seventh-order polynomial and a cut-off length of  $250\ \mu\text{m}$ .

**Adhesion Measurements:** Tack tests were carried out using a custom-built adhesion testing device.<sup>[58,59]</sup> Normal forces were recorded using a 0.25 N load cell (ME-Meßsysteme GmbH, Hennigsdorf, Germany). The surface used for adhesion measurements was the flat face of a cylinder made from epoxy resin, replicating a frosted glass slide (Marienfeld, Lauda Königshofen, Germany). For details see the study by Fischer et al.<sup>[14]</sup>

The measurements were carried out by approaching the sample to the substrate surface at a rate of  $30\ \text{m s}^{-1}$  until a compressive preload of 30 or 60 mN was reached. The sample was held in contact with the surface for 10 s, and then retracted with a velocity of  $10\ \text{m s}^{-1}$  until pull-off occurred. Each sample was measured at three different independent positions (error bars represent standard deviation [SD]). Displacements recorded were corrected for the system compliance  $C = 0.13\ \mu\text{m mN}^{-1}$ .<sup>[14]</sup> The maximum pull-off stress was calculated by dividing the force values by the nominal contact area of  $2.6\ \text{mm}^2$ .<sup>[14]</sup>

**Animal Experiments:** All animal experiments were carried out under anesthesia (auditory measurement) or ex vivo on freshly explanted TM specimens. All experiments were conducted according to the German Animal Welfare Law following the EU directive 2016/63/EU for animal experiments by qualified persons. The Animal Welfare Officer of the Saarland University was informed in advance and the euthanasia methods were fully appropriate. We ensured the minimizing of discomfort, stress, and pain during the experiments using proper anesthesia and analgesics. Furthermore, the animals were kept hydrated and the body temperature was maintained using an electric heating pad. For anesthesia, a mixture of ketamine-hydrochloride ( $80\ \text{mg kg}^{-1}$  body weight [BW] Ursotamin, Serumwerk Bernburg, Germany) and xylazine-hydrochloride ( $10\ \text{mg kg}^{-1}$  BW; Xylazin, Serumwerk Bernburg, Germany) was injected intraperitoneally with an injection volume of  $10\ \text{mL kg}^{-1}$  BW. The anesthesia was maintained by injecting one-third of the initial dose intraperitoneally, typically in 30–40 min intervals. For terminal experiments, the animals were sacrificed in deep anesthesia.

**Surface Roughness Determination and Tack Tests on Explanted Mouse TM:** To analyze the adhesion of film-terminated microstructures and the non-structured control films on the murine TM, tack tests were carried out on explanted TMs. These experiments were conducted in accordance with EU directive 2016/63/EU for animal experiments as acute experiments. The Animal Welfare Officer was informed about them and all experiments were conducted by qualified persons. The preparation of mouse tympanic membranes was carried out as described previously.<sup>[39]</sup> For the preparation of the specimens, the outer ear canal was trimmed down to the bony part. The bony portion of the ear canal that covered a major part of the eardrum was carefully removed by clipping, keeping enough distance to the eardrum to ensure that the TM would not be affected by the preparation. The petrosal bone, containing the tympanic capsule with the eardrum, the middle ear ossicular chain, and the cochlea, was then carefully detached from the skull bone and mounted onto a glass substrate. For the assembly, a two-component methyl methacrylate (Technovit 4004, Kulzer Technik, Hanau, Germany) was used, while ensuring free oscillation of the eardrum. After curing, the glass substrate was mounted to a sample holder. Prior to the adhesion measurements, a negative replica of the membrane was prepared using a two-component silicone (R&S Turboflex.0122 996, CFPM, Tremblay-en-France, France). The components were mixed 1:1 and carefully applied onto the TM, ensuring that the whole membrane was covered, especially including the area under the residual bony parts of the outer ear canal. In addition, it was verified

that no residual air bubbles remained. The molding material was cured at room temperature for  $\approx 5$  min and then gently removed. This negative mold was used to analyze the surface roughness of the TM.

The adhesion tests for real tissue were carried out with a custom-made setup. Adhesive samples were cut under visual control into circular pieces with a diameter of  $\approx 1$  mm using a biopsy punch and carefully fixed on the customized applicator using double-sided tape. This applicator was connected to the load cell (ME-Meßsysteme GmbH, Hennigsdorf, Germany) of our setup (see Section 3.4, Figure 4a). It was aligned to the sample holder under visual control to ensure positioning of the adhesive film parallel to the tympanic membrane surface (Figure 4b). The applicator containing the film was moved toward the TM at a constant speed of  $0.03 \text{ mm s}^{-1}$ , until a compressive stress of  $\approx 25 \text{ kPa}$  was reached, held for 10 s and then pulled off at  $0.1 \text{ mm s}^{-1}$  until total detachment (Figure 4c). The adhesive force was recorded and analyzed. In total, five tympanic membranes were used for the adhesion measurements, in intact and perforated conditions. Seven independently prepared sets of film-terminated and control patches were tested. As further validation, the control patches were tested on both the adhesive and nonadhesive sides. The experiments were carried out in a random sequence.

**Electrophysiological Measurement of Auditory Function by ABRs and DPOAEs Recordings:** The auditory recordings were carried out in a sound-proofed room (camera silent) on a preparation table isolated against vibrations. ABR recordings are a standard method to assess auditory function in both clinical and research setups in humans and laboratory animals.<sup>[60,61]</sup> The click ABRs were carried out as described previously<sup>[62,63]</sup> to detect the auditory threshold in intact and perforated conditions as well as after applying a patch on the perforation. The auditory threshold was characterized as the lowest intensity where the Jewett's wave complex consisting of five positive waves was identifiable.<sup>[61,64]</sup>

DPOAEs were measured with a DPOAE probe, which is used in clinical setup (UGD, Otodynamics, Hatfield, UK) as described previously.<sup>[65]</sup> DPOAE signals were elicited by two pure-tone stimuli (with frequency  $f_1$  and  $f_2$ ) on two different speakers with a level of  $L_1 = 55 \text{ dB SPL}$ ,  $L_2 = 45 \text{ dB SPL}$ , and  $f_2/f_1 = 1.22$ , as described by Engel et al.<sup>[66]</sup> Despite a high number of emitted distortion products, current clinical DPOAE devices only make use of the emitted signal at the frequency component  $2f_2 - f_1$  as a diagnostic parameter. The DPOAE amplitudes were measured between 10 and 18 kHz using 0.5 kHz steps followed by averaging and displayed as signal-to-noise ratio (SNR).<sup>[65,67,68]</sup> DPOAE measurements were carried out in three different conditions: 1) intact TM, 2) perforated TM, and 3) perforated TM with a patch in the same animal.

PDMS patches processed as described earlier were cut manually to  $\approx 1$  mm diameter under microscope control. A perforation was induced in the posterior quadrant of the TM using a suction tube of 1.3 mm outside diameter (KARL STORZ SE & Co. KG, Tuttingen, Germany). The DPOAEs were recorded intact, with perforation and with a patch covering the perforation. Upon completion of the set of measurements, the animal was sacrificed under deep anesthesia, the petrosal bones were explanted and the size of the TM perforation was analyzed using a microscope (MZ10F, Leica, Wetzlar, Germany) and the respective microscopy software (LASX, Leica, Wetzlar, Germany).

**Statistical Analysis:** Continuous variables in bar graphs are represented as mean  $\pm$  SD. In the box and whisker plots, each box represents the range from the first quartile to the third quartile. The median is indicated by a line inside the box, the mean is indicated by a dot. The whiskers represent the ranges from the minimum to the maximum value of each group. The Shapiro-Wilk test was applied to verify the normal distribution of the data. Variance homogeneity was tested by a Levene's test.

For the analysis of adhesive strength analyzed by tack tests on epoxy substrates, the pull-off stresses were compared via a two-sided *t*-test. For the analysis of the DPOAEs and the pull-off stresses *ex vivo*, we used a one-way analysis of variance (ANOVA). For the analysis of the *ex vivo* pull-off stress, the groups were independent, so ANOVA was carried out for normally distributed data. If normal distribution was not given, the Kruskal-Wallis test was used as a nonparametric test with a Dunn's test as posthoc analysis for pairwise comparison. The Bonferroni test was used in case of variance equality for pairwise

comparisons. The results of the DPOAEs and Click-ABR thresholds were analyzed as paired samples. For this purpose, we carried out ANOVA with repeated measures for normally distributed data followed by Levene's test for variance homogeneity and Bonferroni test for pairwise comparison. When normal distribution or variance equality was not given, the DPOAE data were analyzed by Friedman-ANOVA followed by a posthoc analysis with a Dunn's test for pairwise comparisons. In all cases, significance was defined as  $p \leq 0.05$ . For statistical analysis, OriginPro 2020 software was used (OriginLab Corp., North Hampton, USA).

## Supporting Information

Supporting Information is available from the Wiley Online Library or from the author.

## Acknowledgements

The authors acknowledge Joachim Blau for technical support and for designing the *ex vivo* measurement setup. Julian Weiß is acknowledged for confocal microscopy measurements and Dr. Lena Barnefske for the microfabrication of the master structures. Dr. Xuan Zhang is thanked for the support in mechanical calculations and Angela Rutz, for her laboratory assistance. The authors thank Biesterfeld Spezialchemie GmbH (Hamburg, Germany) for providing the polymers and Isaac Ayala Design for the design of the schematic TM graphic shown in Figure 2. The research leading to these results has received funding from the European Research Council under the European Union's HORIZON2020-EU.1.1 program/ ERC PoC Grant Agreement No. 842 613, Advanced Grant "Stick2Heal" to E.A.

## Conflict of Interest

The authors declare no conflict of interest.

## Author Contributions

G.M.L. and K.S. contributed equally to this work. Conceptualization G.M.L., K.S., G.I.W., K.K., E.A.; Roughness and adhesion investigation G.M.L.; *Ex-situ* adhesion investigation G.M.L., K.S., K.K.; Hearing investigation K.S., K.K.; Statistical analysis K.S.; Writing – original draft: G.M.L., K.S. Writing: – Review and editing: G.M.L., K.S., G.I.W., D.H., R.H., K.K., B.S., E.A.

## Data Availability Statement

Research data are not shared.

## Keywords

silicone patches, microstructured adhesives, tympanic membrane perforations, distortion product otoacoustic emissions

Received: May 12, 2021

Revised: June 1, 2021

Published online:

[1] E. Arzt, H. Quan, R. M. McMeeking, R. Hensel, *Prog. Mater. Sci.* **2021**, *120*, 100823.

[2] R. Hensel, K. Moh, E. Arzt, *Adv. Funct. Mater.* **2018**, *28*, 1800865.

- [3] J. S. Kaiser, M. Kamperman, E. J. de Souza, B. Schick, E. Arzt, *Int. J. Artif. Organs* **2011**, *34*, 180.
- [4] M. K. Kwak, C. Pang, H. E. Jeong, H. N. Kim, H. Yoon, H. S. Jung, K. Y. Suh, *Adv. Funct. Mater.* **2011**, *21*, 3606.
- [5] D. M. Drotlef, M. Amjadi, M. Yunusa, M. Sitti, *Adv. Mater.* **2017**, *29*, 1.
- [6] E. Arzt, S. Gorb, R. Spolenak, *Proc. Natl. Acad. Sci. U. S. A* **2003**, *100*, 10603.
- [7] A. Del Campo, C. Greiner, I. Álvarez, E. Arzt, *Adv. Mater.* **2007**, *19*, 1973.
- [8] S. C. L. Fischer, E. Arzt, R. Hensel, *ACS Appl. Mater. Interfaces* **2017**, *9*, 1036.
- [9] V. Tinnemann, L. Hernández, S. C. L. Fischer, E. Arzt, R. Bennewitz, R. Hensel, *Adv. Funct. Mater.* **2019**, *29*, 1807713.
- [10] C. Trojahn, M. Schario, G. Dobos, U. Blume-Peytavi, J. Kottner, *Ski Res. Technol.* **2015**, *21*, 54.
- [11] R. Maiti, L. C. Gerhardt, Z. S. Lee, R. A. Byers, D. Woods, J. A. Sanz-Herrera, S. E. Franklin, R. Lewis, S. J. Matcher, M. J. Carré, *J. Mech. Behav. Biomed. Mater.* **2016**, *62*, 556.
- [12] D. Fuller, K. N. G. Tabor, *Proc. R. Soc. London. A. Math. Phys. Sci.* **1975**, *345*, 327.
- [13] V. Barreau, R. Hensel, N. K. Guimard, A. Ghatak, R. M. McMeeking, E. Arzt, *Adv. Funct. Mater.* **2016**, *26*, 4687.
- [14] S. C. L. Fischer, S. Boyadzhieva, R. Hensel, K. Kruttwig, E. Arzt, *J. Mech. Behav. Biomed. Mater.* **2018**, *80*, 303.
- [15] N. J. Glassmaker, A. Jagota, C.-Y. Hui, W. L. Noderer, M. K. Chaudhury, *Proc. Natl. Acad. Sci.* **2007**, *104*, 10786.
- [16] W. L. Noderer, L. Shen, S. Vajpayee, N. J. Glassmaker, A. Jagota, C. Y. Hui, *Proc. R. Soc. A* **2007**, 2631.
- [17] Z. He, N. M. Moyle, C. Y. Hui, B. Levrard, A. Jagota, *Tribol. Lett.* **2017**, *65*, 1.
- [18] H. Shahsavan, D. Arunbabu, B. Zhao, *Macromol. Mater. Eng.* **2012**, *297*, 743.
- [19] H. Shahsavan, B. Zhao, *Macromolecules* **2014**, *47*, 353.
- [20] P. Hong, M. Bance, P. F. Gratzner, *Int. J. Pediatr. Otorhinolaryngol.* **2013**, *77*, 3.
- [21] E. Dursun, S. Dogru, A. Gungor, H. Cincik, E. Poyrazoglu, T. Ozdemir, *Otolaryngol. – Head Neck Surg.* **2008**, *138*, 353.
- [22] I. Ghanad, M. D. Polanik, D. R. Trakimas, R. M. Knoll, M. Castillo-Bustamante, N. L. Black, E. D. Kozin, A. K. Remenschneider, *Laryngoscope* **2020**, *131*, 392.
- [23] G. Berger, Y. Finkelstein, S. Avraham, M. Himmelfarb, *J. Laryngol. Otol.* **1997**, *111*, 1137.
- [24] R. P. Mehta, J. J. Rosowski, S. E. Voss, E. O'Neil, S. N. Merchant, *Otol. Neurotol.* **2006**, *27*, 136.
- [25] O. A. Sogebi, E. A. Oyewole, T. O. Mabifah, *Ghana Med. J.* **2018**, *52*, 34.
- [26] L. Louw, *J. Laryngol. Otol.* **2010**, *124*, 587.
- [27] P. L. Santa Maria, P. Gottlieb, C. Santa Maria, S. Kim, S. Puria, Y. P. Yang, *Tissue Eng. Part A* **2017**, *23*, 436.
- [28] T. Janssen, H. P. Niedermeyer, W. Arnold, *ORL* **2006**, *68*, 334.
- [29] F. Zhao, H. Wada, T. Koike, D. Stephens, *Clin. Otolaryngol.* **2000**, *25*, 3.
- [30] A. I. Tlumak, P. R. Kileny, *Curr. Opin. Otolaryngol. Head Neck Surg.* **2001**, *9*, 279.
- [31] H. W. LeBourgeois, V. K. Anand, J. R. McAuley, J. D. Dickman, O. Malphurs, *Ear, Nose Throat J.* **2000**, *79*, 610.
- [32] W. Dong, G. Stomackin, X. Lin, G. K. Martin, T. T. Jung, *Hear. Res.* **2019**, *378*, 3.
- [33] F. Zöllner, *J. Laryngol. Otol.* **1955**, *69*, 637.
- [34] H. Wullstein, *Arch. für Ohren-, Nasen-, und Kehlkopfheilkd* **1952**, 422.
- [35] J. M. Hempel, A. Becker, J. Müller, E. Krause, A. Berghaus, T. Braun, *Otol. Neurotol.* **2012**, *33*, 1357.
- [36] S. Branica, K. Dawidowsky, L. Kovač-Bilić, M. Bilić, *Croat. Med. J.* **2019**, *60*, 503.
- [37] M. Farhadi, H. Mirzadeh, A. Solouk, A. Asghari, M. Jalessi, H. Ghanbari, P. Yazdanifard, *J. Biomed. Mater. Res. A* **2011**, *100A*, 549.
- [38] S. Boyadzhieva, S. C. L. Fischer, S. Lösch, A. Rutz, E. Arzt, K. Kruttwig, *J. Vis. Exp.* **2018**, 2018, 57573.
- [39] S. Boyadzhieva, K. Sorg, M. Danner, S. C. L. Fischer, R. Hensel, B. Schick, G. Wenzel, E. Arzt, K. Kruttwig, *Polymers* **2019**, *11*, 942.
- [40] C. Creton, M. Ciccotti, *Reports Prog. Phys.* **2016**, *79*, 46601.
- [41] A. E. Kovalev, K. Dening, B. N. J. Persson, S. N. Gorb, *Beilstein J. Nanotechnol.* **2014**, *5*, 1341.
- [42] H. Shahsavan, B. Zhao, *Soft Matter* **2012**, *8*, 8281.
- [43] L. Caminos, J. Garcia-Manrique, A. Lima-Rodriguez, A. Gonzalez-Herrera, *Appl. Bionics Biomech.* **2018**, *2018*, 1.
- [44] I. O. for S. ISO, *Self Adhesive Tapes – Determination of Peel Adhesion Properties*, **2007**.
- [45] I. O. for S. ISO, *Self Adhesive Tapes – Measurement of Peel Adhesion from Stainless Steel or from Its Own Backing*, **1997**.
- [46] C. S. Davis, D. Martina, C. Creton, A. Lindner, A. J. Crosby, *Langmuir* **2012**, *28*, 14899.
- [47] J. M. Eubel, Design Und Herstellung Eines Haftsystem Zur Anwendung Auf Dem Trommelfell, Universität des Saarlandes, **2019**.
- [48] B. Mikolaszek, J. Kazlauske, A. Larsson, M. Sznitowska, *Polymers* **2020**, *12*, 1520.
- [49] K. Yu, J. Hou, Z. Jin, K. Wu, S. Xu, N. Yang, Y. Shen, T. Tang, S. Guo, *J. Drug Deliv. Sci. Technol.* **2018**, *46*, 173.
- [50] C. M. Blankenship, L. L. Hunter, D. H. Keefe, M. Patrick Feeney, D. K. Brown, A. McCune, D. F. Fitzpatrick, L. Lin, in *Ear Hear.*, Lippincott Williams And Wilkins, Philadelphia, PA **2018**, pp. 1075–1090.
- [51] D. Colon, U. Verdugo-Raab, C. Alvarez, T. Steffens, S. Marcrum, S. Kolb, C. Herr, D. Twardella, *Noise Heal.* **2016**, *18*, 288.
- [52] L. A. Ohlms, B. L. Lonsbury-Martin, G. K. Martin, *Otolaryngol. – Head Neck Surg.*, **1990**, *103*, 52.
- [53] J. E. O. Amadasun, *J. Laryngol. Otol.* **2002**, *116*, 181.
- [54] Z. Lou, Y. Wang, K. Su, *Eur. Arch. Oto-Rhino-Laryngol.* **2014**, *271*, 2153.
- [55] I. Saliba, *Clin. Otolaryngol.* **2008**, *33*, 610.
- [56] M. K. Park, K. H. Kim, J. D. Lee, B. D. Lee, *Otolaryngol. Head. Neck Surg.* **2011**, *145*, 581.
- [57] G. Aslan, L. Uzun, *Oper. Tech. Otolaryngol. – Head Neck Surg.* **2011**, *22*, 173.
- [58] S. C. L. Fischer, K. Kruttwig, V. Bandmann, R. Hensel, E. Arzt, *Macromol. Mater. Eng.* **2017**, *302*, 1.
- [59] E. Kroner, J. Blau, E. Arzt, *Rev. Sci. Instrum.* **2012**, *83*, 2.
- [60] J. F. Willott, *Curr. Protoc. Neurosci.* **2006**, *34*, 8.21B.1.
- [61] L. Rüttiger, U. Zimmermann, M. Knipper, *Orl* **2017**, *79*, 93.
- [62] K. Sorg, P. Stahn, L. Pillong, M. P. Hinsberger, L. Heimann, H.-J. Foth, B. Schick, G. I. Wenzel, *J. Biomed. Opt.* **2019**, *24*, 1.
- [63] S. A. L. Schacht, P. Stahn, M. Hinsberger, B. Schick, G. I. Wenzel, *J. Biomed. Opt.* **2018**, *23*, 1.
- [64] Q. Y. Zheng, K. R. Johnson, L. C. Erway, *Hear. Res.* **1999**, *130*, 94.
- [65] D. J. Hecker, J. Lohscheller, C. A. Bader, W. Delb, B. Schick, J. Długaiczky, *IEEE Trans. Biomed. Eng.* **2011**, *58*, 2369.
- [66] J. Engel, C. Braig, L. Rüttiger, S. Kuhn, U. Zimmermann, N. Blin, M. Sausbier, H. Kalbacher, S. Münkner, K. Rohbock, P. Ruth, H. Winter, M. Knipper, *Neuroscience* **2006**, *143*, 837.
- [67] T. Schimmang, J. Tan, M. Müller, U. Zimmermann, K. Rohbock, I. Köpschall, A. Limberger, L. Minichiello, M. Knipper, *Development* **2003**, *130*, 4741.
- [68] B. Fell, S. Eckrich, K. Blum, T. Eckrich, D. Hecker, G. J. Obermair, S. Münkner, V. Flockerzi, B. Schick, J. Engel, *J. Neurosci.* **2016**, *36*, 11024.

Supporting Information

Self-Adhesive Silicone Microstructures for the Treatment of  
Tympanic Membrane Perforations

*Gabriela Moreira Lana\**, *Katharina Sorg\**, *Gentiana Ioana Wenzel*, *Dietmar Hecker*,  
*René Hensel*, *Bernhard Schick*, *Klaus Kruttwig*, *Eduard Arzt\**

\*corresponding author: [eduard.arzt@leibniz-inm.de](mailto:eduard.arzt@leibniz-inm.de), ORCID 0000-0002-0834-4540

Gabriela Moreira Lana, Dr. René Hensel, Dr. Klaus Kruttwig, Prof. Dr. Eduard Arzt  
INM – Leibniz Institute for New Materials  
Campus D2 2, 66123 Saarbrücken, Germany  
Email: [eduard.arzt@leibniz-inm.de](mailto:eduard.arzt@leibniz-inm.de)

Gabriela Moreira Lana, Prof. Dr. Eduard Arzt  
Department of Materials Science and Engineering  
Saarland University  
Campus D2 2, 66123 Saarbrücken, Germany

Katharina Sorg, Prof. Dr. Gentiana Ioana Wenzel, Dr. Dietmar Hecker, Prof. Dr. Bernhard Schick  
Department of Otorhinolaryngology  
Saarland University Medical Center, 66421 Homburg, Germany  
Email: [katharina.Sorg@uks.eu](mailto:katharina.Sorg@uks.eu)

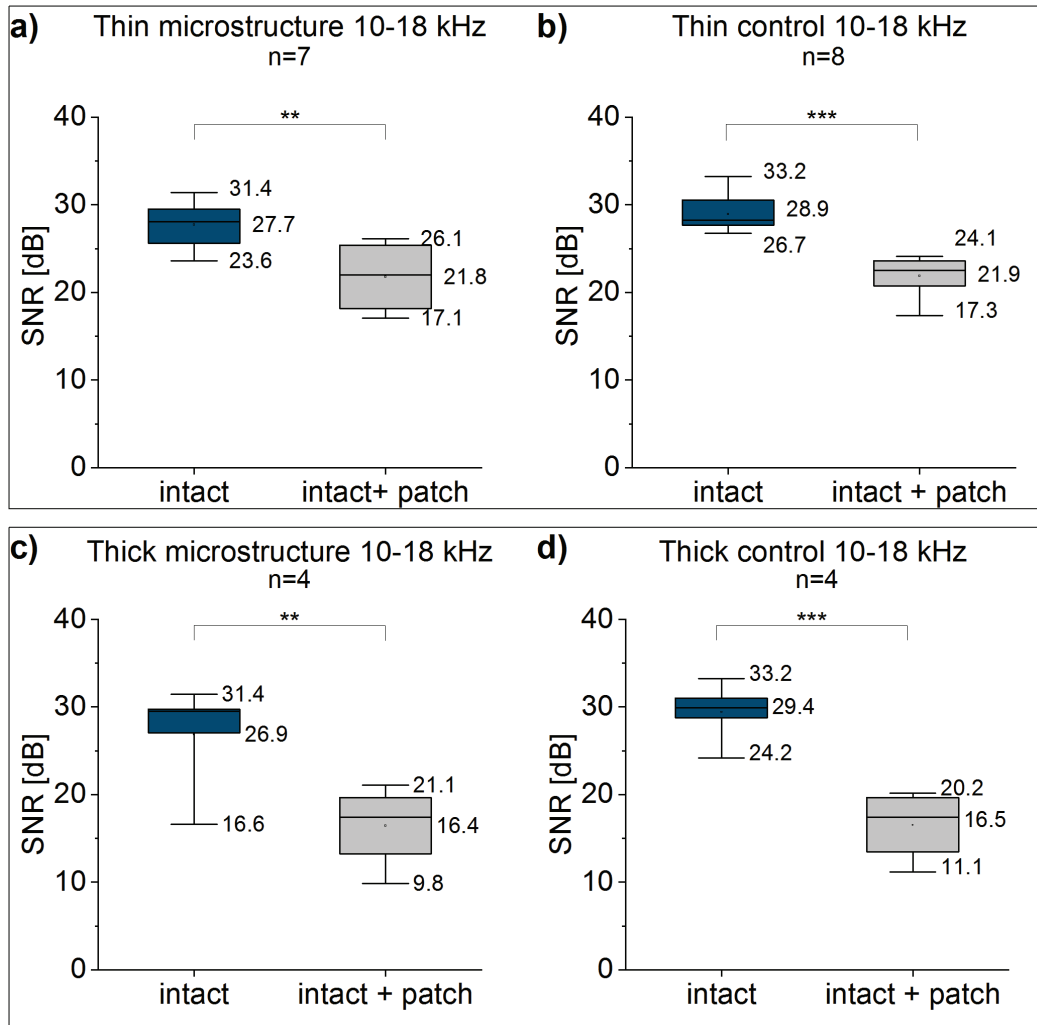


**Figure S1.** Analysis of the hearing function via DPOAE measurements over the frequency range of 10-18 kHz only on intact condition: The DPOAE signals on intact membranes without a patch (intact) and after application of thin (a, b) or thick (c, d) microstructure and unstructured control patches (intact + patch). The DPOAE signals were significantly decreased after application of patches on the intact TM in all cases. \*\* indicates  $p < 0.01$ , \*\*\* indicates  $p < 0.001$ . The number of replicas is indicated above each plot.

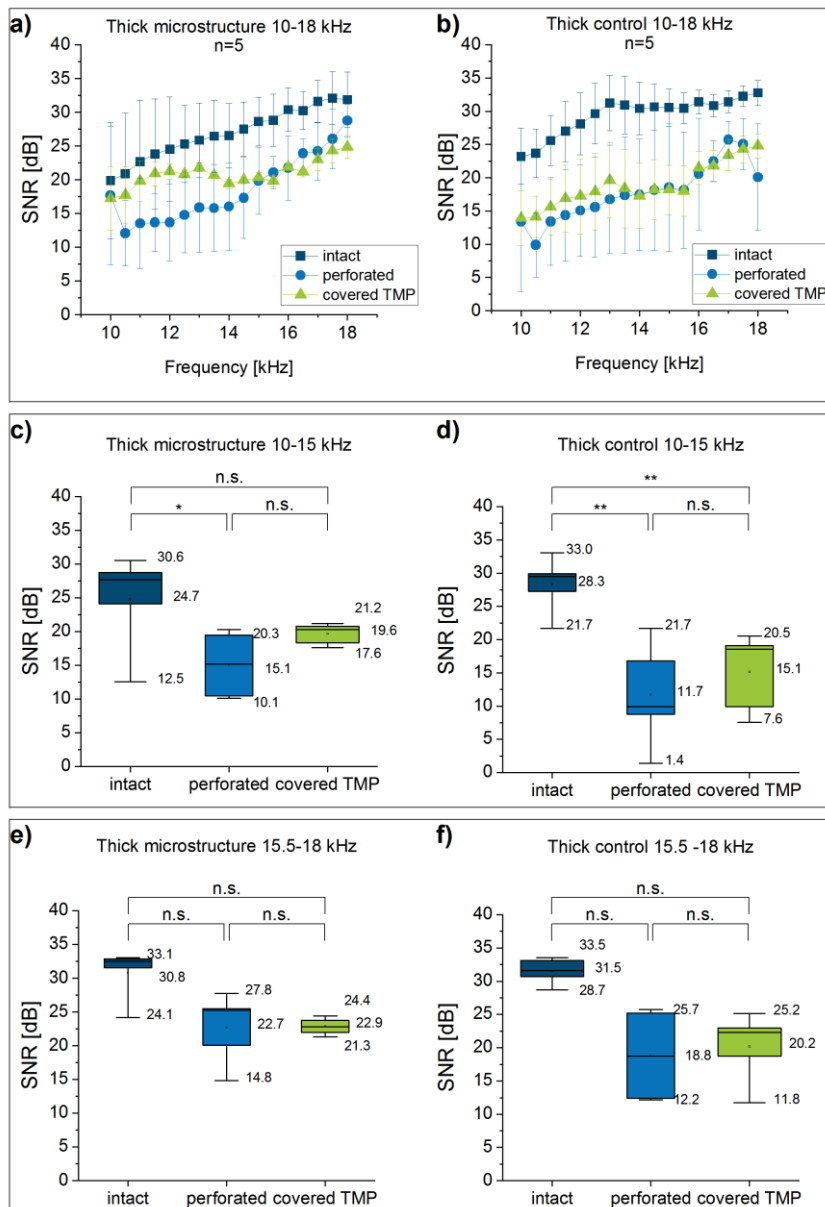


**Figure S2.** Analysis of the hearing function by DPOAE measurements after the application of thick microstructured patches (a, c, e) and related unstructured thick control patches (b, d, f) in comparison to the intact and perforated condition. The average measurements demonstrated significantly lower DPOAE signals in the frequency range from 10-15 kHz after perforation that could not be increased by patching of the perforation, neither by thick microstructures or thick control patches (c, d). In the higher frequency range, no significant change in any conditions could be observed, also (e, f). \* indicates  $p < 0.05$ , \*\* indicates  $p < 0.01$  and n.s.= non-significant. The number of replicas is indicated in a and b (n=5).

## References

1. Abbasi F, Mirzadeh H (2003) Properties of poly(dimethylsiloxane)/hydrogel multicomponent systems. *J Polym Sci Part B Polym Phys* 41:2145–2156
2. Abbasi F, Mirzadeh H, Simjoo M (2006) Hydrophilic interpenetrating polymer networks of poly(dimethyl siloxane) (PDMS) as biomaterial for cochlear implants. *J Biomater Sci Polym Ed* 17:341–355
3. Abrams J (2015) Traumatische Trommelfellperforation — schienen oder abwarten? *HNO Nachrichten* 45:25–27
4. Afolabi OA, Aremu SK, Alabi BS, Segun-Busari S (2009) Traumatic tympanic membrane perforation: An aetiological profile. *BMC Res Notes* 2:
5. Arzt E, Quan H, McMeeking RM, Hensel R (2021) Functional surface microstructures inspired by nature – From adhesion and wetting principles to sustainable new devices. *Prog Mater Sci* 119:100778
6. Aslan G, Uzun L (2011) Adhesive strip patching for tympanic membrane perforations. *Oper Tech Otolaryngol - Head Neck Surg* 22:173–174
7. Baik S, Lee HJ, Kim DW, Kim JW, Lee Y, Pang C (2019) Bioinspired Adhesive Architectures: From Skin Patch to Integrated Bioelectronics. *Adv Mater* 31:1803309
8. Barreau V, Hensel R, Guimard NK, Ghatak A, McMeeking RM, Arzt E (2016) Fibrillar Elastomeric Micropatterns Create Tunable Adhesion Even to Rough Surfaces. *Adv Funct Mater* 26:4687–4694
9. Bell AG (1881) LXVIII. *Upon the production of sound by radiant energy*. London, Edinburgh, Dublin *Philos Mag J Sci* 11:510–528
10. Berger G, Finkelstein Y, Avraham S, Himmelfarb M (1997) Patterns of hearing loss in non-explosive blast injury of the ear. *J Laryngol Otol* 111:1137–41
11. Blazer DG, Domnitz S, Liverman CT, Adults C on A and AHHC for, Policy B on HS, Division H and M, National Academies of Sciences E and M (2016) *Hearing Health Care Services: Improving Access and Quality*.
12. Boyadzhieva S, Fischer SCL, Lösch S, Rutz A, Arzt E, Kruttwig K (2018) Thin film composite silicon elastomers for cell culture and skin applications: Manufacturing and characterization. *J Vis Exp* 2018:57573
13. Boyadzhieva S, Sorg K, Danner M, Fischer SCL, Hensel R, Schick B, Wenzel G, Arzt E,

- Kruttwig K (2019) A Self-Adhesive Elastomeric Wound Scaffold for Sensitive Adhesion to Tissue. *Polymers (Basel)* 11:942
14. Branica S, Dawidowsky K, Kovač-Bilić L, Bilić M (2019) Silicon foil patching for blast tympanic membrane perforation: A retrospective study. *Croat Med J* 60:503–507
  15. Browing G, Gatehouse S (1992) The prevalence of middle ear disease in the adult British population. *Clin Otolaryngol Allied Sci* 17:317–321
  16. Caminos L, Garcia-Manrique J, Lima-Rodriguez A, Gonzalez-Herrera A (2018) Analysis of the mechanical properties of the human tympanic membrane and its influence on the dynamic behaviour of the human hearing system. *Appl Bionics Biomech* 2018:
  17. Camnitz PS, Bost WS (1985) Traumatic perforations of the tympanic membrane: early closure with paper tape patching. *Otolaryngol Head Neck Surg* 93:220–3
  18. Chen J, Zheng J, Gao Q, Zhang J, Zhang J, Omisore O, Wang L, Li H (2018) Polydimethylsiloxane (PDMS)-Based Flexible Resistive Strain Sensors for Wearable Applications. *Appl Sci* 8:345
  19. Chien W, Lin FR (2012) Prevalence of hearing aid use among older adults in the United States. *Arch Intern Med* 172:292–293
  20. Cunningham LL, Tucci DL (2017) Hearing Loss in Adults. *N Engl J Med* 377:2465
  21. da Lilly-Tariah OB, Somefun AO (2007) Traumatic perforation of the tympanic membrane in University of Port Harcourt Teaching Hospital, Port Harcourt. Nigeria. *Niger Postgrad Med J* 14:121–4
  22. Dawood MR (2014) Evaluation of Spontaneous Healing of Traumatic Tympanic Membrane Perforation. *Gen Med Open Access* 2:24–29
  23. Deng Z, Wu J, Qiu J, Wang J, Tian Y, Li Y, Jin Y (2009) Comparison of porcine acellular dermis and dura mater as natural scaffolds for bioengineering tympanic membranes. *Tissue Eng - Part A* 15:3729–3739
  24. Dirksen M, Sorg K, Heimann L, Langenbacher A, Schick B, Wenzel GI (2021) Einfluss verschiedener Distanzen einer Laserlichtquelle auf die optische Aktivierung des Hörsystems an drei unterschiedlichen Stimulationsorten des Hörorgans. *Laryngo-Rhino-Otologie* 100:
  25. Dong W, Stomackin G, Lin X, Martin GK, Jung TT (2019) Distortion product otoacoustic emissions: Sensitive measures of tympanic -membrane perforation and healing processes in a gerbil model. *Hear Res* 378:3–12
  26. Duck GP, Seung CS, Sung WK, Youn TK (2005) Development of flexible self adhesive patch

- for professional heat stress monitoring service. Conf Proc IEEE Eng Med Biol Soc URL: <https://pubmed.ncbi.nlm.nih.gov/17281054/>
27. Dursun E, Dogru S, Gungor A, Cincik H, Poyrazoglu E, Ozdemir T (2008) Comparison of paper-patch, fat, and perichondrium myringoplasty in repair of small tympanic membrane perforations. *Otolaryngol - Head Neck Surg* 138:353–356
  28. Farhadi M, Mirzadeh H, Solouk A, Asghari A, Jalessi M, Ghanbari H, Yazdanifard P (2012) Collagen-immobilized patch for repairing small tympanic membrane perforations: In vitro and in vivo assays. *J Biomed Mater Res - Part A* 100 A:549–553
  29. Fell B, Eckrich S, Blum K, Eckrich T, Hecker D, Obermair GJ, Münkner S, Flockerzi V, Schick B, Engel J (2016)  $\alpha 2\delta 2$  controls the function and trans-synaptic coupling of cav1.3 channels in mouse inner hair cells and is essential for normal hearing. *J Neurosci* 36:11024–11036
  30. Fischer SCL, Kruttwig K, Bandmann V, Hensel R, Arzt E (2017) Adhesion and Cellular Compatibility of Silicone-Based Skin Adhesives. *Macromol Mater Eng* 302:1600526
  31. Fischer SCL, Boyadzhieva S, Hensel R, Kruttwig K, Arzt E (2018) Adhesion and relaxation of a soft elastomer on surfaces with skin like roughness. *J Mech Behav Biomed Mater* 80:303–310
  32. Foth HJ, Färber S, Gauer A, Wagner R (2000) Thermal damage threshold at 633 nm of tympanic membrane of pig. *Hear Res* 142:71–78
  33. Fridberger A, Ren T (2006) Local mechanical stimulation of the hearing organ by laser irradiation. *Neuroreport* 17:33–7
  34. Gaur S, Sinha ON, Bhushan A, Batni G (2017) Observations on Tympanic Membrane Perforations (Safe Type) and Hearing Loss. *Indian J Otolaryngol Head Neck Surg* 69:29–34
  35. GBD 2019 Hearing Loss Collaborators (2021) Hearing loss prevalence and years lived with disability, 1990–2019: findings from the Global Burden of Disease Study 2019. *Lancet* 397:996–1009
  36. Geneva: World Health Organization (2021) World Report On Hearing.
  37. Ghanad I, Polanik MD, Trakimas DR, Knoll RM, Castillo-Bustamante M, Black NL, Kozin ED, Remenschneider AK (2020) A Systematic Review of Nonautologous Graft Materials Used in Human Tympanoplasty. *Laryngoscope* 131:392–400
  38. Glassmaker NJ, Jagota A, Hui CY, Noderer WL, Chaudhury MK (2007) Biologically inspired crack trapping for enhanced adhesion. *Proc Natl Acad Sci U S A* 104:10786–10791
  39. Golz A, Goldenberg D, Netzer A, Fradis M, Westerman ST, Westerman LM, Joachims HZ (2003) Paper patching for chronic tympanic membrane perforations. *Otolaryngol Head Neck*

- Surg 128:565–70
40. Goyal V, Rajguru S, Matic AI, Stock SR, Richter C-P (2012) Acute Damage Threshold for Infrared Neural Stimulation of the Cochlea: Functional and Histological Evaluation. *Anat Rec Adv Integr Anat Evol Biol* 295:1987–1999
  41. Griffin WL (1979) A retrospective study of traumatic tympanic membrane perforations in a clinical practice. *Laryngoscope* 89:261–282
  42. Guinan JJ, Backus BC, Lilaonitkul W, Aharonson V (2003) Medial Olivocochlear Efferent Reflex in Humans: Otoacoustic Emission (OAE) Measurement Issues and the Advantages of Stimulus Frequency OAEs. *JARO - J Assoc Res Otolaryngol* 4:521–540
  43. Haynes DS, Vos JD, Labadie RF (2005) Acellular allograft dermal matrix for tympanoplasty. *Curr Opin Otolaryngol Head Neck Surg* 13:283–286
  44. He Z, Moyle NM, Hui CY, Levrard B, Jagota A (2017) Adhesion and Friction Enhancement of Film-Terminated Structures against Rough Surfaces. *Tribol Lett* 65:1–8
  45. Heimann L, Carlein C, Sorg K, Diller R, Langenbacher A, Schick B, Wenzel GI (2021) Wavelength-specific optoacoustic-induced vibrations of the guinea pig tympanic membrane. *J Biomed Opt* 26:38001
  46. Heimann L, Sorg K, Engel J, Langenbacher A, Schick B, Wenzel GI (2021) Growth functions of acoustically and optoacoustically induced ABR waves in the mouse model.
  47. Heitmann D, Scheffler B, Abrams J, Gerstner AOH (2021) Spontaneous course of traumatic tympanic membrane perforations. *HNO* 69:192–197
  48. Hempel JM, Becker A, Müller J, Krause E, Berghaus A, Braun T (2012) Traumatic tympanic membrane perforations: Clinical and audiometric findings in 198 patients. *Otol Neurotol* 33:1357–1362
  49. Hensel R, Moh K, Arzt E (2018) Engineering Micropatterned Dry Adhesives: From Contact Theory to Handling Applications. *Adv Funct Mater* 28:1800865
  50. Hernandez VH, Gehrt A, Reuter K, Jing Z, Jeschke M, Schulz AM, Hoch G, Bartels M, Vogt G, Garnham CW, Yawo H, Fukazawa Y, Augustine GJ, Bamberg E, Kügler S, Salditt T, De Hoz L, Strenzke N, Moser T (2014) Optogenetic stimulation of the auditory pathway. *J Clin Invest* 124:1114–1129
  51. Hof JR, Anteunis LJC, Chenault MN, Van Dijk P (2005) Otoacoustic emissions at compensated middle ear pressure in children. *Int J Audiol* 44:317–320
  52. Hong P, Bance M, Gratzner PF (2013) Repair of tympanic membrane perforation using novel

- adjuvant therapies: A contemporary review of experimental and tissue engineering studies. *Int J Pediatr Otorhinolaryngol* 77:3–12
53. Hwang I, Kim HN, Seong M, Lee S-H, Kang M, Yi H, Bae WG, Kwak MK, Jeong HE (2018) Multifunctional Smart Skin Adhesive Patches for Advanced Health Care. *Adv Healthc Mater* 7:1800275
  54. Jackler RK (2019) *Ear Surgery Illustrated : A Comprehensive Atlas of Otologic Microsurgical Techniques*. Thieme, New York
  55. Jeong SH, Zhang S, Hjort K, Hilborn J, Wu Z (2016) PDMS-Based Elastomer Tuned Soft, Stretchable, and Sticky for Epidermal Electronics. *Adv Mater* 28:5830–5836
  56. Jian XH, Dong FL, Xu J, Li ZJ, Jiao Y, Cui YY (2018) Frequency Domain Analysis of Multiwavelength Photoacoustic Signals for Differentiating Tissue Components. *Int J Thermophys* 39:1–9
  57. Kaftan H, Noack M, Friedrich N, Völzke H, Hosemann W (2008) Prävalenz chronischer Trommelfellperforationen in der Erwachsenen Bevölkerung. *HNO* 56:145–150
  58. Kallweit N, Baumhoff P, Krueger A, Tinne N, Kral A, Ripken T, Maier H (2016) Optoacoustic effect is responsible for laser-induced cochlear responses. *Sci Rep* 6:28141
  59. Kim J, Kim DW, Baik S, Hwang GW, Kim T il, Pang C (2019) Snail-Inspired Dry Adhesive with Embedded Microstructures for Enhancement of Energy Dissipation. *Adv Mater Technol* 4:
  60. Kim YJ, Kim HJ, Kim HL, Kim HJ, Kim HS, Lee TR, Shin DW, Seo YR (2017) A Protective Mechanism of Visible Red Light in Normal Human Dermal Fibroblasts: Enhancement of GADD45A-Mediated DNA Repair Activity. *J Invest Dermatol* 137:466–474
  61. Klatt J, Barcellona P, Bennett R, Bokareva OS, Feth H, Rasch A, Reith P, Buhmann SY (2017) Strong van der Waals Adhesion of a Polymer Film on Rough Substrates. *Langmuir* 33:5298–5303
  62. Kochkin S (2007) MarkeTrak VII : Obstacles to adult non-user adoption of hearing aids. *Hear J* 60:24–50
  63. Kozin ED, Black NL, Cheng JT, Cotler MJ, McKenna MJ, Lee DJ, Lewis JA, Rosowski JJ, Remenschneider AK (2016) Design, fabrication, and in vitro testing of novel three-dimensionally printed tympanic membrane grafts. *Hear Res* 340:
  64. Kral A, Hartmann R, Mortazavi D, Klinke R (1998) Spatial resolution of cochlear implants: the electrical field and excitation of auditory afferents. *Hear Res* 121:11–28
  65. Kraus F, Hagen R (2015) Ätiologie und Therapie der traumatischen Trommelfellperforation.

- Laryngorhinootologie 94:596–600
66. Krmpot AJ, Janjetovic KD, Misirkic MS, Vucicevic LM, Pantelic D V., Vasiljevic DM, Popadic DM, Jelenkovic BM, Trajkovic VS (2010) Protective effect of autophagy in laser-induced glioma cell death in vitro. *Lasers Surg Med* 42:338–347
  67. Kwak MK, Pang C, Jeong HE, Kim HN, Yoon H, Jung HS, Suh KY (2011) Towards the next level of bioinspired dry adhesives: New designs and applications. *Adv Funct Mater* 21:3606–3616
  68. Kwak MK, Jeong HE, Suh KY (2011) Rational design and enhanced biocompatibility of a dry adhesive medical skin patch. *Adv Mater* 23:3949–3953
  69. Laidlaw DW, Costantino PD, Govindaraj S, Hiltzik DH, Catalano PJ (2001) Tympanic Membrane Repair With a Dermal Allograft. *Laryngoscope* 111:702–707
  70. Leavitt J, Fatone M, Hestdalen C, Obringer JW, Tillinghast HS (1997) Mutagenic activity of high-energy 532 nm ultra-short laser pulses. *Radiat Res* 147:490–494
  71. LeBourgeois HW, Anand VK, McAuley JR, Dickman JD, Malphurs O (2000) Effect of Tympanic Perforations on the Detection of Distortion-product Otoacoustic Emissions. *Ear, Nose Throat J* 79:610–618
  72. Lenarz T, Boenninghaus H-G (2012) Hals-Nasen-Ohrenheilkunde. 14th edition. Springer-Verlag Berlin Heidelberg
  73. Lin X, Meenderink SWF, Stomackin G, Jung TT, Martin GK, Dong W (2021) Forward and Reverse Middle Ear Transmission in Gerbil with a Normal or Spontaneously Healed Tympanic Membrane. *JARO - J Assoc Res Otolaryngol* 22:261–274
  74. Losi P, Briganti E, Magera A, Spiller D, Ristori C, Battolla B, Balderi M, Kull S, Balbarini A, Di Stefano R, Soldani G (2010) Tissue response to poly(ether)urethane-polydimethylsiloxane-fibrin composite scaffolds for controlled delivery of pro-angiogenic growth factors. *Biomaterials* 31:5336–5344
  75. Lou ZC, Lou ZH, Zhang QP (2012) Traumatic tympanic membrane perforations: A study of etiology and factors affecting outcome. *Am J Otolaryngol - Head Neck Med Surg* 33:549–555
  76. Louw L (2010) Acquired cholesteatoma pathogenesis: Stepwise explanations. *J Laryngol Otol* 124:587–593
  77. Mager T, Morena DLD La, Senn V, Schlotte J, Derrico A, Feldbauer K, Wrobel C, Jung S, Bodensiek K, Rankovic V, Browne L, Huet A, Jüttner J, Wood PG, Letzkus JJ, Moser T, Bamberg E (2018) High frequency neural spiking and auditory signaling by ultrafast red-shifted

- optogenetics. *Nat Commun* 9:1–14
78. McFeely WJ, Bojrab DI, Kartush JM (2000) Tympanic membrane perforation repair using AlloDerm. *Otolaryngol - Head Neck Surg* 123:17–21
  79. Mehta RP, Rosowski JJ, Voss SE, O’Neil E, Merchant SN (2006) Determinants of Hearing Loss in Perforations of the Tympanic Membrane. *Otol Neurotol* 27:136–143
  80. Mikolaszek B, Kazlauske J, Larsson A, Sznitowska M (2020) Controlled Drug Release by the Pore Structure in Polydimethylsiloxane Transdermal Patches. *Polymers (Basel)* 12:1520
  81. Møller AR (2011) *Epidemiology of Tinnitus in Adults*. Springer, New York, NY URL: [https://link.springer.com/chapter/10.1007/978-1-60761-145-5\\_5](https://link.springer.com/chapter/10.1007/978-1-60761-145-5_5)
  82. Moon TH, Lee MY, Jung JY, Ahn JC, Chang SY, Chung PS, Rhee CK, Kim YH, Suh MW (2016) Safety assessment of trans-tympanic photobiomodulation. *Lasers Med Sci* 31:323–333
  83. Moreira Lana G, Sorg K, Wenzel GI, Hecker D, Hensel R, Schick B, Kruttwig K, Arzt E (2021) Self-Adhesive Silicone Microstructures for the Treatment of Tympanic Membrane Perforations. *Adv NanoBiomed Res* 2100057
  84. Mota C, Danti S, D’Alessandro D, Trombi L, Ricci C, Puppi D, Dinucci D, Milazzo M, Stefanini C, Chiellini F, Moroni L, Berrettini S (2015) Multiscale fabrication of biomimetic scaffolds for tympanic membrane tissue engineering. *Biofabrication* 7:
  85. Noderer WL, Shen L, Vajpayee S, Glassmaker NJ, Jagota A, Hui CY (2007) Enhanced adhesion and compliance of film-terminated fibrillar surfaces. *Proc R Soc A Math Phys Eng Sci* 463:2631–2654
  86. Nordvik O, Laugen Heggdal PO, Brännström J, Vassbotn F, Aarstad AK, Aarstad HJ (2018) Generic quality of life in persons with hearing loss: A systematic literature review. *BMC Ear, Nose Throat Disord* 18:1–13
  87. Norman JJ, Desai TA (2005) Control of cellular organization in three dimensions using a microfabricated polydimethylsiloxane-collagen composite tissue scaffold. *Tissue Eng* 11:378–386
  88. Obringer JW, Phipps S, Johnson MD (1999) High Energy, Ultrashort Pulse Green Laser-Light Exposure of Cultured Human Cells Yields Evidence of DNA Damage. *Def Tech Inf Cent*
  89. Olusany BO, Neumann KJ, Saunders JE (2014) The global burden of disabling hearing impairment: a call to action. *Bull World Health Organ* 92:367–373
  90. Orji FT, Agu CC (2008) Determinants of spontaneous healing in traumatic perforations of the tympanic membrane. *Clin Otolaryngol* 33:420–426

91. Ott MC, Lundy LB (2015) Tympanic membrane perforation in adults. <http://dx.doi.org/101080/00325481200111445496> 110:81–84
92. Owens DK, Wendt RC (1969) Estimation of the surface free energy of polymers. *J Appl Polym Sci* 13:1741–1747
93. Owens JJ, McCoy MJ, Lonsbury-Martin BL, Martin GK (1993) Otoacoustic emissions in children with normal ears, middle ear dysfunction, and ventilating tubes. URL: <https://europepmc.org/article/med/8424474>
94. Pannu KK, Chadha S, Kumar D, Preeti (2011) Evaluation of Hearing Loss in Tympanic Membrane Perforation. *Indian J Otolaryngol Head Neck Surg* 63:208–213
95. Parekh A, Mantle B, Banks J, Swartz JD, Badylak SF, Dohar JE, Hebda PA (2009) Repair of the tympanic membrane with urinary bladder matrix. *Laryngoscope* 119:1206–1213
96. Park AH, Hughes CW, Jackson A, Hunter L, McGill L, Simonsen SE, Alder SC, Shu XZ, Prestwich GD (2006) Crosslinked hydrogels for tympanic membrane repair. *Otolaryngol - Head Neck Surg* 135:877–883
97. Park H, Hong SN, Kim HS, Han JJ, Chung J, Seo MW, Oh SH, Chang SO, Lee JH (2015) Determinants of conductive hearing loss in tympanic membrane perforation. *Clin Exp Otorhinolaryngol* 8:92–96
98. Park MK, Kim KH, Lee JD, Lee BD (2011) Repair of large traumatic tympanic membrane perforation with a Steri-Strips patch. *Otolaryngol Head Neck Surg* 145:581–5
99. Pillong L, Stahn P, Hinsberger M, Sorg K, Schick B, Wenzel GI (2020) Cytotoxicity studies of an optoacoustic stimulation strategy for the development of laser-based hearing aids. *J Biomed Opt* 25:1
100. Rhee C-K, He P, Jung JY, Ahn J-C, Chung P-S, Lee MY, Suh M-W (2013) Effect of low-level laser treatment on cochlea hair-cell recovery after ototoxic hearing loss. *J Biomed Opt* 18:128003
101. Rudin R, Svärdsudd K, Tibblin G, Hallén O (2009) Middle Ear Disease in Samples from the General Population: Prevalence and Incidence of Otitis Media and its Sequelae the Study of Men Born in 1913–23. <http://dx.doi.org/103109/00016488309132896> 96:237–246
102. Ruf S, Hougaard S (2011) EuroTrak I : A Consumer Survey About Hearing Aids.
103. Sagiv D, Migirov L, Glikson E, Mansour J, Yousovich R, Wolf M, Shapira Y (2018) Traumatic Perforation of the Tympanic Membrane: A Review of 80 Cases. *J Emerg Med* 54:186–190
104. Schiebler TH, Schmidt W (2002) *Anatomie*. 8th edition. Springer Berlin Heidelberg
105. Schmucker C, Kapp P, Motschall E, Loehler J, Meerpohl JJ (2019) Prevalence of hearing loss

- and use of hearing aids among children and adolescents in Germany: A systematic review. *BMC Public Health* 19:1–10
106. Schultz M, Baumhoff P, Maier H, Teudt IU, Krüger A, Lenarz T, Kral A (2012) Nanosecond laser pulse stimulation of the inner ear—a wavelength study. *Biomed Opt Express* 3:3332–45
  107. Shahsavan H, Arunbabu D, Zhao B (2012) Biomimetic modification of polymeric surfaces: A promising pathway for tuning of wetting and adhesion. *Macromol Mater Eng* 297:743–760
  108. Shahsavan H, Zhao B (2014) Bioinspired functionally graded adhesive materials: Synergetic interplay of top viscous-elastic layers with base micropillars. *Macromolecules* 47:353–364
  109. Shield B (2018) Hearing Loss - Numbers and Costs Evaluation of the social and economic costs of hearing impairment. A report for Hear-it. Brunel Univ London 159
  110. Simsek G, Akin I (2014) Early paper patching versus observation in patients with traumatic eardrum perforations: Comparisons of anatomical and functional outcomes. *J Craniofac Surg* 25:2030–2032
  111. Sorg K, Stahn P, Pillong L, Hinsberger MP, Heimann L, Foth H-J, Schick B, Wenzel GI (2019) First biocompatibility margins for optical stimulation at the eardrum via 532-nm laser pulses in a mouse model. *J Biomed Opt* 24:1
  112. Sorg K, Heimann L, Lana GM, Langenbucher A, Schick B, Arzt E, Wenzel GI (2021) Optoacoustically induced auditory brainstem responses in the mouse model enhanced through an absorbing film. *J Biomed Opt* 26:98001
  113. Sorg K, Heimann L, Lana GM, Stahn P, Engel J, Arzt E, Langenbucher A, Schick B, Wenzel G (2021) Increase of optoacoustic-induced auditory brainstem response amplitudes using an absorbing patch. Optical Society of America, Munich. URL: <http://www.osapublishing.org/abstract.cfm?URI=ECBO-2021-ETu5B.2>
  114. Stahn P, Lim HH, Hinsberger MP, Sorg K, Pillong L, Kannengießer M, Schreiter C, Foth H-J, Langenbucher A, Schick B, Wenzel GI (2019) Frequency-specific activation of the peripheral auditory system using optoacoustic laser stimulation. *Sci Rep* 9:4171
  115. Stenklev NC, Vik O, Laukli E (2004) The aging ear: an otomicroscopic and tympanometric study. *Acta Otolaryngol* 124:69–76
  116. Teh BM, Marano RJ, Shen Y, Friedland PL, Dilley RJ, Atlas MD (2013) Tissue engineering of the tympanic membrane. *Tissue Eng Part B Rev* 19:116–32
  117. Thomas X (2003) Silicone adhesives in healthcare applications. *Dow Corning Healthc Ind* 1–6
  118. Thomsen S (1991) PATHOLOGIC ANALYSIS OF PHOTOTHERMAL AND

- PHOTOMECHANICAL EFFECTS OF LASER–TISSUE INTERACTIONS. *Photochem Photobiol* 53:825–835
119. Tlumak AI, Kileny PR (2001) Parameters that affect the measurement of otoacoustic emissions. *Curr Opin Otolaryngol Head Neck Surg* 9:279–283
  120. Ueda H, Nakata S, Hoshino M (1998) Effects of effusion in the middle ear and perforation of the tympanic membrane on otoacoustic emissions in guinea pigs. *Hear Res* 122:41–46
  121. Verma RU, Guex AA, Hancock KE, Durakovic N, McKay CM, Slama MCC, Brown MC, Lee DJ (2014) Auditory responses to electric and infrared neural stimulation of the rat cochlear nucleus. *Hear Res* 310:69–75
  122. Villar-Fernandez MA, Lopez-Escamez JA (2015) Outlook for Tissue Engineering of the Tympanic Membrane. *Audiol Res* 5:117
  123. Voss SE, Rosowski JJ, Merchant SN, Peake WT (2001) Middle-ear function with tympanic-membrane perforations. I. Measurements and mechanisms. *J Acoust Soc Am* 110:1432–1444
  124. Voss SE, Rosowski JJ, Merchant SN, Peake WT (2001) Middle-ear function with tympanic-membrane perforations. II. A simple model. *J Acoust Soc Am* 110:1445–1452
  125. Voss SE, Rosowski JJ, Merchant SN, Peake WT (2001) How do tympanic-membrane perforations affect human middle-ear sound transmission? *Acta Otolaryngol* 121:169–173
  126. Wada H, Ohyama K, Kobayashi T, Koike T, Noguchi SI (1995) Effect of middle ear on otoacoustic emissions. *Int J Audiol* 34:161–176
  127. Wang J, Xia M, Lu J, Li C, Tian X, Tian L (2015) Performance analysis of the beam shaping method on optical auditory neural stimulation in vivo. *Lasers Med Sci* 30:1533–1540
  128. Wani A, Rehman A, Lateef S, Malik R, Ahmed A, Ahmad W, Kirmani M (2016) Traumatic tympanic membrane perforation: An overview. *Indian J Otol* 22:100
  129. Wenzel GI, Balster S, Zhang K, Lim HH, Reich U, Massow O, Lubatschowski H, Ertmer W, Lenarz T, Reuter G (2009) Green laser light activates the inner ear. *J Biomed Opt* 14:44007
  130. Wenzel GI, Lim HH, Zhang K, Balster S, Massow O, Ilgner J, Lubatschowski H, Reuter G, Lenarz T (2010) Effects of Green Light Application at Ear Drum and Middle Ear Level. Baltimore, USA
  131. Werz J, Goldberg-Bockhorn E, Wigand M, Hahn J, Mytilineos D, Riepl R (2019) Traumatische Trommelfellperforationen: Diagnose, Therapie und Prognose – eine retrospektive Analyse. Abstr und Posterband – 90 Jahresversammlung der Dtsch Gesellschaft für HNO-Heilkunde, Kopf- und Hals-Chirurgie eV, Bonn – Digit der Hno-heilkd 98:2019

132. Willott JF (2006) Measurement of the Auditory Brainstem Response (ABR) to Study Auditory Sensitivity in Mice. *Curr Protoc Neurosci* 34:8.21B.1-8.21B.12
133. World Health Organization (2017) Global costs of unaddressed hearing loss and cost-effectiveness of interventions: a WHO report, 2017. World Health Organization
134. World Health Organization (2018) Addressing The Rising Prevalence of Hearing Loss. World Heal Organ Geneva, Switz 1
135. Yu K, Hou J, Jin Z, Wu K, Xu S, Yang N, Shen Y, Tang T, Guo S (2018) A cochlear implant loaded with dexamethasone and coated with hyaluronic acid to inhibit fibroblast adhesion and proliferation. *J Drug Deliv Sci Technol* 46:173–181
136. Zhang K, Wenzel G, Balster S, Lim H, Lubatschowski H, Lenarz T, Ertmer W, Reuter G (2009) Optoacoustic induced vibrations within the inner ear. *Opt Express* 17:23037–23043
137. Zhang K, Zhang Y, Li J, Wang Q (2016) A contrastive analysis of laser heating between the human and guinea pig cochlea by numerical simulations. *Biomed Eng Online* 15:59
138. Zhang KY, Wenzel GI, Balster S, Lim HH, Lubatschowski H, Lenarz T, Ertmer W, Reuter G (2009) Optoacoustic induced vibrations within the inner ear. *Opt Express* 17:23037
139. Zheng J, Shen W, He DZZ, Long KB, Madison LD, Dallos P (2000) Prestin is the motor protein of cochlear outer hair cells. *Nature* 405:149–155
140. Zhou X, Jen PH-S, Seburn KL, Frankel WN, Zheng QY (2006) Auditory brainstem responses in 10 inbred strains of mice. *Brain Res* 1091:16–26
141. Zuccotti A, Lee SC, Campanelli D, Singer W, Satheesh S V, Patriarchi T, Geisler H-S, Köpschall I, Rohbock K, Nothwang HG, Hu J, Hell JW, Schimmang T, Rüttiger L, Knipper M (2013) L-type CaV1.2 deletion in the cochlea but not in the brainstem reduces noise vulnerability: implication for CaV1.2-mediated control of cochlear BDNF expression. *Front Mol Neurosci* 6:20

## Further publications of the author

- Frech, M., Teichler, S., Feld, C., Bouchard, C., Berberich, H., Sorg, K., ... & Neubauer, A. (2018). MYB induces the expression of the oncogenic corepressor SKI in acute myeloid leukemia. *Oncotarget*, 9(32), 22423.
- Pillong, L., Stahn, P., Hinsberger, M., Sorg, K., Schick, B., & Wenzel, G. (2018). Untersuchungen zur Biokompatibilität optischer Stimulation mithilfe von 532nm-Laserpulsen anhand humaner Fibroblasten. *Laryngo-Rhino-Otologie*, 97(S 02), 10209.
- Eckrich, S., Hecker, D., Sorg, K., Blum, K., Fischer, K., Münkner, S., ... & Engel, J. (2019). Cochlea-specific deletion of Cav1.3 calcium channels arrests inner hair cell differentiation and unravels pitfalls of conditional mouse models. *Frontiers in cellular neuroscience*, 13, 225.
- Boyadzhieva, S., Sorg, K., Danner, M., Fischer, S. C., Hensel, R., Schick, B., ... & Kruttwig, K. (2019). A Self-Adhesive Elastomeric Wound Scaffold for Sensitive Adhesion to Tissue. *Polymers*, 11(6), 942.
- Stahn, P., Lim, H. H., Hinsberger, M. P., Sorg, K., Pillong, L., Kannengießer, M., ... & Wenzel, G. I. (2019). Frequency-specific activation of the peripheral auditory system using optoacoustic laser stimulation. *Scientific reports*, 9(1), 1-13.
- Heimann, L., Carlein, C., Sorg, K., Diller, R., Langenbucher, A., Schick, B., & Wenzel, G. I. (2021). Wavelength-specific optoacoustic-induced vibrations of the guinea pig tympanic membrane. *Journal of Biomedical Optics*, 26(3), 038001.
- Sorg, K., L. Heimann, L., Moreira Lana, G., Stahn, P., Engel, J., Arzt, E., Langenbucher, A., Schick, B., & Wenzel, G. I. "Increase of optoacoustic-induced auditory brainstem response amplitudes using an absorbing patch," in European Conferences on Biomedical Optics 2021 (ECBO), OSA Technical Digest (Optical Society of America, 2021), paper ETu5B.
- Dirksen, M., Sorg, K., Heimann, L., Langenbucher, A., Schick, B., & Wenzel, G. I. (2021). Einfluss verschiedener Distanzen einer Laserlichtquelle auf die optische Aktivierung des Hörsystems an drei unterschiedlichen Stimulationsorten des Hörorgans. *Laryngo-Rhino-Otologie*, 100(S 02).

## Danksagung

Mein Dank gebührt einer Reihe von Menschen, die zur Entstehung dieser Arbeit maßgeblich beigetragen und mich auf meinem Weg dahin begleitet haben. Ich danke meiner Doktormutter Frau Prof. Engel, dass sie mir die Möglichkeit gab, unter ihrer Betreuung und Fürsorge an diesem spannenden Thema arbeiten zu können. Herrn Prof. Schick gebührt mein Dank dafür, dass er mir die Möglichkeit gab, in seiner Klinik in der Arbeitsgruppe „LaserHearingAids“ die Experimente durchführen zu können. Außerdem danke ich Herrn Prof. Arzt, der mir die großartige Möglichkeit gab, in Kooperation mit seinem Institut und seiner Arbeitsgruppe, dieses großartige Forschungsprojekt begleiten und durchführen zu können.

Des Weiteren danke ich meinen Arbeitskollegen und -Kolleginnen aus Homburg, allen voran Frau Prof. Wenzel, für ihre Betreuung meiner Doktorarbeit und ihren unermüdlichen Einsatz bei der Durchführung der Experimente und beim Korrekturlesen unserer Arbeiten. Danke, dass man bei dir immer ein offenes Ohr fand und Du trotz deines Klinikalltages immer alles gegeben hast, um uns in allen Bereichen bestmöglich zu unterstützen! Außerdem danke ich meinen Kolleginnen aus dem Labor, Carolin Bick, Ulrike Bechtel und Silke Wemmert, die mir beim Durchführen der Experimente geholfen haben. Außerdem danke ich meinen Mitstreitern und Mitstreiterinnen Florian Bochen, Lukas Pillong, Sandrina Körner und Larissa Heimann. Ihr habt mir den Alltag versüßt und durch den gegebenen Teamgeist lief die Arbeit viel leichter von der Hand! Außerdem danke ich meinen Kollegen aus Saarbrücken Klaus Kruttwig und Gabriela Moreira Lana für die wundervolle Zusammenarbeit, die immer geprägt war von angeregten Diskussionen, qualitativvollen Experimenten und viel Spaß, was damit maßgeblich zum Gelingen dieser Arbeit beigetragen hat! Der gesamten Arbeitsgruppe aus Saarbrücken danke ich für die Unterstützung bei den Experimenten und für die Hilfe bei der Entstehung unseres gemeinsamen Manuskriptes.

Ein besonderer Dank geht an meine Familie und an meine Freunde. Danke dafür, dass ihr bedingungslos hinter mir standet, auch in stressigen Phasen mit Verständnis reagiert habt und immer ein offenes Ohr für mich hattet. Ohne euren Rückhalt und eure Unterstützung wäre diese Arbeit in dieser Form nie möglich gewesen. Ein weiterer Dank geht an einen besonderen Menschen, der mich zwar auf einem nur kurzen, aber dafür dem wichtigsten Teil meiner Doktorarbeit, begleitet und enorm unterstützt hat. Danke dafür, dass Du immer da bist, auch wenn es brennt!

## Lebenslauf

Aus datenschutzrechtlichen Gründen wird der Lebenslauf in der elektronischen Fassung der Dissertation nicht veröffentlicht.

